Thermodynamic and Kinetic Studies of Sulfur Geochemistry

by

Mark Alan Williamson

A Dissertation submitted to the Faculty of
the Virginia Polytechnic Institute and State University
in partial fulfillment of the requirements of the degree of

DOCTOR OF PHILOSOPHY

in Geological Sciences

APPROVED:

J. Donald Rimstidt, Chair

Robert J. Bodnar

G. V. Gibbs

James R. Craig

Roe Hoan Yoon

August, 1992
Blacksburg, Virginia

Abstract

The thermodynamic properties of aqueous sulfur species were estimated using a structure-based, group contribution additivity method that is based upon first-order approximations. Structural groups were chosen so as to minimize subjectivity and maximize the ease of recognition and include: (1) S_n^*, polymeric sulfur (as 1/n, where n is the length of the longest continuous sulfur chain in the species), (2) O_3S^{IV}; (3) O_3S^{VI}; (4) O_2S^{III} and (5) bridging oxygen. In addition, a modified "charge-to-size" ratio (C) is used to model the coulombic interaction between ions and the solvent. Multiple linear regressions of these thermodynamic data were performed in terms of structural groups to yield fundamental equations for the model. Regression coefficients were used to estimate thermodynamic properties of a number of aqueous species for which no experimental data currently exist. Model-derived thermodynamic data were used to find the thermodynamic stability of intermediate sulfur species that occur during the aqueous oxidation of sulfide minerals, which identified at least one thermodynamically feasible pathway for the overall reaction. The data were also used to construct an Eh-pH diagram for aqueous sulfur species with average sulfur oxidation states less than sulfate (VI). The structure-thermodynamic correlation was used to determine the likely structure of the aqueous $S_2O_5^{2-}$ ion, which has been debated over the past 50 years.

The rate of decomposition of the ferric thiosulfate complex was observed to vary as the square of the concentration of the complex. The decomposition of this complex in acid solutions is strongly dependent on temperature, E_a = 120(±15) kJ mol^{-1}. The rate of reaction increases was

observed to increase with increasing ionic strength, consistent with the interaction of two positively charged ions to form the activated complex. This study resolves many of the inconsistencies found in earlier studies and shows that reaction with H^+ is a more important sink for $S_2O_3^{2-}$ than rection with Fe^{3+} when pH > ~1.7.

Comprehensive rate laws for aqueous pyrite oxidation were produced using experimentally determined data and data reported in the literature. Rate data available in the literature for the reaction of pyrite with dissolved oxygen (DO) to were compiled to produce a rate law that is applicable over three and one half orders of magnitude in DO concentration over the pH range 2-10. A series of batch, and mixed flow reactor experiments were performed to determine the effect of SO_4^{2-}, Cl^-, ionic strength and dissolved oxygen on the rate of reaction of pyrite with ferric iron. Only dissolved oxygen was found to have any appreciable effect. The results of this study were combined with kinetic data reported in the literature to formulate rate laws that are applicable over a six order of magnitude range in Fe^{3+} and Fe^{2+} concentration for the pH range ~0.5-3.0. Fundamental rates laws were formulated for each system and showed that the reaction order for ferric iron changed, thus suggesting a change in reaction mechanism. An observed rate correlation with the Fe^{3+}/Fe^{2+} ratio indicates that the rate is proportional to Eh, and is best modelled by a non-ideal, non-site specific Freundlich multilayer isotherm. Because rate is observed to be positively correlated with the concentration of the aqueous oxidant only, the rate determining step for the aqueous oxidaion of pyrite can be identified as the electron transfer from the mineral to the oxidant.

Acknowledgements

It is perhaps a more daunting task to accurately acknowledge those who have contributed to the successful completion of a dissertation than it is to complete the work itself. For my own part, there is no one with whom I ever shared time during my tenure at Virginia Tech that did not contribute to my ability to complete the task I set before myself. However, in keeping with tradition and good form (neither particularly prominent features of my character) I would like to acknowledge a few noteworthy persons.

My dissertation committee deserves special note insofar as they have always prompted me to examine my research problems in ways that were not always immediately obvious to me. This was never truer than during my preliminary exams. They helped me learn to reason more creatively, which is a tool that to my mind far outstrips the acquisition of pure knowledge alone. Of this committee, Don Rimstidt, my advisor and friend, deserves the greatest accolades. He has consistently provided me with every opportunity to succeed, cheered my victories and consoled me during my failures. I will always remain grateful to him for his genuine concern and effort on my behalf. The National Science Foundation and Sigma Xi generously supported my research at Virginia Tech.

The graduate students in the department of geology have proven time and again to be a reliable source of companionship, information and support. Their laughter, complaining, cheering, swearing, praying, cursing, sweating and toil-filled hours have been an inspiration and memories of them will remain with me for years to come. I thank them all for being part of that diverse body of personalities that has become so significant to the success of

this department and so dear to me. Similarly, the staff of this department receives far too little credit for their efforts and in my eyes have not gone unnoticed.

Inherent to the successful completion of a doctoral dissertation is significant absent- and single-mindedness on the part of the author (at least for me), which is a burden all too often carried by those closest to them. For their endless patience and love, I humbly thank *all* my friends and the members of my family, particularly my wife and son, Becky and Zach.

> "So I guess I gotta lite out for the territory ahead of the rest, 'cause Aunt Sally, she's gonna 'dopt me an' civ'lize me and I just can't stand it. I been there before."
>
> -Mark Twain *in Huckelberry Finn*

Table of Contents

List of Figures

List of Tables

Chapter 1: Introduction

Sulfur ranks fifteenth in crustal abundance (Mason, 1966), far below the geochemically abundant elements like silicon, alumimum, or iron, but it plays a critical role in the earth's geochemistry and in modern society. Sulfur is abundant in many geologic environments, including in sedimentary (4250 ppm), metamorphic (700 ppm) and igneous rocks (486 ppm), fumarolic gases (0.2-1.6 volume %) and seawater (885 ppm) (Wedepohl, 1984). It is present in seafloor hydrothermal systems (black smokers) as well as terrestrial caldera lakes (Takano, 1987). Details of the sulfur' geochemical cycle outlined by Smil (1985) indicate that sulfide, S(-II), elemental sulfur, S(0), and sulfate, S(+VI), are the most important species in nature. However, numerous species with intermediate oxidation states (e.g. thiosulfate, $S_2O_3^{2-}$, and tetrathionate, $S_4O_6^{2-}$) that have persistent lifetimes in aqueous solutions and may participitate in the chemical pathway that allows eight electrons to be exchanged during the transformation of sulfide to sulfate and *vice versa*. This dissertation is a collection of three studies of the thermodynamics and kinetics of sulfur geochemistry and is intended to further our understanding of the stability and reactivity of this element.

As intermediate metastable oxidation states for sulfur in aqueous solutions are increasingly recognized as important species in ore deposit formation (Stoffreggen, 1986; Spirakis, 1991), sulfide oxidation kinetics (Goldhaber, 1983; Moses et al., 1987), volcanic eruption sequences (Takano, 1987), acid rain formation (Graedel and Goldberg, 1983) and sulfur cycling in sedimentary environments (Jorgensen, 1990), the demand for a complete set of internally consistent thermodynamic data has grown. Chapter 2 presents a study

which correlates structure and thermodynamic properties of aqueous sulfur anions utilizing a simple additivity model which addresses this need. It also illustrates a technique for estimating thermodynamic data that produces accurate results, involves minimal subjectivity and is not calculation intensive.

Thiosulfate ($S_2O_3^{2-}$) is a common sulfur oxy-anion which occurs in a variety of geochemically interesting environments, but despite its apparent importance, an understanding of its reactivity under naturally occurring conditions is far from complete. The complex that thiosulfate forms with ferric iron has been suggested as a key intermediate in the formation of uranium roll-front deposits (Granger and Warren, 1974). As thiosulfate has been identified in solutions emanating from sulfide mineral tailings piles (Wolkoff and Larose, 1975), the reactivity of the ferric-thiosulfate complex may be a key intermediate reaction involved in the oxidation of sulfide sulfur to fully oxidized sulfate. The study reported in Chapter 3 is a step toward understanding the geochemical reactivity of this complex and provides insight into the rate and mechanism of the reaction between thiosulfate and ferric iron.

As the most common sulfide mineral, pyrite is a significant link in the global cycling of sulfur and is involved in the formation of acid mine drainage, a persistent environmental problem. However, much remains to be learned about the factors which control its oxidation and weathering which leads to the formation of sulfate that is eventually returned to the oceans. Chapter 4 presents a study of the kinetics of aqueous pyrite oxidation by dissolved oxygen and ferric iron, and reports rate laws that are valid over very wide ranges of solution composition. Some of the data reported in this chapter were collected by William D. Newcomb and his efforts are sincerely appreciated. This study identifys the

rate-determining step for the aqueous oxidation of pyrite and moves us closer to understanding the specific mechanism by which this important reaction occurs.

REFERENCES

Goldhaber M. B. (1983) Experimental study of metastable sulfur oxyanion formation during pyrite oxidation at pH 6-9 and 30°C. *Am. Jour. Sci.* **283**, 193-217.

Graedel T. E. and Goldberg K. I. (1983) Kinetic studies of raindrop chemistry 1. Inorganic and organic processes. *J. Geophys. Res.* **88**, 10865-10882.

Granger H. C. and Warren C. G. (1974) Zoning in the altered tongue asociated with roll-type uranium deposits. Symposium on the formation of uranium ore deposits, Athens, Greece. pp. 185-199

Jorgensen B. B. (1990) A thiosulfate shunt in the sulfur cycle of marine sediments. *Science* **249**, 152-154.

Mason, B. (1966) Principles of Geochemistry. 3rd ed., Wiley.

Moses C. O. Nordstrom, D.K., Herman, J.S., Mills, A.L. (1987) Aqueous pyrite oxidation by dissolved oxygen and by ferric iron. *Geochimica et Cosmochimica Acta* **51**, 1561-1571.

Smil, V. (1985) Carbon, Nitrogen, Sulfur; Human Interferences in Grand Biospheric Cycles. Plenum Press, New York.

Spirakis C. S. (1991) The possible role of thiosulfate in the precipitation of ^{34}S-rich barite in some Mississippi Valley-type ore deposits. *Mineral. Deposita* **24**, 60-65.

Stoffreggen R. (1986) Observations on the behavior of gold during supergene oxidation at Summitville, Colorado, USA, and implications for electrum stability in the weathering environment. *App. Geochem.* **1**, 549-558.

Takano B. (1987) Correlation of volcanic activity with sulfur oxyanion speciation in a crater lake. *Science* **235**, 1545-1712.

Wedepohl, K.H. (1984) Sulfur in the Earth's Crust, It's Origin and Natural Cycle, in Sulfur, its Significance fro Chemistry for the Geo-, Bio- and Cosmophere and Technology. (Müller, A. and Krebs, B., eds.) Studies in Inorganic Chemistry, vol. 5, Elsevier, Amsterdam.

Wolkoff A. W. and Larose R. H. (1975) Separation and detection of low concentrations of polythionates by high speed anion exchange liquid chromatography. *Anal. Chem.* **47**, 1003-1008.

Chapter 2: Correlation Between Structure and Thermodynamic Properties of Aqueous Sulfur Species

ABSTRACT

The thermodynamic properties of aqueous sulfur species can be estimated using a structure-based, group contribution additivity method that is based upon first-order approximations. Free energy and enthalpy data used to calibrate the additivity model were critically selected from a variety of sources. Structural groups were chosen so as to minimize subjectivity and maximize the ease of recognition. We have chosen five fundamental groups to represent the major structural components: (1) S_n^*, polymeric sulfur (as 1/n, where n is the length of the longest continuous sulfur chain in the species), (2) O_3S^{IV}; (3) O_3S^{VI}; (4) O_2S^{III} and (5) bridging oxygen. In addition, a modified "charge-to-size" ratio (C) is used to model the coulombic interaction between ions and the solvent. Thermodynamic data were broken into two sets, one for monovalent species and another for divalent species. Multiple linear regressions of these thermodynamic data were performed in terms of structural groups to yield the following relationships

$$\Delta G_{f\ \text{divalent}}^{\circ} = -176.7O_3S^{IV} - 1270.4O_3S^{VI} - 691.8O_2S^{III} + 1954.5S_n^* + 757.3O - 1182.2C + 55.0$$

$$\Delta H_{f\ \text{divalent}}^{\circ} = -231.3O_3S^{IV} - 1316.9O_3S^{VI} - 734.1O_2S^{III} + 2006.5S_n^* + 734.7O - 1212.5C - 33.2$$

$$\Delta G_{f\ \text{monovalent}}^{\circ} = -536.9O_3S^{IV} - 635.1O_3S^{VI} - 351.7O_2S^{III} - 128.0S_n^* - 140.3O - 828.0C + 64.1$$

$$\Delta H_{f\ \text{monovalent}}^{\circ} = -105.4O_3S^{IV} - 366.5O_3S^{VI} - 0.0O_2S^{III} + 505.8S_n^* + 0.0O + 0.0C - 520.8$$

R^2 values for regressions exceeded 0.9999 and all residuals were normally distributed. Large values for the regression coefficients indicate that the choice of structural parameters is significant. These coefficients were used to estimate thermodynamic properties of a number of aqueous species for which no experimental data currently exist.

Model-derived thermodynamic data were used to find the thermodynamic stability of intermediate sulfur species that occur during the aqueous oxidation of sulfide minerals. This exercise identified at least one thermodynamically feasible pathway for the overall reaction. The data were also used to construct an Eh-pH diagram for aqueous sulfur species with average sulfur oxidation states less than sulfate (VI). The structure-thermodynamic correlation was used to determine the likely structure of the aqueous $S_2O_5^{2-}$ ion, which has been debated over the past 50 years.

INTRODUCTION

Geochemists have traditionally been concerned only with sulfide and sulfate species. The inter-conversion of these two species requires the transfer of eight electrons and despite the fact that only one, or at most two, electrons are transferred in any one reaction step (Basolo and Pearson, 1967), little attention has been directed toward developing an understanding of the chemistry of the series of metastable sulfur species which must occur as intermediates in this process. Metastability of most aqueous sulfur species is probably best viewed from the standpoint of the octet rule. Sulfide (S^{2-}) and sulfate (SO_4^{2-}) both possess fully occupied outermost atomic orbitals and are therefore stable, while intermediate

species (e.g. $S_2O_4^{2-}$) must lose or gain electrons to achieve full stability. Figure 1 shows the sulfur species which are known to have significant lifetimes in aqueous solutions and illustrates the major groups within this system: polysulfides, S_n^{2-}; sulfane monosulfonic acids (polythiosulfates), $S_nO_3^{2-}$; sulfane disulfonic acids (polythionates), $S_nO_6^{2-}$; sulfite, SO_3^{2-} and sulfate, SO_4^{2-}. Thermodynamic data have been tabulated for portions of the aqueous sulfur system (Maronny, 1959; Schwartzenbach and Fischer, 1960; Barner and Scheuerman, 1978; Brewer, 1982; Wagman, et al., 1982; Murowchick, 1984), although a complete, self-consistent data set has not been produced.

As intermediate metastable oxidation states for sulfur in aqueous solutions are increasingly recognized as important species in ore deposit formation (Stoffreggen, 1986; Spirakis, 1991), sulfide oxidation kinetics (Goldhaber, 1983; Moses et al., 1987), volcanic eruption sequences (Takano, 1987; Takano and Watanuki, 1990), acid rain formation (Graedel and Goldberg, 1983) and sulfur cycling in sedimentary environments (Jorgensen, 1990), the demand for a complete set of internally consistent thermodynamic data has grown. Fulfillment of this need will necessarily involve either time intensive, systematic measurement of thermodynamic properties of all aqueous sulfur species or, more practically, the development of a fundamentally sound correlation and estimation method. Because of their metastability, many aqueous sulfoxy intermediates do not participate in equilibria which would allow accurate determination of their thermodynamic properties. Therefore, development of a correlation and estimation methodology offers the

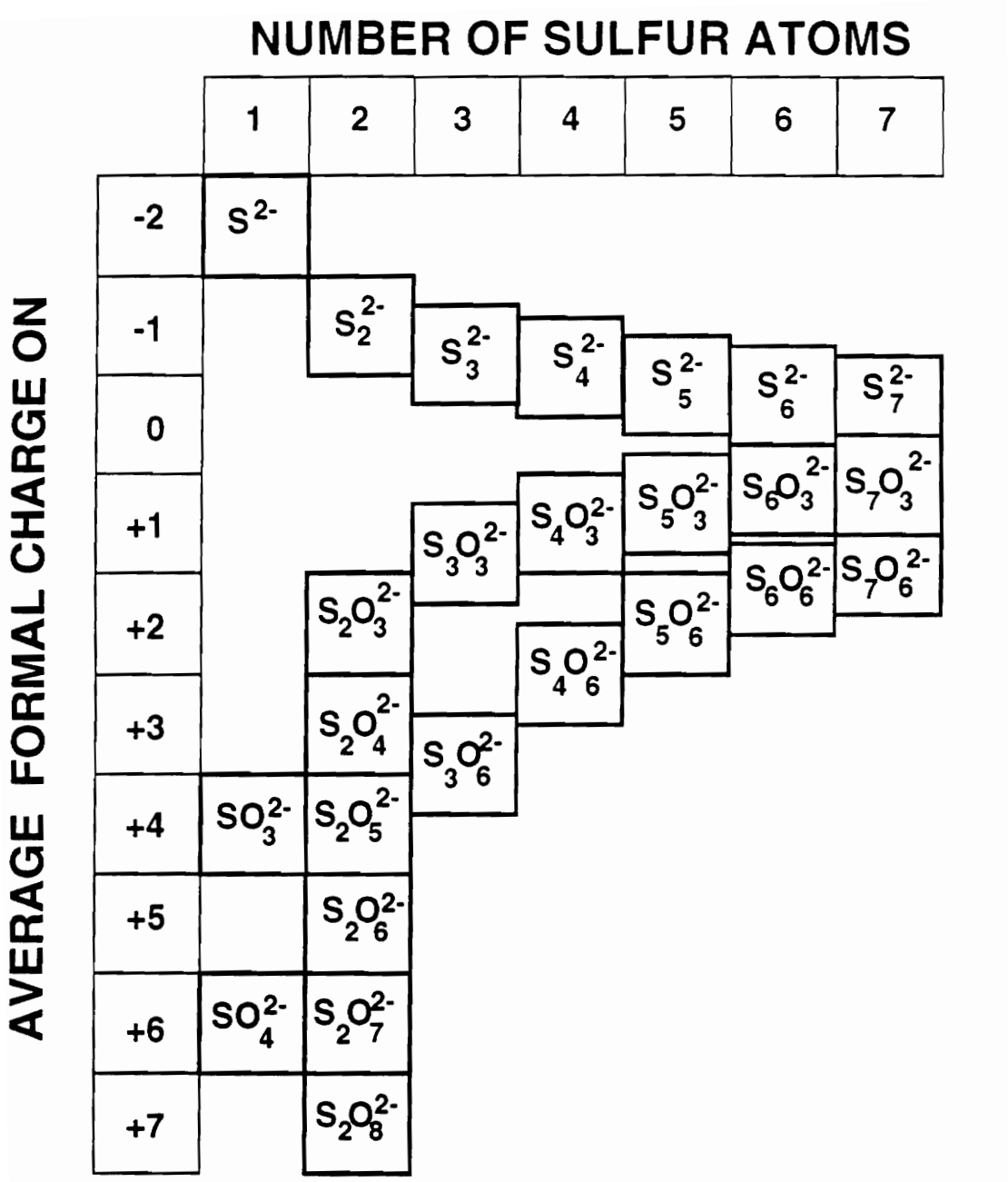

Figure 1. Diagram showing relationships among aqueous sulfur species that are either thermodynamically stable or have significant metastable persistance.

possibility of assessing thermodynamic properties for species that might otherwise evade quantification.

Procedures to estimate thermodynamic properties for mineral phases (see Chermak and Rimstidt, 1989, or Nordstrom and Munoz, 1985, for a brief review), aqueous complexes (Langmuir, 1979), and organic compounds (Janz, 1958) have received a significant amount of attention and are fundamentally based upon systematic relationships between atomic composition and ΔG_f^o and ΔH_f^o of species that may or may not be adjusted according to structural considerations. An approach recognizing the additivity of structural units was first advanced by Parks and Huffman (1932). Their method resulted from an extensive systematic study of the thermodynamic properties of liquid paraffin hydrocarbons and produced two fundamental equations for calculating the entropy and free energy of these compounds using the total number of carbon atoms and the number of methyl (or aliphatic) branches on main, straight chains. Their approach was a zeroth approximation of molar quantities based upon simple additive contributions from constituent atoms in the molecular structure. To progress to the next higher, or first-order approximation, the immediate environment of a given constituent atom must be considered. Estimation procedures involving this level of approximation effectively recognize the dependence of molar properties of a substance on consistent contribution from groups of atoms, regardless of overall molecular structure. This method of group contributions has been used extensively in studies directed toward the estimation of thermodynamic properties of minerals (see Chermak and Rimstidt, 1989, and references therein). For

approximations beyond the first order, contributions toward thermodynamic properties from given atoms are regarded as a function of more and more distant, remote structural features of the molecule. These higher order estimations generally improve the accuracy with which thermodynamic properties may be estimated (Leffler and Grunwald, 1963), but only at the expense of employing additional fitting parameters. Methods employing statistical thermodynamics (Pitzer, 1940) and group equations (Taylor et al., 1946) involve such sophisticated approximations. These techniques are particularly precise, having been used to great advantage in the study of long chain aliphatic, gaseous hydrocarbons, but are, as would be expected, calculation intensive. In sum, several techniques for estimation of thermodynamic properties are available, with the method of group contributions, based upon first-order additivity approximations, being particularly attractive because of its relatively good accuracy and great simplicity. Additionally, any method which seeks to correlate thermodynamic properties with structure will, in all cases, be limited by the quality of the experimental data used to calibrate the model. As a result of the complexity of the system S-O-H, many thermodynamic measurements for species shown in Fig. 1 have been hard won and are generally not as accurately known as simpler systems. This consideration serves to further heighten the appeal of a group contribution methodology. According to Janz (1958), this method allows acceptably accurate estimation of thermodynamic properties with minimal data, is not particularly calculation intensive and lends itself to easy application through recognition of logical, consistent structural features.

Although several approaches exist for estimating thermodynamic properties and have been fruitfully employed during the study of uncharged molecules (hydrocarbons and silicate minerals), we are aware of no effort which has been directed toward estimation of thermodynamic data for specific aqueous ionic species. In the present study, we report the results of our efforts to understand and model the thermodynamic properties of aqueous sulfur anions using a structure-based, group contribution methodology.

METHODS

Our approach to construction of a group contribution methodology to model the thermodynamic properties of aqueous sulfur anions requires three principle steps: (1) critical selection of thermodynamic data from literature sources to calibrate the model, (2) identification of logical, easily recognized groups of structure for the system and (3) multiple linear regression to determine the contribution from each of the fundamental groups (independent variables, x_n) to thermodynamic properties (dependent variable, y)

$$y = \Sigma m_i x_i + b \qquad (1)$$

If free energy or enthalpy (dependent variable) are regressed against a series of fundamental, structure-based parameters (independent variables), the following is obtained

$$\Delta G_f^\circ = \Sigma g_i n_i + b \quad (2)$$

$$\Delta H_f^\circ = \Sigma h_i n_i + b \quad (3)$$

where n_i is the number of occurrences of a fundamental structural unit, i, within the molecule and g_i is the statistical leverage coefficient, similar to the slope term of a simple linear regression. An analogous relationship may be used for enthalpy. We outline our approach to each of these tasks below.

Selection of Data Used to Calibrate the Model

The free energy and enthalpy data used to calibrate the additivity model were selected from a variety of sources. Often there was a wide variation in the reported values; for example, the reported ΔG_f° values for thiosulfate, $S_2O_3^{2-}$ range from -513.4 kJ·mol^{-1} (Mel et al., 1956) to -598.3 kJ·mol^{-1} (Latimer, 1952). We used concepts discussed in Nordstrom and Munoz (1985, Chapter 12) as guides in selecting what we feel are the best and most internally consistent set of ΔG_f° and ΔH_f° values. Accordingly, we have searched the literature, extracted data, and tabulated values from several sources. Any datum which differed significantly from several other determination of the same value was considered unacceptable. We have avoided selecting data from compilations in which the author(s) have made adjustments to original empirical determinations to improve consistency within their own work (e.g. Brewer, 1982). Similarly, we have avoided use of data that are estimates (e.g. $S_2O_5^{2-}$, Latimer, 1952). Where possible, we made selections of data based upon reliability of the

experimental procedures. During initial regressions of thermodynamic properties against structural groups, some thermodynamic data were identified as being significantly inconsistent with all other data (e.g. $S_2O_5^{2-}$ and $S_2O_6^{2-}$, discussed below) and were rejected on those grounds from the final thermodynamic dataset reported in Table 1. Rationale for particular values listed in Table 1 is discussed in the following paragraphs.

Polysulfides, S_n^{2-}

The chemical properties of polymeric sulfur chains of up to five sulfurs, the range of polysulfide lengths expected to occur in appreciable quantities in aqueous solutions (Pickering and Tobolsky, 1972), are related to the inverse of the chain length (n). Figure 2 shows experimental pK_1 and pK_2 values of sulfanes for n=4 and 5 (Schwartzenbach and Fischer, 1960), the estimated value pK_2 of H_2S (Schoonen and Barnes, 1988), and the pK_1 and pK_2 values derived from extended Hückel molecular orbital calculation on planar sulfane structures (Meyer et al., 1977) plotted against 1/n. Schoonen and Barnes (1988) argued that pK_1 and pK_2 values of a sulfane of infinite chain length should be identical and used this use this assumption to extend the 1/n relationship for pK_1 to zero. The intercept was then used to extrapolate to 1/n = 1 to derive an estimate for pK_2 of H_2S. The calculations of Meyer et al. (1977) suggest that for 1/n = 1 to 0.2 the relationship between pK and 1/n is linear, but begins to fall off for chain lengths greater than 5. However, we extrapolated the values from Meyer et al. (1977) for 1/n = 1 to 0.2 (Meyer et al., 1977, indicate data for 1/n<0.2 are approximate) back to 1/n = 0 (infinite chain length) and found that the

Table 1. Selected thermodynamic data for aqueous sulfur species and corresponding structural groups. See Table 2 for a description of each parameter.

SPECIES	ΔG_f^o, kJ·mol^{-1}	ΔH_f^o kJ·mol^{-1}	O_3S^{IV}	O_3S^{VI}	O_2S^{III}	O	S_n^*	C
S^{2-}	117.7	33.3	0	0	0	0	1	1.6
S_2^{2-}	84.5	-	0	0	0	0	0.500	0.80
S_3^{2-}	83.5	-	0	0	0	0	0.333	0.53
S_4^{2-}	66.5	-	0	0	0	0	0.250	0.40
S_5^{2-}	65.9	-	0	0	0	0	0.200	0.32
S_6^{2-}	67.1	-	0	0	0	0	0.167	0.27
$S_2O_3^{2-}$	-543.8	-659.8	0	1	0	0	0.500	0.26
$S_4O_6^{2-}$	-1055.5	-1236.3	1	1	0	0	0.250	0.13
$S_2O_4^{2-}$	-600.3	-753.5	0	0	2	0	0	0.21
SO_3^{2-}	-486.0	-637.6	1	0	0	0	0	0.31
$S_2O_8^{2-}$	-1114.6	-1344.7	0	2	0	2	0	0.12
SO_4^{2-}	-744.6	-909.4	0	1	0	1	0	0.24
HS^-	12.08	-15.0	0	0	0	0	1	0.21
HS_4^-	28.1	-	0	0	0	0	0.25	0.083
HS_5^-	31.9	-	0	0	0	0	0.2	0.068
$HS_2O_3^-$	-553.8	-634.4	1	0	0	0	0.5	0.057
$HS_2O_4^-$	-614.5	-	0	0	2	0	0	0.047
HSO_3^-	-528.0	-626.2	1	0	0	0	0	0.066
HSO_4^-	-755.9	-887.3	0	1	0	1	0	0.054

intercept determined by Schoonen and Barnes (1988) is almost exactly the mid-point of the range defined by Meyer et al.'s (1977) data. Thus, we feel further assured that the value estimated by Schoonen and Barnes (1988) is reasonable, even though the 1/n relationship may not be linear for all values of n. Nonetheless, this figure clearly shows the utility of the 1/n relationship to model the properties of polymeric sulfur species over short intervals.

Because experimental data are only available for tetra- and penta-sulfide we have been compelled to use one thermodynamic estimate in our data base for HS^- to more tightly constrain the contribution of polymeric sulfur toward thermodynamic properties of aqueous sulfur anions. The ΔG_f^o $[H_2S_{(aq)}]$, -27.83 kJ·mol^{-1}, taken from Wagman et al. (1982) was combined with its first dissociation constant, pK_1 = 6.975 (Millero, 1983), to calculate ΔG_f^o $[HS^-$ = 12.08 kJ·mol^{-1}. This value for HS^- was then used in combination with a value of pK_2 = 18.5 (Schoonen and Barnes, 1988) to calculate $\Delta G_f^o[S^{2-}]$= 117.7 kJ·mol^{-1}. Combining the literature value for $H_2S_{(aq)}$ and HS^- with the equilibrium constants, $pK_{n=2}$ = -19.68, $pK_{n=3}$ = -19.50, $pK_{n=4}$ = -16.52, $pK_{n=5}$ = -16.41, from (Boulegue and Michard, 1978) for

$$H_2S + \frac{n}{8}S_8 = S_n^{2-} + 2H^+$$

$$n=2\text{-}5$$

we calculated values of ΔG_f^o for each of the polysulfides. Table 1 lists ΔG_f^o values calculated for polysulfides which were subsequently used for modeling.

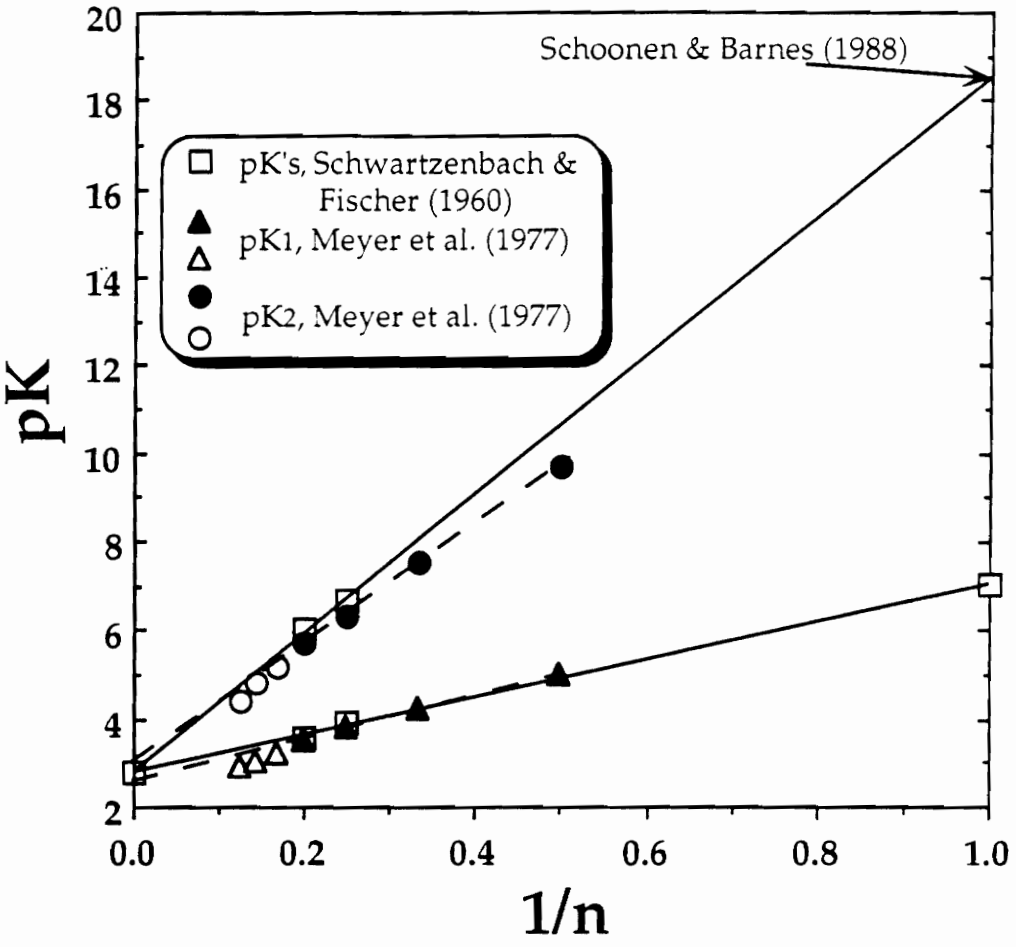

Figure 2. Schoonen and Barnes (1988) used the relationship between pK2 values for aqueous polysulfide species and 1/n, where n is the length of the polymeric sulfur chain (first suggested by the work of Meyer et al., 1977), to estimate a pK2 value for H_2S.

HS_n^-

Dissociation constants, pK_2, reported by Schwartzenbach and Fisher (1960), corrected for infinite dilution at 20°C, for H_2S_4, pK_2 = 6.66 and H_2S_5, pK_2 = 6.02 coupled with pK_2 of H_2S of 18.5 were used to calculate free energy values for HS^-, HS_4^-, HS_5^-. No temperature correction was made as it would probably be smaller than the error in the original determination made by Schwartzenbach and Fischer (1960). Values for ΔG_f° of these species are summarized in Table 1.

$S_2O_3^{2-}$

ΔG_f° and ΔH_f° were chosen from (Cobble et al., 1972) who derived these values from

(1) calorimetric studies of the heat of oxidation of thiosulfate by Br_2

$$S_2O_3^{2-} + 4Br_2 + 5H_2O \rightarrow 2SO_4^{2-} + 10H^+ + 8Br^-$$

with supplemental data for the reaction taken from contemporary NBS compilations, the

(2) solubility of Ag_2S in sulfite solutions

$$2Ag + S_2O_3^{2-} = Ag_2S + SO_3^{2-}$$

coupled with heat capacities (see references in Cobble et al., 1972) and subsequent third law analysis, and the

(3) solubility of hydrated calcium sulfite in pure water and in the presence of sulfur (see discussion in Cobble et al., 1972)

$$CaSO_3 \cdot \tfrac{1}{2}H_2O = Ca^{2+} + SO_3^{2-} + \tfrac{1}{2}H_2O$$

$$CaSO_3 \cdot \tfrac{1}{2}H_2O + \tfrac{1}{8}S = Ca^{2+} + S_2O_3^{2-} + \tfrac{1}{2}H_2O$$

These two expressions may then be combined to form

$$SO_3^{2-} + \tfrac{1}{8}S = S_2O_3^{2-}$$

Values calculated from each of these three approaches were averaged by Cobble et al. (1972) to produce the value which we tabulate in Table 1.

$HS_2O_3^-$

ΔG_f^o was calculated from the free energy value for thiosulfate (Cobble et al., 1972) and the pK_2 [$H_2S_2O_3$] (= 1.72 at infinite dilution) as determined by Page (1953). This value was evaluated in the present study by examining the correlation between equilibrium constants of a series of sulfate and thiosulfate complexes (Langmuir, 1979). Figure 3 is a graph of the dissociation constants (Smith and Martell, 1976) of thiosulfate *versus* the dissociation constants of sulfate complexes with Ba, Ca, Co, K, Mg, Mn, Na, Ni, Sr and Zn. Using the least squares fit to this set of data and a pK_2 value for H_2SO_4 of 1.99 (Smith and Martell, 1976), a pK_2 for $H_2S_2O_3$ is estimated to be 1.73, in good agreement with the work by Page (1953).

ΔH_f^o is based upon C_p values from Olafsson et al. (1978).

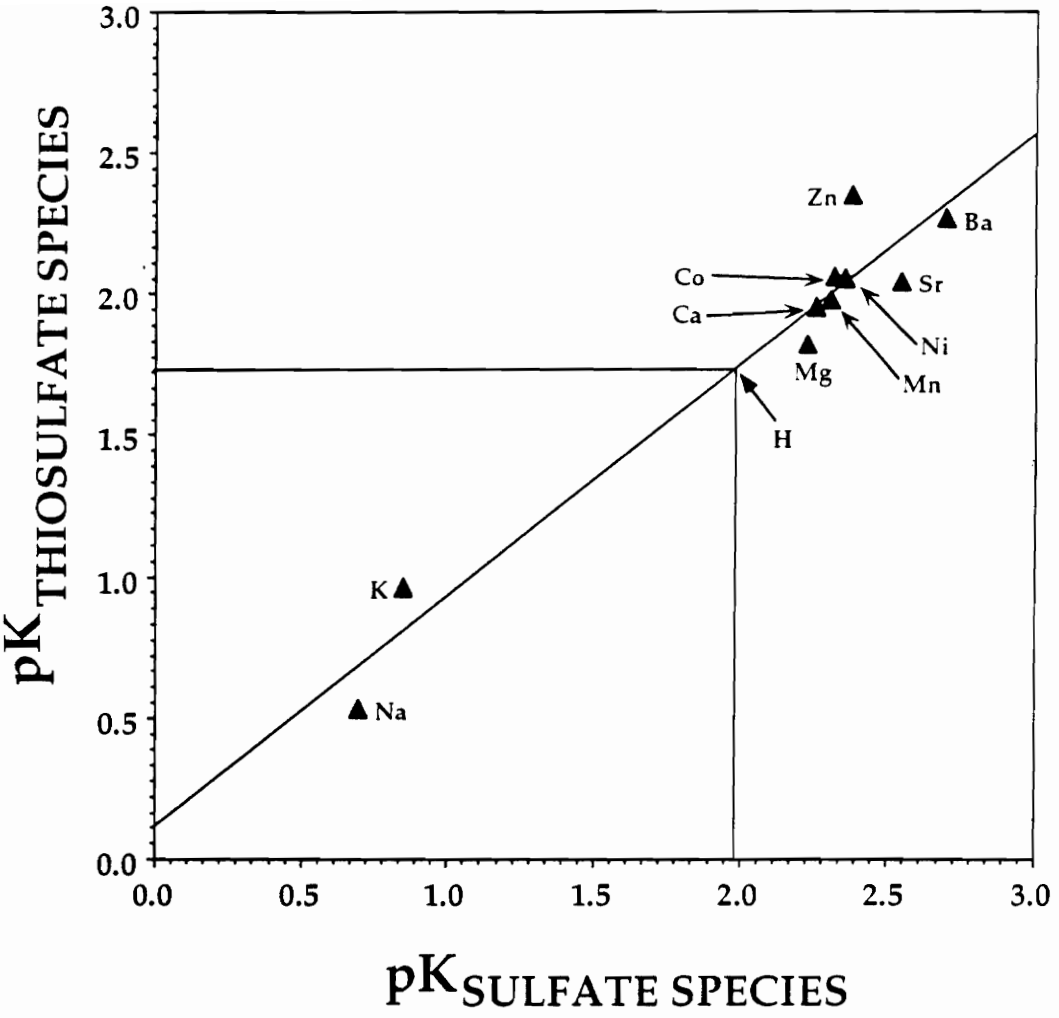

Figure 3. The pK2 value for $H_2S_2O_3$ can be estimated using the relationship between dissociation constants for a series of complexes of thiosulfate and sulfate (Langmuir, 1979). The linear least squares regression line shown in this figure (R2 = 0.943) was used to correlate the pK2 value for H_2SO_4 with an estimated value for $H_2S_2O_3$, determined to be 1.73.

$S_2O_4^{2-}$

ΔG_f^o value from Wagman et al. (1982) was accepted and is probably based upon the reaction

$$S_2O_4^{2-} + 2Ag(NH_3)_2^+ + 2H_2O = 2SO_3^{2-} + 2Ag + 4NH_4^+$$

studied by (McMillan et al., 1942).

$HS_2O_4^-$

ΔG_f^o was calculated in the present study using the free energy value for $S_2O_4^{2-}$ (Wagman et al., 1982) coupled with the second dissociation constant for $H_2S_2O_4$(aq), $pK_2 = 2.45$ (Jellenik, 1911).

$S_4O_6^{2-}$

ΔG_f^o and ΔH_f^o were selected from Cobble et al. (1972). ΔG_f^o was calculated from the solubility of $K_2S_4O_6$ and an estimated activity coefficient of 1.21 at 25°C. ΔH_f^o is based upon determinations of heat of solution of $K_2S_4O_6$ at various temperatures and concentrations.

SO_3^{2-}

ΔG_f^o value from Cobble, et al. (1972) was accepted as it is accurately fixed from the second dissociation constant of $H_2SO_{3(aq)}$ at infinite dilution, $pK_2 = 7.2$. ΔH_f^o value was taken from Cobble, et al. (1972), who base their estimate upon calorimetric measurements for the heat of dissociation of HSO_3^-(aq).

HSO_3^-

ΔG_f° and ΔH_f° from Wagman et al. (1982) were accepted as they are based upon extensive solubility data of $SO_2(g)$ to form $H_2SO_3(aq)$ combined with the first dissociation constant of this acid, $pK_1 = 1.85$ (Huss and Eckert, 1977).

SO_4^{2-}

ΔG_f° and ΔH_f° values from Wagman et al. (1982) were accepted. Although key thermodynamic values from CODATA (Cox et al., 1989) for ΔH_f° are in agreement with the value in Wagman et al. (1982), no value for ΔG_f° is tabulated in CODATA.

HSO_4^-

ΔG_f° and ΔH_f° values from Wagman, et al. (1982) were accepted and are consistent with the well-characterized second dissociation constant for sulfuric acid, $pK_2 = 1.99$ (Smith and Martell, 1971).

$S_2O_8^{2-}$

ΔG_f° and ΔH_f° Values for peroxymonosulfate range from -1114.6 $kJ \cdot mol^{-1}$ (Wagman et al., 1982) to -1189.9 $kJ \cdot mol^{-1}$ (Barner and Scheuerman, 1978) for free energy and -1344.7 $kJ \cdot mol^{-1}$ (Wagman et al., 1982) to -1467.3 $kJ \cdot mol^{-1}$ (Barner and Scheuerman, 1978) for enthalpy. We have accepted the values from Wagman et al. (1982). This choice was made as Wagman et al. (1982) is a fairly standard source of data, and no details of experimental determination were available for any tabulated values to

enable more critical selection. During regression analysis, this datum was not identified as an outlier and, thus, could not be eliminated from the dataset, so it was retained.

Structural Partitioning

For any scheme which seeks to estimate the thermodynamic properties of a class of compounds based upon first order approximations, fundamental structural groups must be identified. Further, the choice of these groups should be made so as to minimize subjectivity and maximize the ease of recognition.

As illustrated in Figure 4, structural (or perhaps more properly, connectivity) similarities exist between the major classes of aqueous sulfur species shown in Figure 1: polysulfides, sulfane monosulfonic acids (here termed polythiosulfates) and sulfane disulfonic acids (generally referred to as polythionates). Polysulfides consist of charged polymeric sulfur chains with an ionic charge of -2 or -1, depending on whether or not the species is protonated. The shaded arrows in Figure 4 indicate that the charge on these species is *localized* towards the ends of the chain (Meyer et al., 1977). Thiosulfate is a derivative of the sulfate, SO_4^{2-}, structure in which one of the oxygen atoms is replaced with a sulfur atom (hence the nomenclature *thio*sulfate). This substituted position may be extended to become a polysulfur chain, giving rise to the complete series, S_n-SO_3^{2-}. Electron density within these species tends, as would be expected, to be weighted towards the SO_3 group (as oxygen is particularly electronegative) until the polymeric sulfur chain is long enough to effectively isolate the two ends of

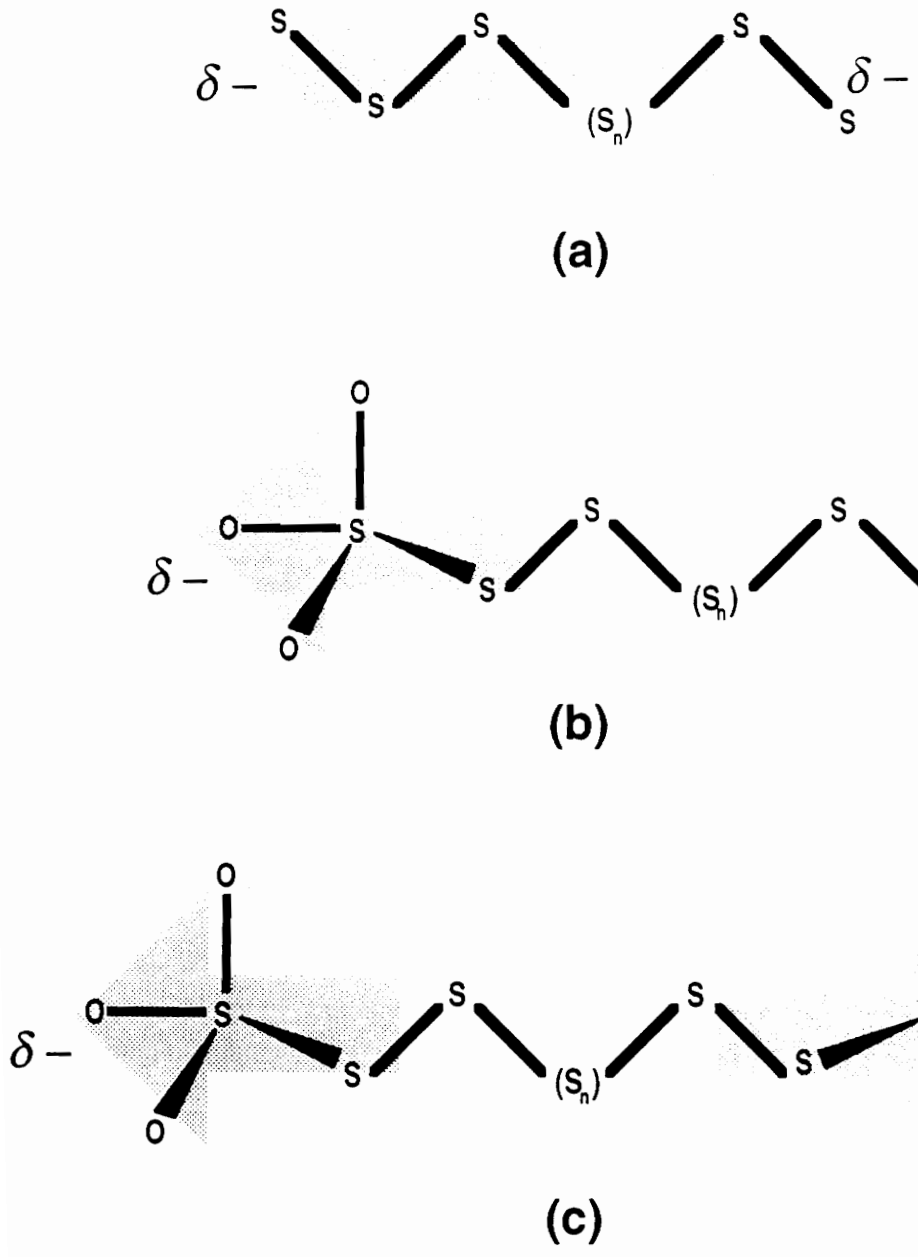

Figure 4. A polymeric sulfur chain is common to several classes of aqueous sulfur species, which are shown in this figure: (a) polysulfides, (b) sulfane monosulfonic acids (polythiosulfates) and (c) sulfane disulfonic acids (polythionates). The shaded arrows in the figure illustrate the general directional shift in charge distribution in these species. This results in a partial negative charge, d-, localized at the ends of the chains.

the structure, which allows a modest accumulation of charge on the "sulfide" end (Meyer et al., 1977). Similar to the sulfane monosulfonic acids, polythionates consist of a nearly neutral polymeric chain of sulfur atoms which is terminated by *two* SO_3 groups. In this structure also, electron density is localized about the more electronegative oxygen atoms found in terminal SO_3 groups.

Aqueous sulfur species other than polysulfides, polythiosulfates and polythionates include sulfite, SO_3^{2-}, peroxymonosulfate, $S_2O_8^{2-}$ and dithionite, $S_2O_6^{2-}$. Although these species are not members of the major groups of aqueous sulfur anions outlined above, they possess fundamental groups of structure that are common to all.

We have chosen five fundamental groups to represent the major components: (1) polymeric sulfur (as 1/n, where n is the length of the longest continuous sulfur chain in the species), (2) O_3S^{IV}; (3) O_3S^{VI}; (4) O_2S^{III} and (5) bridging oxygen. In addition, a modified "charge-to-size" ratio is used to model the coulombic interaction between ions and the solvent. These choices were made primarily by examination of the structure, or connectivity, of the atoms in various species.

As 1/n is well correlated with properties of sulfur chains, where n is the length of the chain, this term must be used as a fundamental parameter. Indeed, it is the common structural group among polysulfides, polythiosulfates and polythionates (Fig. 4). The occurrence of this fundamental group within a species structure is recognized by sulfur-sulfur bonds and the term 1/n is calculated using the number of sulfur atoms in a

bonded row as n. Thus, tetrasulfide, S_4^{2-}, has a 1/n term of 0.25, as does tetrathionate, $S_4O_6^{2-}$.

The necessary distinction between O_3S^{IV} and O_3S^{VI} sites is evident upon examination of the structure and reactivity of polythionates. For these species, the average oxidation state of sulfur within the two groups of oxygen atoms is +5, which is probably more accurately considered a resonance structure wherein the oxidation state varies from +4 to +6. Sulfur in the S(VI) (e.g. SO_4^{2-}) has an electronic configuration $1s^2 2s^2 2p^6$ where all electrons are paired, there are no partially filled orbitals and the octet rule is obeyed and this species is particularly stable. Further, S(V) (i.e. $S_2O_6^{2-}$) is not known in the geochemical environment and S(IV) (e.g. SO_3^{2-}) is. Hence, a resonance structure in which sulfur can vary from S(VI) to S(IV) is expected to be more stable than a single state of S(V). Experimental studies of the charge density in crystalline polythionates suggest that the two sulfite groups at either end of the polythionate chain differ (Christidis et al., 1985). Hence, we have chosen to deal with polythionates as if they have a O_3S^{IV} at one end and a O_3S^{VI} at the other end.

Recognition of either of these groups is based upon location of a sulfur grouped by three oxygen atoms and calculating the formal charge on the sulfur atom. The SO_3 group in sulfane monosulfonic acids is always considered O_3S^{IV}, polythionates will always contain one each, O_3S^{IV} and O_3S^{VI}. Sulfite, SO_3^{2-}, is straightforward, O_3S^{IV}. Aqueous sulfur species which have higher average oxidation states for sulfur are characterized, as might be expected, by an increased number of oxygen atoms in the structure. The persulfate ion, $S_2O_8^{2-}$, is composed of two sulfates, SO_4^{2-},

which are linked through an oxygen bridge (Cotton and Wilkinson, 1972). Hence, we represent the structure of this ion as two O_3S^{VI} (high sulfur oxidation state) groups with two bridging oxygens. Similarly, sulfate may be considered to be made up of one O_3S^{VI} group and one bridging oxygen (that happens to be but singly bonded). With this approach, use of an O_4S^{VI} term is avoided as it is effectively represented as a linear combination of already established fundamental groups, which helps strengthen the statistical reliability of the resultant O_3S^{VI} term.

A regression term was include for the occurrence of O_2S^{III}groups as observed in $S_2O_4^{2-}$. This fundamental group occurs in only one species found in our database, but comprises a portion of other species that our model seeks to predict such as $S_2O_5^{2-}$ and $S_2O_7^{2-}$.

Lastly, a term was chosen to account for ionic charge (Z) relative to a weighted sum of the atoms in the ion

$$C = \frac{Z^2}{n_T} \tag{4}$$

where n_T is defined as

$$n_T = E_S S_\Sigma + E_O O_\Sigma + E_H H_\Sigma \tag{5}$$

where E is the Pauling electronegativity of the atom (E_S = 2.5; E_O = 3.5; E_H = 2.1) and S_Σ, O_Σ and H_Σ are the total numbers of sulfur, oxygen, and hydrogen atoms, respectively, in the ion. Although the exact theoretical basis of such charge-to-size terms is not clearcut (Huheey, 1983) they have

repeatedly proved to be useful in modeling the behavior of aqueous ions (Latimer, 1939; Sterns, 1969). In general, however, this term arises because for ions in aqueous solution, small ions of high charge have the largest enthalpy of hydration as they attract the water molecules most strongly. In the present model, this term uses electronegativity values to account for the manner in which charge is distributed about the ion, affecting the enthalpy of hydration and, hence, the free energy and enthalpy of formation of the species.

Our structural partitioning scheme is summarized in Table 2, which provides graphical as well as verbal description of parameters. The structural parameters that we have chosen to model the aqueous sulfur species are intended to minimized subjectivity of assignment because they are readily recognizable.

Regression Methods

Multiple linear regression of thermodynamic data for the species listed in Table 1 was performed in terms of regression parameters discussed in the previous section. Critically evaluated thermodynamic data were divided into two datasets; divalent (unprotonated) species and monovalent (monoprotonated) species. We found this distinction necessary because the ΔG_f^o and ΔH_f^o values for hydrolysis of the aqueous sulfur species varies in a non-systematic way from species to species, depending on whether the hydrogen is associated with a sulfur atom (e.g. SO_3^{2-}) or oxygen (e.g. SO_4^{2-}).

Table 2. Structural parameters used in the present model are designed to minimize subjectivity, maximize ease of recognition and are summarized here. See text for detailed explanation of each parameter.

PARA-METER	SPECIES	STRUCTURE	NOTES
O_2S^{III}	$S_2O_4^{2-}$, **dithionite**	$O_2S\text{-}SO_2$	Group of two oxygens surrounding a sulfur atom with a +3 formal charge.
O_3S^{IV}	$S_4O_6^{2-}$, **tetrathionate**	$O_3S\text{-}S\text{-}S\text{-}S\ O_3$	Group of three oxygen atoms surrounding a sulfur atom with a +4 formal charge and is found at one end of polythionates.
O_3S^{VI}	" "	$O_3S\text{-}S\text{-}S\text{-}SO_3$ $O_3S\text{-}S\text{-}S\text{-}S$	Three oxygen atoms surrounding a sulfur with a formal charge of +6 at the other end of $S_xO_6^{2-}$ and all $S_xO_3^{2-}$
$S_n^{\bullet}$	" " $S_4O_3^{2-}$, **tetra-thiosulfate**	$O_3S\text{-}S\text{-}S\text{-}SO_3$ $O_3S\text{-}S\text{-}S\text{-}S$	The reciprocal of the number of sulfur atoms, n, in the longest continuous chain. $S_n^{\bullet} = 1/n$
O	$S_2O_8^{2-}$, **peroxy-monosulfate**	$O_3S\text{-}O\text{-}O\text{-}SO_3$	Bridging oxygens that occur whenever the ratio of oxygen to sulfur in the molecular formula exceeds 3:1.
C	$S_2O_3^{2-}$, **thiosulfate**	$S\text{-}SO_3$ $\frac{4}{2(2.5)+3(3.5)} = 0.16$	"Charge-to-size" ratio (C) is the squared species' charge (Z^2) divided by the sum of the number of each atoms (n) multiplied by its electronegativity (E_n). $C = \frac{Z^2}{\Sigma n_i E_n}$

RESULTS

Coefficients for g_i and h_i produced by the multiple linear regressions are listed in Table 3. Table 4 lists model-predicted ΔG_f^o and ΔH_f^o values for species used to calibrate the model, with associated residuals. For the divalent dataset, the average difference between literature and model-predicted ΔG_f^o is 0.062% and for ΔH_f^o, <0.000001%. Similarly for the monovalent dataset, residuals average 0.30% for ΔG_f^o and <0.000001% for ΔH_f^o. The fit of ΔH_f^o appears better in part because the dataset contains fewer values. Also note that there are more regressors than data for the monovalent ΔH_f^o model and only one more datum than regressors for the divalent set. For both datasets, residuals followed a normal Gaussian distribution, suggesting that all of the systematic variations in the data are fit by the model.

Regression-generated coefficients for the contribution of each parameter toward overall ΔG_f^o and ΔH_f^o were used to calculate thermodynamic properties of a host of aqueous species. Thus, a virtually complete, internally consistent thermodynamic dataset for aqueous, ionic sulfur-containing species was generated.

Values for ΔG_f^o and ΔH_f^o of aqueous sulfur species not used to calibrate the model were calculated by summing g_i n_i (or h_i n_i) values for all fundamental groups which occur in the structure times the number of occurrences of each. For example, consider the species, $S_2O_8^{2-}$. From equation (1), the charge-to-size ratio (C) is calculated as

$$C = \frac{(-2)^2}{2.5(2) + 3.5(8) + 2.1(0)} = 0.1212 \qquad (6)$$

Table 3. Results of multiple linear regression to determine the contribution to overall ΔH_f^o and ΔG_f^o by individual first-order groups. Because enthalpy models are over determined systems (i.e. the number of regressors is nearly the same as the number of enthalpy data) errors are meaningless and are not reported.

TERM	g_i kJ·mol^{-1}	ERROR* kJ·mol^{-1}	h_i kJ·mol^{-1}	ERROR* kJ·mol^{-1}
DI-VALENT				
Intercept	55.0	3.05	-33.1	-
O_3S^{IV}	-176.7	8.7	-231.3	-
O_3S^{VI}	-1270.4	16.1	-1316.9	-
O_2S^{III}	-691.8	8.7	-734.1	-
S_n^*	1954.5	43.9	2006.5	-
O	757.3	18.4	734.7	-
C	-1182.2	28.2	-1212.5	-
MONO-VALENT				
Intercept	64.1	6.6	-520.8	-
O_3S^{IV}	-536.9	7.44	-105.4	-
O_3S^{VI}	-635.1	14.2	-366.5	-
O_2S^{III}	-351.7	8.1	-	-
S_n^*	128.0	38.9	505.8	-
O	-140.3	18.9	-	-
C	-828.0	208.7	-	-

*Standard Error of Estimate

Table 4. Comparison of model-generated data with data for species used to calibrate the model. Residuals are normally distributed.

SPECIES	$\Delta G^{o}_{f,pred}$ kJ·mol^{-1}	RESIDUAL	$\Delta H^{o}_{f,pred}$ kJ·mol^{-1}	RESIDUAL
S^{2-}	117.7	-0.22	33.3	0
S_2^{2-}	84.5	-1.97	-	-
S_3^{2-}	83.5	8.16	-	-
S_4^{2-}	66.5	-4.24	-	-
S_5^{2-}	65.9	-1.70	-	-
S_6^{2-}	67.1	0.94	-	-
$S_2O_3^{2-}$	-543.8	-1.04	-659.8	0
$S_4O_6^{2-}$	-1055.5	1.04	-1236.3	0
$S_2O_4^{2-}$	-600.3	0	-753.5	0
SO_3^{2-}	-486.0	-1.04	-637.6	0
$S_2O_8^{2-}$	-1114.6	-0.09	-1344.7	0
SO_4^{2-}	-744.6	0.19	-909.4	0
HS^-	12.1	0.02	-15.0	0
HS_4^-	27.7	-0.40	-	-
HS_5^-	33.0	-1.10	-	-
$HS_2O_3^-$	-554.0	0.20	-634.4	0
$HS_2O_4^-$	-614.5	0	-	-
HSO_3^-	-527.6	0.40	-626.2	0
HSO_4^-	-755.9	0	-887.3	0

As discussed earlier, we represent $S_2O_8^{2-}$ with two O_3S^{VI} groups and two bridging oxygens. Thus, the overall free energy of formation of this species may be estimated as follows

$$\Delta G_f^o = 2(g_{O_3S^{VI}}) + 2(g_O) + 0.1212(g_C) + b \qquad (7)$$

$$= 2(-1267.7) + 2(754.3) + 0.1212(-1183.0) + 55.5 \text{ kJ mol}^{-1}$$

$$= -1114.6 \text{ kJ mol}^{-1}$$

The error (precision) associated with this estimate may be calculated by taking the square root of the sum of the squares of the standard error of coefficients used in the free energy calculation, as follows (Taylor, 1982; Table 2)

$$\text{Error} = \sqrt{\left[2(2.01)^2\right] + \left[2(2.29)^2\right] + \left[0.1212(3.52)^2\right] + 0.38^2} \text{ kJ mol}^{-1} \qquad (8)$$

$$= \pm 4.5 \text{ kJ mol}^{-1} \qquad (1\sigma)$$

Tables 5a and 5b list estimated ΔG_f^o and ΔH_f^o values for all of the known aqueous sulfur species not already listed in Table 4, along with the associated error for the estimation. All values in this table were calculated using regression coefficients from Table 2 except ΔH_f^o for $HS_2O_5^{2-}$ and $HS_2O_7^{2-}$, which were estimated using a relationship between ΔG_f^o and ΔH_f^o discussed below.

As a measure of the self-consistency of the model-generated ΔG_f^o values, the pK_2 values for nine sulfur or sulfoxy acids were calculated with model-generated data and compared with literature-cited pK_2's. The

Table 5a Model-generated thermodynamic data for divalent aqueous sulfur species. Limits of error are calculated as the square root of the sum of squares of standard error associated with fundamental groups in Table 2 used to estimate values for each species.

SPECIES	O_3S^{IV}	O_3S^{VI}	O_2S^{III}	S_n^*	O	C	ΔH_f^o kJ·mol^{-1}	ΔG_f^o kJ·mol^{-1}
S^{2-}	0	0	0	1	0	1.600	33.3 ± 0.0	118.0 ± 56.6
S_2^{2-}	0	0	0	0.5	0	0.800	0.1 ± 0.0	86.5 ± 40.0
S_3^{2-}	0	0	0	0.333	0	0.533	-11.7 ± 0.0	75.4 ± 32.7
S_4^{2-}	0	0	0	0.25	0	0.400	-16.6 ± 0.0	70.8 ± 28.3
S_5^{2-}	0	0	0	0.2	0	0.320	-19.9 ± 0.0	67.6 ± 25.4
S_6^{2-}	0	0	0	0.167	0	0.267	-21.4 ± 0.0	66.2 ± 23.2
$S_2O_3^{2-}$	0	1	0	0.5	0	0.258	-659.8 ± 0.0	-543.2 ± 37.8
$S_3O_3^{2-}$	0	1	0	0.333	0	0.222	-951.4 ± 0.0	-827.2 ± 32.9
$S_4O_3^{2-}$	0	1	0	0.25	0	0.195	-1085.1 ± 0.0	-957.4 ± 30.0
$S_5O_3^{2-}$	0	1	0	0.2	0	0.174	-1159.7 ± 0.0	-1030.1 ± 28.0
$S_6O_3^{2-}$	0	1	0	0.167	0	0.157	-1205.2 ± 0.0	-1074.4 ± 26.6
$S_7O_3^{2-}$	0	1	0	0.143	0	0.143	-1236.4 ± 0.0	-1104.8 ± 25.5
$S_2O_6^{2-}$	1	1	0	0.5	0	0.154	-764.7 ± 0.0	-596.7 ± 37.7
$S_3O_6^{2-}$	1	1	0	0.333	0	0.140	-1083.4 ± 0.0	-907.1 ± 33.0
$S_4O_6^{2-}$	1	1	0	0.25	0	0.129	-1236.2 ± 0.0	-1056.0 ± 30.4
$S_5O_6^{2-}$	1	1	0	0.2	0	0.119	-1324.9 ± 0.0	-1142.3 ± 28.6
$S_6O_6^{2-}$	1	1	0	0.167	0	0.111	-1381.0 ± 0.0	-1197.0 ± 27.3
$S_7O_6^{2-}$	1	1	0	0.143	0	0.104	-1420.4 ± 0.0	-1235.4 ± 26.4
$S_2O_4^{2-}$	0	0	2	0.5	0	0.211	-753.4 ± 0.0	-600.2 ± 35.9
SO_3^{2-}	1	0	0	0	0	0.308	-637.6 ± 0.0	-485.4 ± 18.0
$S_2O_5^{2-}$	0	0	2	0	1	0.178	-982.3 ± 0.0	-781.4 ± 25.2
$S_2O_7^{2-}$	1	1	0	0	1	0.136	-1011.1 ± 0.0	-795.1 ± 28.0
$S_2O_8^{2-}$	0	2	0	0	2	0.121	-1344.6 ± 0.0	-1114.5 ± 36.0
SO_4^{2-}	0	1	0	0	1	0.242	-909.3 ± 0.0	-744.7 ± 28.2

Table 5b. Model-generated thermodynamic data for divalent aqueous sulfur species. Limits of error are calculated as the square root of the sum of squares of standard error associated with fundamental groups in Table 2 used to estimate values for each species.

SPECIES	O_3S^{IV}	O_3S^{VI}	O_2S^{III}	S_n^*	O	C	ΔH_f^o kJ·mol^{-1}	ΔG_f^o kJ·mol^{-1}
HS^-	0	0	0	1	0	0.217	-15.0 ± 0.0	12.1 ± 104.8
HS_2^-	0	0	0	0.5	0	0.141	-267.9 ± 0.0	11.5 ± 83.0
HS_3^-	0	0	0	0.333	0	0.104	-352.4 ± 0.0	20.5 ± 71.0
HS_4^-	0	0	0	0.25	0	0.083	-394.4 ± 0.0	27.7 ± 63.1
HS_5^-	0	0	0	0.2	0	0.068	-419.6 ± 0.0	33.0 ± 57.4
HS_6^-	0	0	0	0.167	0	0.058	-436.3 ± 0.0	37.1 ± 53.0
$HS_2O_3^-$	0	1	0	0.5	0	0.057	-634.4 ± 0.0	-554.0 ± 58.6
$HS_3O_3^-$	0	1	0	0.333	0	0.050	-718.9 ± 0.0	-471.4 ± 52.3
$HS_4O_3^-$	0	1	0	0.25	0	0.044	-760.9 ± 0.0	-477.4 ± 48.6
$HS_5O_3^-$	0	1	0	0.2	0	0.040	-786.1 ± 0.0	-480.2 ± 45.8
$HS_6O_3^-$	0	1	0	0.167	0	0.036	-802.8 ± 0.0	-481.4 ± 43.5
$HS_7O_3^-$	0	1	0	0.143	0	0.033	-815.0 ± 0.0	-482.0 ± 41.5
$HS_2O_6^-$	1	1	0	0.5	0	0.036	-739.8 ± 0.0	-1073.4 ± 50.7
$*HS_2O_4^-$	0	0	2	0.5	0	0.047	-720.5 ± 0.0	-614.5 ± 54.4
HSO_3^-	1	0	0	0	0	0.066	-626.2 ± 0.0	-527.6 ± 54.3
$*HS_2O_5^-$	0	0	2	0	1	0.041	-1218.8 ± 0.0	-998.5 ± 47.5
$HS_2O_7^-$	0	2	0	0	1	0.032	-1253.8 ± 0.0	-1372.6 ± 46.3
$HS_2O_8^-$	0	2	0	0	2	0.028	-1253.8 ± 0.0	-1510.3 ± 48.6
HSO_4^-	0	1	0	0	1	0.054	-887.3 ± 0.0	-755.8 ± 53.9

excellent agreement of this comparison is shown in Figure 5, indicating that the model is able to reproduce experimentally observed behavior of these species with good accuracy.

DISCUSSION

As shown in Figures 6a and 6b, the agreement between model-generated ΔG_f^o and ΔH_f^o values and literature data used to calibrate the model is remarkably good ($R^2 > 0.9999$). The generally large values of g_i and h_i for the divalent data set (Table 2) are indicative that each of the chosen parameters makes a significant contribution to calculated thermodynamic values of species used to calibrate the model. In contrast, the paucity of literature data for monovalent species, particularly for ΔH_f^o, resulted in regression coefficients that are unevenly weighted toward O_3S^{IV} and O_3S^{VI}. Some coefficients (e.g. h_i O_2S^{III}) were necessarily set at zero as no thermodynamic data that incorporated that group were available to calibrate the model. Additionally, some parameters (e.g. h_i C) were statistically determined to be zero (i.e. they did not contribute significantly to the regression). Thus, limits are placed on the ability of this model to predict thermodynamic values of species which require use of these parameters.

A comparison between ΔH_f^o and ΔG_f^o serves as a check of the systematic nature of the estimated thermodynamic properties. Figures 7a and 7b show graphs of $\Delta H_{f\,\text{Literature}}^o$ values *versus* model-generated ΔG_f^o for di- and monovalent species. Overlain on these plots are data for model-generated ΔH_f^o values. As can be seen clearly from the figures, the

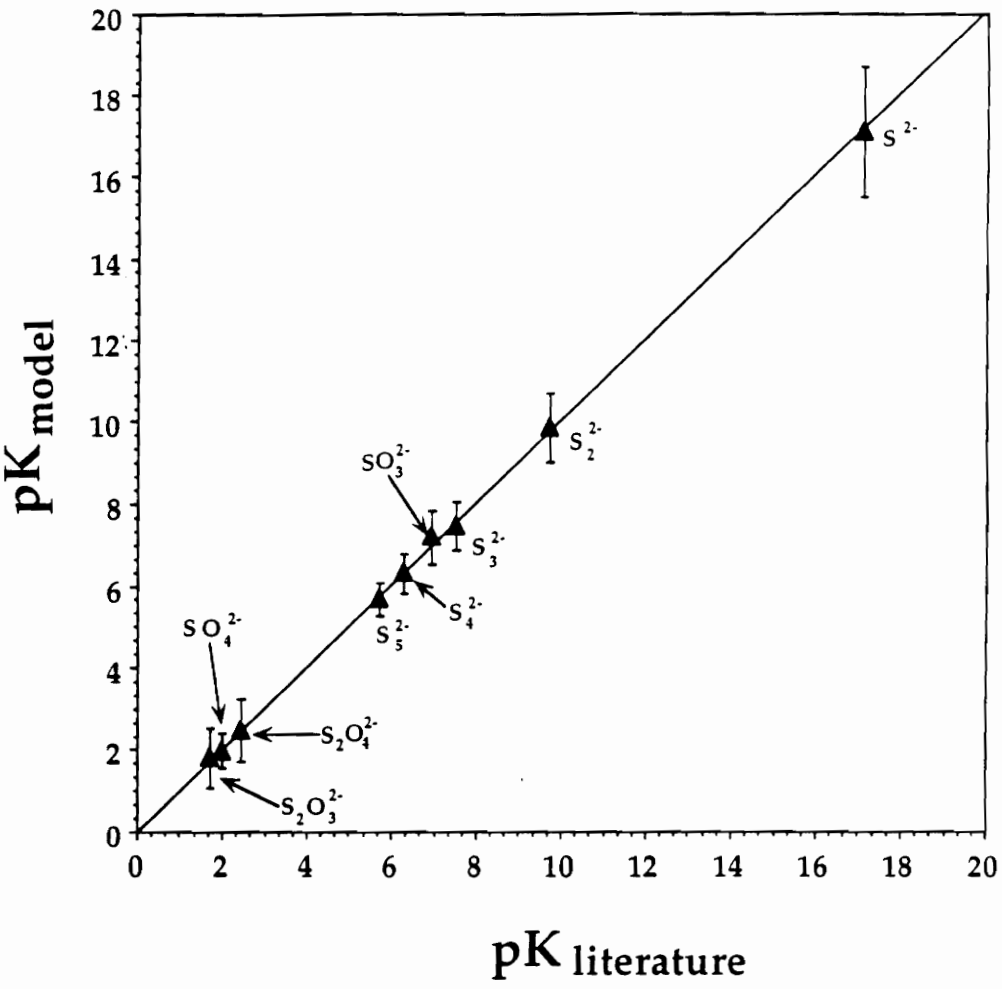

Figure 5. Acid dissociation constants, pK, calculated from model-generated free energy values for nine aqueous sulfur species, HS^-, HS_2^-, HS_3^-, HS_4^-, HS_5^-, HSO_3^-, $HS_2O_4^-$, HSO_4^- and $HS_2O_3^-$, are in excellent agreement with empirically determined values (R2 = 0.999).

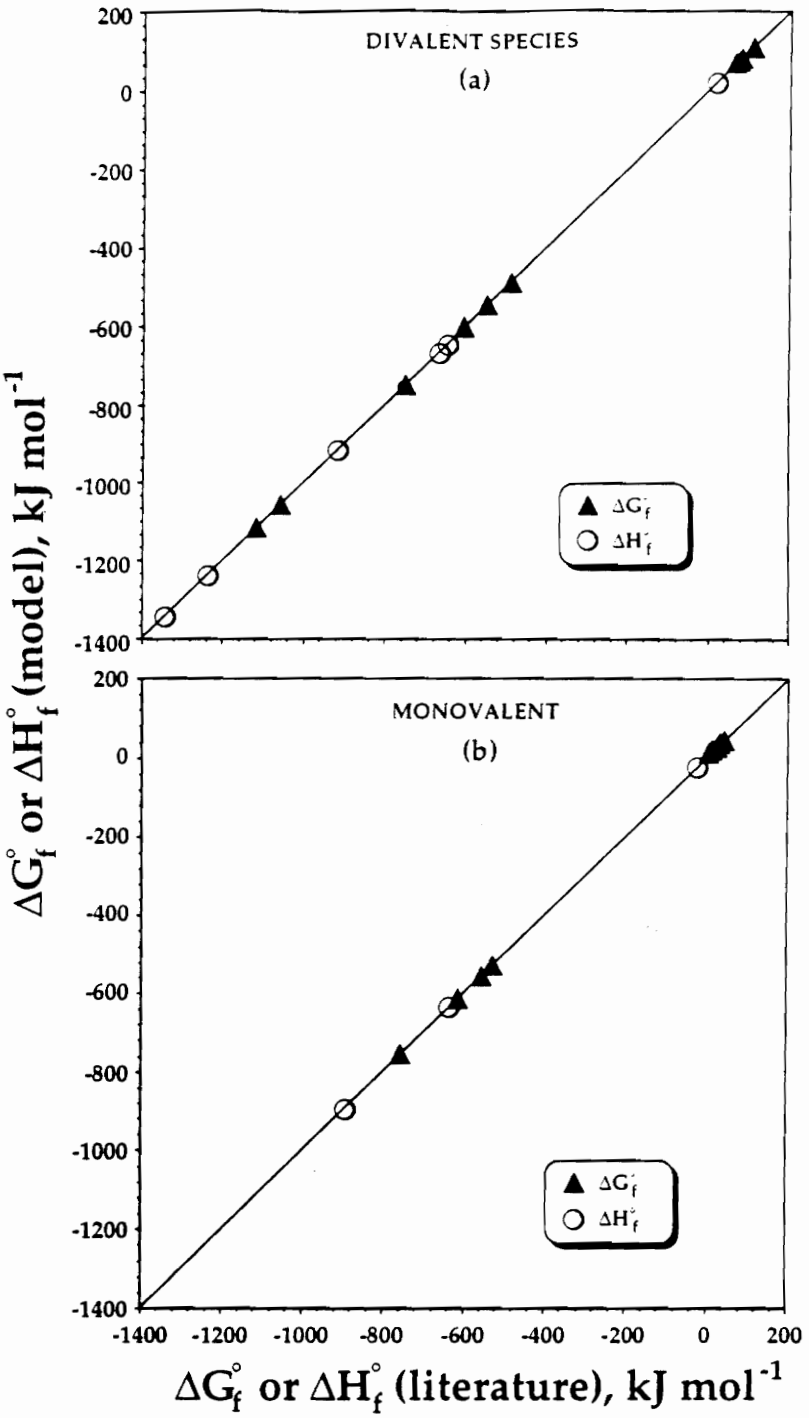

Figure 6. The excellent agreement between model-generated and literature free energy and enthalpy illustrates the firm correlation between thermodynamic properties and structure for aqueous sulfur species. Agreement extends over two orders of magnitude for both free energy and enthalpy for both divalent (6a, top) and monovalent (6b, bottom) species.

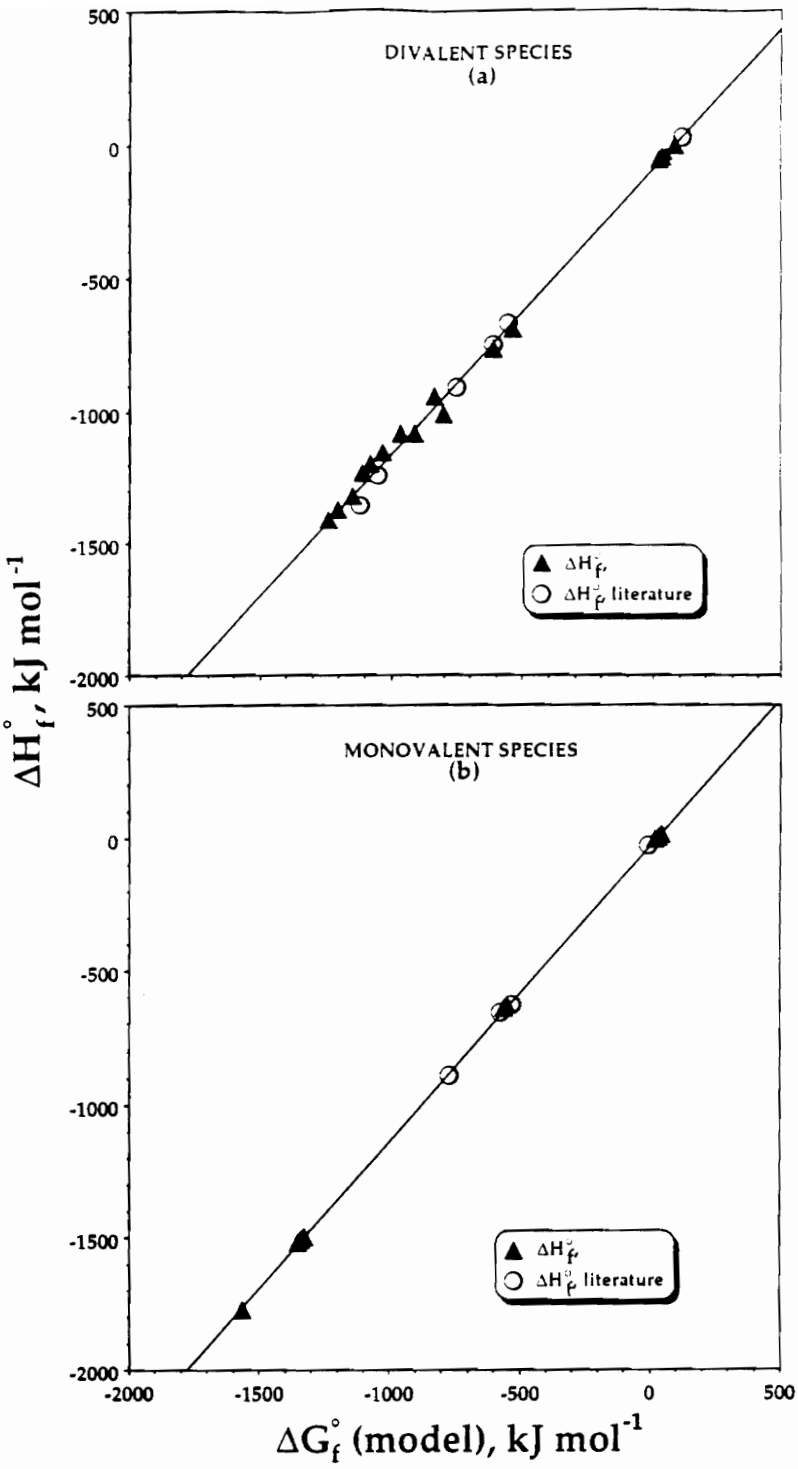

Figure 7. Because entropy is generally a small quantity at 298K, it has little influence on free energy, which is controlled primarily by enthalpy. Hence, a correlation between enthalpy and free energy is demonstrated in this figure (R2 = 0.999). This trend is more clearly pronounced for the divalent species (7a, top) than in the monovalent ones (7b, bottom).

regression model values are colinear with the trend established by empirical observation which is not surprising since ΔG_f^o will be least influenced by ΔS_f^o, a typically small quantity at 298K. R^2 values for linear regression of data in Figures 7a and 7b are both >0.999. The regression line shown in Figure 7b is described by

$$\Delta H_f^o = 1.13\ \Delta G_f^o - 26.09 \qquad (9)$$

This relationship can be used to estimate the ΔH_f^o of species which could not be directly estimated using h_i, (e.g. $HS_2O_5^{2-}$) utilizing model-generated ΔG_f^o values. Estimates of ΔH_f^o for these species are tabulated in Table 5b and are marked with an asterisk.

Comparison of the estimates from this study with estimates of others for divalent polysulfides is shown in Figure 8 and indicates that there is good agreement for ΔG_f^o, (except for S^{2-})but a significant discrepancy in terms of ΔH_f^o. The free energy data generated by the current model are essentially coincident with selected values from Murowchick (1984) and Wagman et al. (1982), for n = 2-5. The free energy value tabulated by these workers for S^{2-} is apparently based upon a pK_2 for H_2S that is lower than the currently accepted value of 17.1, thereby resulting in a ΔG_f^o value for S^{2-} that is too low (85.5 kJ mol^{-1}), thus inconsistent with the trend in the polysulfide series. The enthalpy values produced in the present study do not agree well with values cited by Brewer (1982) for n = 2-5, whose estimates are based on values reported by Maronny (1959) for S_2^{2-} and S_3^{2-}. For comparison, Figure 8 also shows enthalpy values that were estimated

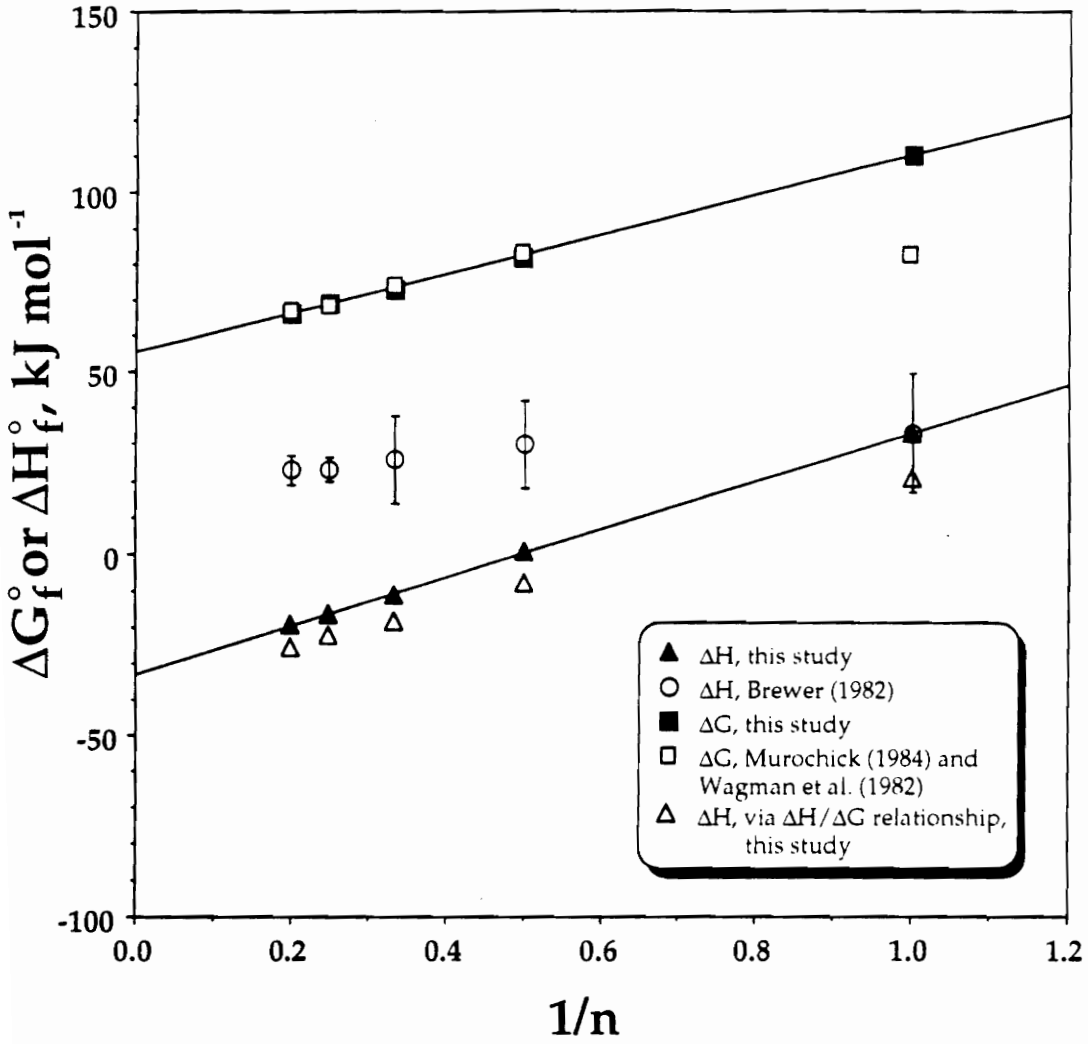

Figure 8. Model-generated free energy for divalent polysulfides, S_n^{2-}, are in good agreement with literature data for n = 2 thru 5. A noticeable difference exists for enthalpy, which suggests that values currently in the literature need revision. Error bars for data points from the present study ar eno larger than the size of the points plotted.

in the present study using the linear relationship between ΔH_f^o and ΔG_f^o, and are clearly seen to be consistent with enthalpy values generated directly from the regression model. Thus, it would appear that enthalpy values currently in use for polysulfide species are as much as 50 kJ mol^{-1} too positive

The strength of the additivity method used here is that it creates a database wherein the thermodynamic properties of the polysulfide species are consistent with other aqueous sulfur ions. The approach has been able to avoid many of the difficulties encountered during the experimental study of these particularly labile and reactive species. Maronny's (1959) work is based on the assumption that disulfide to pentasulfide ions are all simultaneously present in solution and that reactions among these species are potential determining, which is a dubious position (Schwartzenbach and Fisher, 1960; Schoonen and Barnes, 1988). Indeed, Schwartzenbach and Fisher (1960) fully discredit the cell measurements of Maronny (1959) which have to date been the basis for nearly all data for aqueous polysulfide species.

For the polysulfides and sulfane monosulfonic acids, second dissociation constants, pK_2, calculated with model-generated data are observed to decrease as a function of chain length and qualitatively follow the charge on terminal atoms as calculated by Meyer et al. (1977)(Fig. 9). Hence, we are encouraged that the choice of $1/n$ as a parameter to model these species is effective and that our values for polysulfides and sulfane monosulfonic acids are reasonable. The qualitative correlation between our model pK values and the charge distribution calculation by Meyer, et

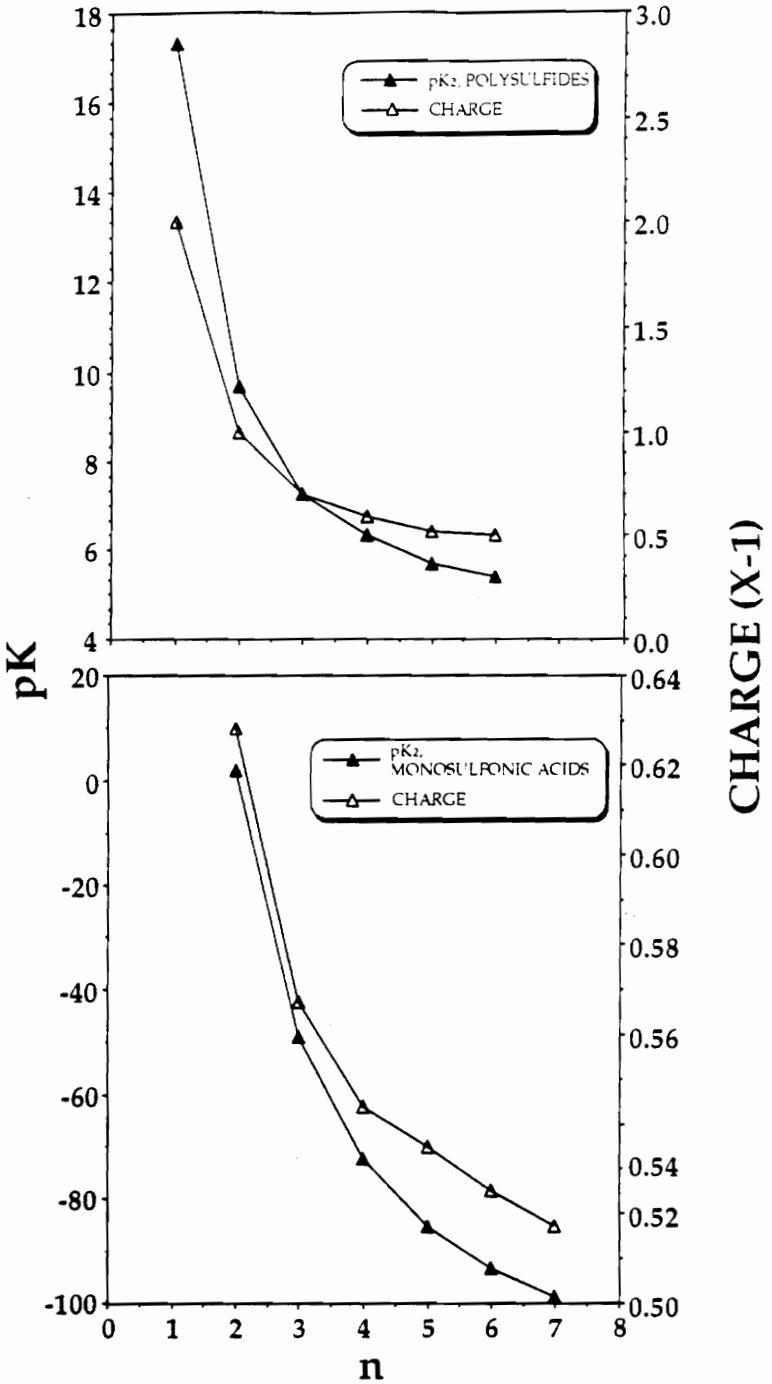

Figure 9. Acid dissociation constants, pK2 for polysulfides (10a, top)and sulfane monosulfonic acids (10b, bottom) qualitatively follw the charge on the terminal atoms of each species, as calculated by Meyer, et al. (1977), suggesting that the data produced in the present study is well correlated with the distribution of electrons in the molecules.

al. (1977) is an important observation and suggests that our model-generated free energy data may be used reliably to calculate equilibrium speciation of these species as a function of pH. For example, at neutral pH's the fully dissociated form of the polythiosulfates acids will predominate in solution. Only as the pH approaches 1.75 (i.e. in some acid mine drainage; Barton, 1978) will significant changes in speciation occur, and then only for thiosulfate, $S_2O_3^{2-}$, as it has the highest pK_2.

For polysulfides ($H_2S_xO_6$), however, our results were inconclusive, as calculation of pK_2 values for this series of acids produced unreasonable values. For example, using model-generated data, we initially calculated a pK_2 for disulfane disulfonic acid ($H_2S_4O_6$; $\Delta G_f^o[HS_4O_6^{2-}]$ = -1114.8 kJ mol^{-1}) of approximately +10. This result disagrees with data plotted in Figure 10, which clearly shows the expected pK_2 for a 0.25M $Na_2S_4O_6$ solution (unadjusted pH of approximately 3.5) to be less than zero: the acid should be fully dissociated.

We used a pK_2 value for $H_2S_4O_6$ estimated from Figure 10 (pK = 2.3) to calculate $\Delta G_f^o[HS_4O_6^{2-}]$ = -1042 kJ mol^{-1}, which is some 72.8 kJ more positive than the model estimate. We regressed this new estimate with the other thermodynamic data to evaluate its validity. Interestingly, when this value was added to the thermodynamic database, a resulting multiple linear regression maintained a high R^2 (> 0.999) and the residuals remained normally distributed. This suggests that the approximation for pK_2 of $H_2S_4O_6$ derived from Figure 10 is reasonable. We are hesitant, however, to take too much stock in this estimated pK value due to its approximate nature relative to other critically selected data. Further, the

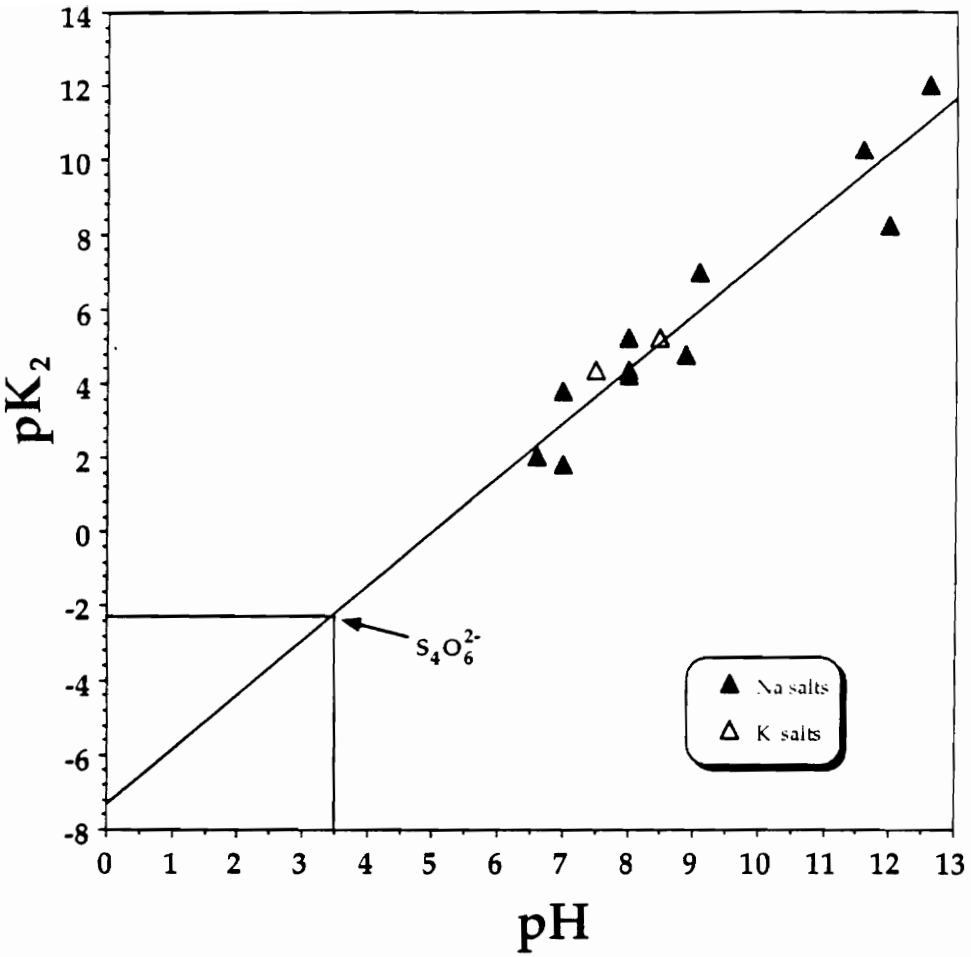

Figure 10. A relationship exists between the unadjusted pH of approximately 0.25M solutions of inorganic salts and the second acid dissociation constant for the anionic species. This figure shows a graph of pK2 values as a function of unadjusted pH for a series of solutions of inorganic sodium salts (solid points) and potassium salts (open points). The observed pH for a 0.25 M sodium tetrathionate solution, $S_4O_6^{2-}$ of about 3.5 suggests that the pK2 of this species is less than zero. Data for this figure are approximate were are taken from Budavari et al. (1989) and Weast et al. (1981).

low pK estimated in Fig. 10 indicates that protonated polythionates will not be found in the geochemical environment and hence should not be important species. The general lack of agreement between model-generated $\Delta G_f^o[HS_4O_6^{2-}]$ and that calculated using the pK_2 estimate for $HS_4O_6^{2-}$ from Figure 10 illustrates an important point. In order to obtain the most reliable model-estimates from any multiple linear regression model, it is desirable to have data from all branches of the system for calibration of the model. When all branches are not represented in the calibration, flexures can develop in the model that limit the ability to predict unknown values. Thus, although our model offers estimates for the thermodynamic properties of protonated polythionate species, which currently do not exist in the literature, their reliability can only improve through incorporation of at least one data point for the series during model calibration.

Despite the apparent utility of the method described here to estimate thermodynamic properties of aqueous sulfur species, caution should be exercised when extending the model beyond its intended limits. The good correlation between 1/n and the chemical properties of aqueous sulfur chains for n = 1 - 6 may be linear over the short interval described in this study, but may not extend beyond this range. This caveat can be demonstrated by considering aliphatic dicarboxylic acids, which can be used as analogies for polysulfides. Figure 11 shows a good linear relationship between pK values for a series of these acids (Sergeant and Dempsey, 1979) and 1/n for relatively short chain lengths, $n < 5$. However, for longer chains this linear relationship becomes less reliable. It is that polymeric

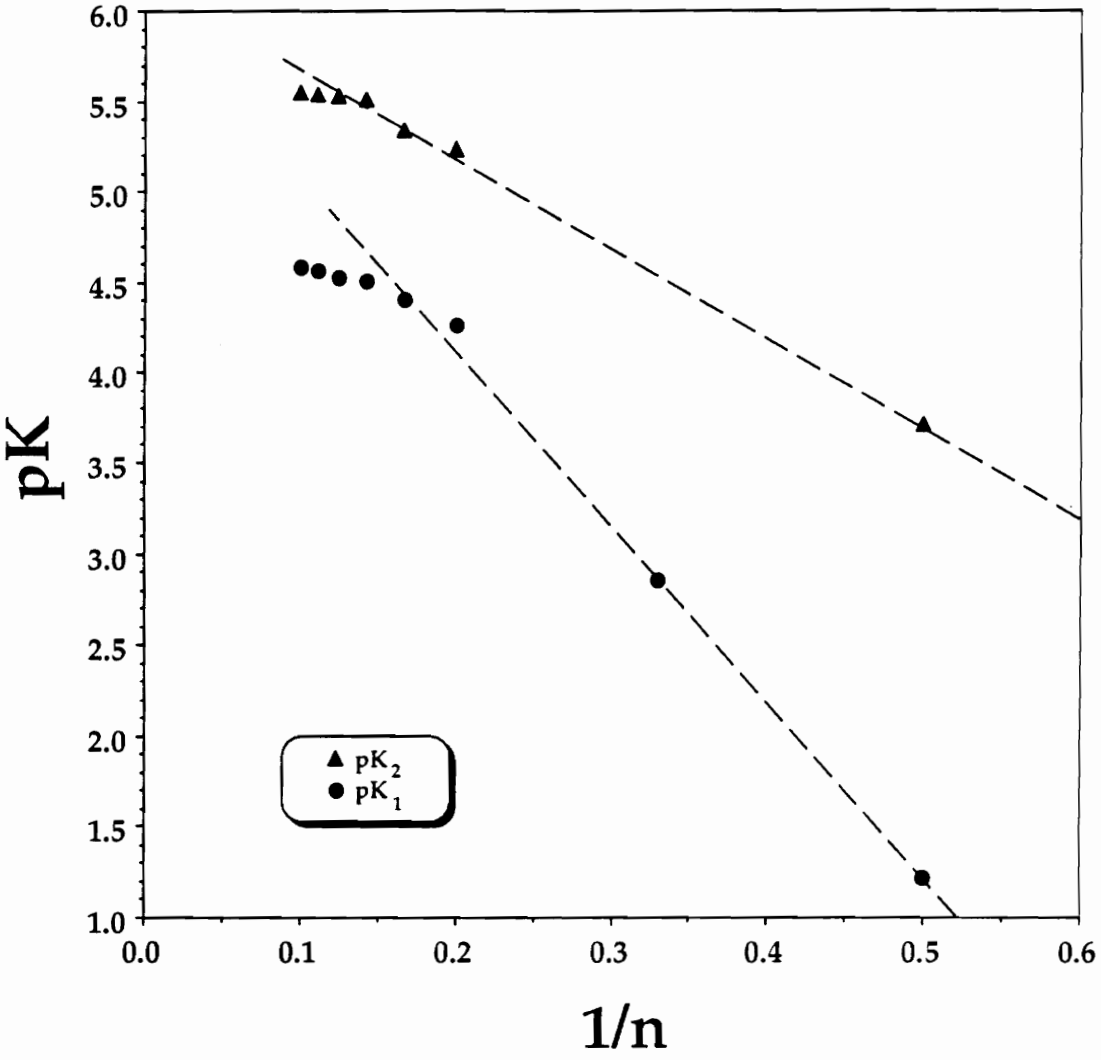

Figure 11. Though linear over a restricted range, pK values for aliphatic dicarboxylic acids (Sergent and Dempsey, 1979) tend to become non-linear with increasing chain length. This trend may also be true of aqueous polymeric sulfur species and, therefore, caution is warrented when calculating data with the present model beyond the optimal range of confidence of the model ($n > 6$).

sulfur systems will show similar behavior, as suggested by the calculations of Meyer et al. (1977; Fig. 2). Thus, estimates made using the 1/n model will be less reliable when extrapolated beyond n = 6 to estimate thermodynamic properties for particularly long chain species such as polythionates, $S_nO_6^{2-}$, where n>>6 (Steudel et al 1987).

Oxidation of Low Valence Sulfur

An immediate use for the estimates produced by this model is to consider the process of oxidation of low valence sulfur species to produce aqueous sulfate. Intermediate metastable oxidation states for sulfur in aqueous solutions are recognized as important species in sulfide mineral oxidation reactions (Goldhaber, 1983; Moses et al., 1987). Although they are not thermodynamically stable, thiosulfate, $S_2O_3^{2-}$, tetrathionate, $S_4O_6^{2-}$, trithionate, $S_3O_6^{2-}$ and sulfite, SO_3^{2-} have been identified during studies of inorganic pyrite oxidation (Goldhaber, 1983; Moses et al., 1987). It is possible that during the overall oxidation of sulfide to sulfate, sulfur must pass through one or more these key aqueous species.

Oxidation of sulfide to sulfate requires the transfer of eight electrons and it is unlikely that more than two are transferred in any one reaction step (Basolo and Pearson, 1967; Nordstrom, 1982). Hence, there must be several reaction intermediates for the overall process. Typical sulfide mineral oxidation reactions are far from equilibrium; free energies of reaction for the oxidation of common sulfide minerals by oxygen to produce sulfate, hydrogen ions, and release of cations to solution are on the order of 1400 kJ mol^{-1}. The overall reaction appears to be irreversible

because of this large free energy change. However, the occurrence of several metastable aqueous sulfur species that may be intermediates in the overall process suggests the possibility of smaller, reversible steps that individually account for much smaller changes in energy.

It is reasonable to expect that while unstable, fleeting transition states between metastable intermediates will be energetic high points, the overall sequence of aqueous sulfur intermediates must proceed down a free energy gradient to sulfate. To illustrate this point, it is instructive to consider the thermodynamic stability of intermediate species, relative to the end product of sulfide mineral oxidation, sulfate. In Figure 12, we modify Figure 1 to show, in a third dimension, ΔG_r^o for each species with O_2 to form SO_4^{2-} and H^+, as calculated using model-generated data. This figure illustrates a series of free energy stairsteps down which the overall oxidation reaction might be expected to descend. As $S_2O_3^{2-}$, $S_3O_6^{2-}$, $S_4O_6^{2-}$ and SO_3^{2-}, the prominent species in solution during a pyrite oxidation experiment, skirt energetic high points in this figure, a mechanistic hypothesis couched in terms of these reservoirs is thermodynamically feasible.

Metastable Aqueous Sulfur Speciation

With the growing recognition of metastable aqueous sulfur species in natural environments, as well as during laboratory-based pyrite oxidation experiments, questions about conditions which favor the predominance of certain species will arise. Because of the overwhelming thermodynamic stability of sulfide and sulfate sulfur relative to

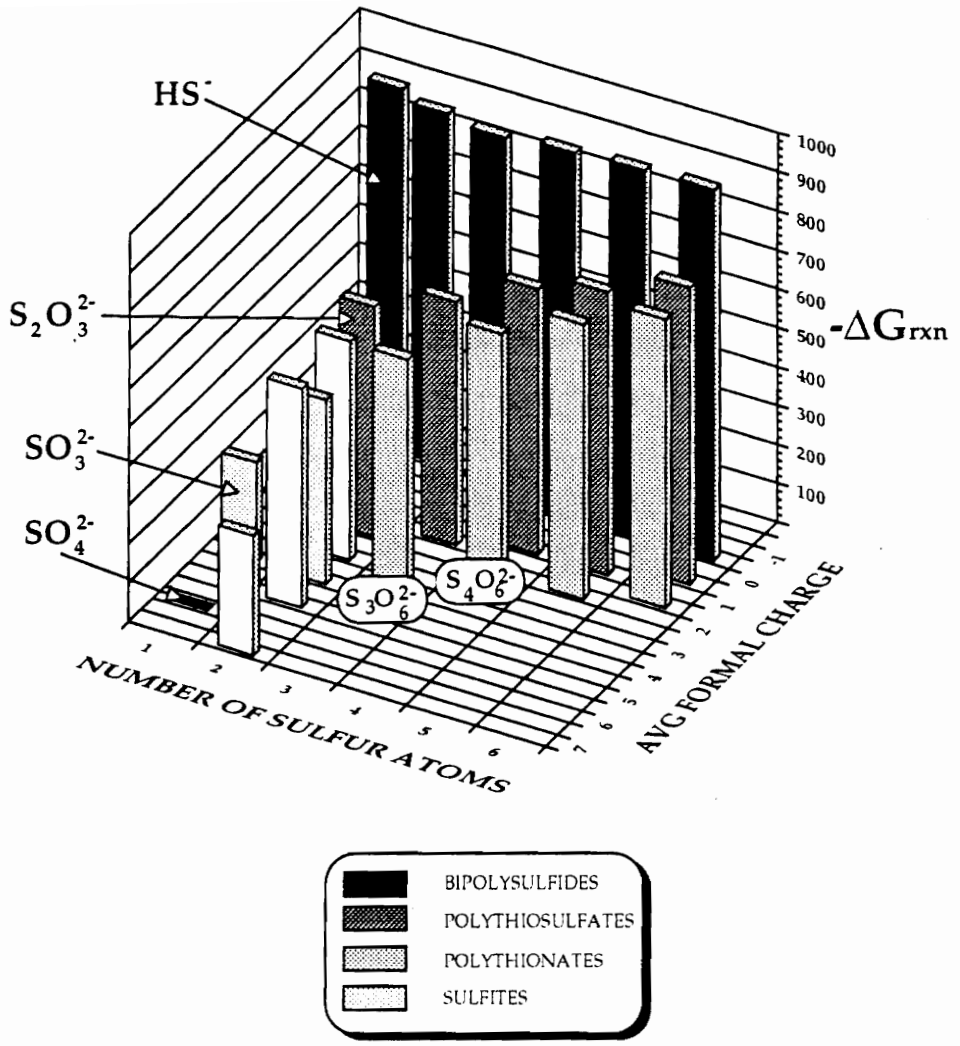

Figure 12. Modification of Figure 1 shows, in a third dimension, ΔG^{o}_{rxn} for $\left(\frac{1}{x}\right)S_xO_y^{2-} + \left(1-\frac{1}{x}\right)H_2O + \left(\frac{3x - y + 1}{2x}\right)O_2 = SO_4^{2-} + \left(2 - \frac{2}{x}\right)H^+$ thereby illustrating the overall free energy decline expected to drive the oxidation of sulfide sulfur to sulfate.

intermediate forms, stability field diagrams in the literature typically do not bother to show the stability fields for such species as polysulfides, thiosulfate or sulfite. Using model-generated free energy data, we have constructed an Eh-pH diagram, using the program SOLUPLOT (Bethke, 1978), that considers all intermediate species, except elemental sulfur, whose average sulfur oxidation state is lower than sulfate. The results of our efforts are shown in Figure 13, which clearly shows that stability fields with significant area exist for thiosulfate, its conjugate acid, and tetrathionate ($S_4O_6^{2-}$). For environments in which reduced forms of sulfur are exposed to more oxidizing conditions, it is doubtful if any redox equilibria will be obtained and kinetic factors will necessarily need to be considered when modeling such systems. However, several intermediates are expected to have significant contributions to the bulk composition of the system, therefore requiring that modeling efforts speciate these anions as a means of accurately describing aqueous chemical evolution.

The Structure of $S_2O_5^{2-}$ Debate

The correlation presented in this report links the thermodynamic properties of ionic sulfur species with their structure, thus allowing the estimation of properties for species for which no data currently exist. Conversely, however, given accurate thermodynamic data it is reasonable to expect that the most likely structure for a species may be predicted. Further, in instances where specific structural details are in question, our method may be used to great advantage to reconcile differences. For example, consider the pyrosulfite ion, $S_2O_5^{2-}$, also known as disulfite.

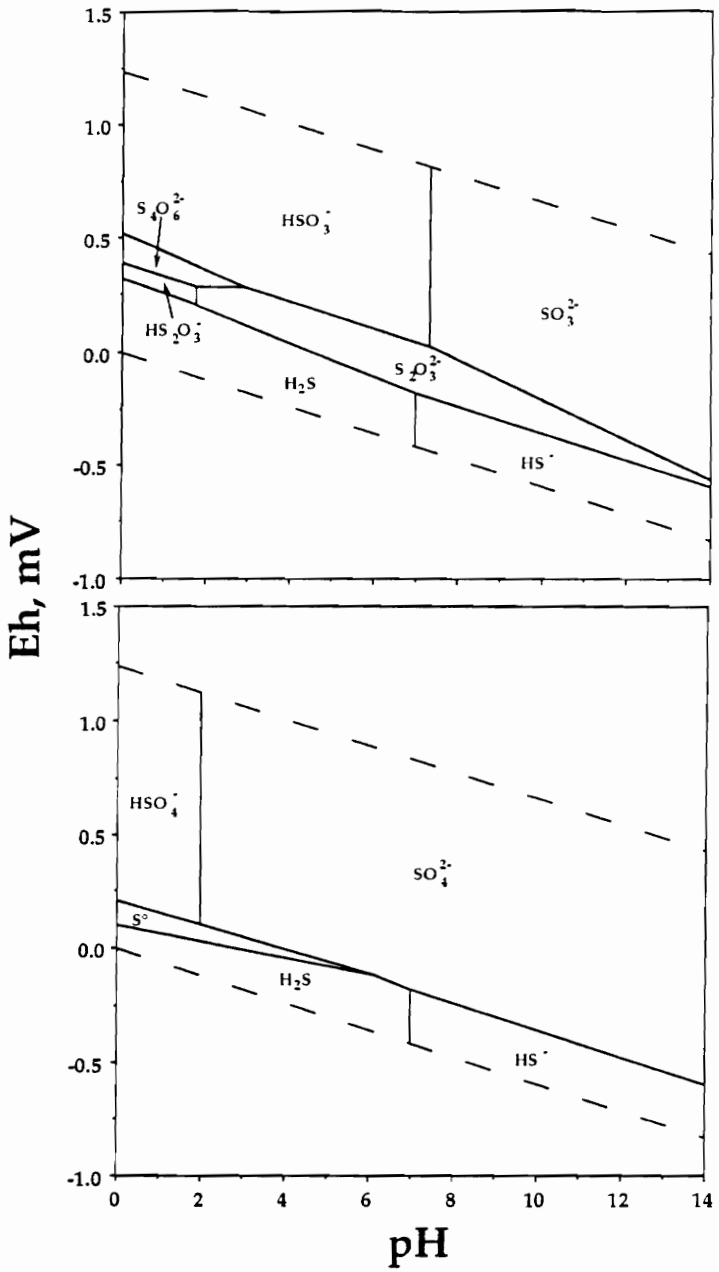

Figure 13. Using model-derived thermodynamic data as input to the program SOLUPLOT, an Eh-pH diagram of aqueous sulfur species with average formal charge on sulfur less than sulfate (+6), other than elemental sulfur shows that stability fields with significant area exist for thiosulfate, its conjugate acid, and tetrathionate (14a, top). For comparison, Figure 14b (lower) shows for comparison a diagram with elemental sulfur and sulfate species.

The specific structure of this anion was first addressed by Zachariasen (1932) and was later confirmed by Lindquist and Mörtsell (1957). In his discussion of the structure of the potassium salt, Zachariasen (1932) emphasized the inconsistency between his determined S-S bonds with the formula given by chemists of the day incorporating an S-O-S linkage. Raman studies by Simon and Kriegsman (1953) of aqueous solutions of $S_2O_5^{2-}$ offered evidence supporting a symmetrical O_2S-O-SO_2 structure for the aquated species. This result was contested by Herlinger and Long (1969), who suggested that their Raman band assignments argued for an asymmetrical O_2S-SO_3 arrangement. Most recently, however, work by Connick et al. (1982) examined the intensity of Raman bands as a function of concentration for $S_2O_5^{2-}$ solutions. Their work suggests that band assignments by Herlinger and Long (1969) may have been in error and leaves the matter unresolved. Although the solid salts of $S_2O_5^{2-}$ apparently contain an S-S bond, does the molecule rearrange in aqueous solution to produce an S-O-S linkage?

Thermodynamic data for $S_2O_5^{2-}$ is far from abundant in the literature, with most compilations (Wagman et al., 1982; Barner and Scheuerman, 1978; Woods and Garrels, 1990) relying on estimations for this species by Latimer (1952) of ΔH_f° = -971 kJ mol^{-1} and ΔG_f° = -791 kJ mol^{-1}. Connick et al. (1982) studied the equilbrium between bisulfite, HSO_3^- and its dimer $S_2O_5^{2-}$

$$2HSO_3^- = S_2O_5^{2-} + H_2O \qquad (10)$$

as a function of ionic strength, from which a value for the equilibrium constant at infinite dilution may be obtained (K = 0.31). Using this accurately obtained equilibrium constant, a ΔG_f^o value for water of 237.19 kJ mol^{-1}, and our model-generated value for HSO_3^{-1} of 527.7 kJ mol^{-1}, we calculate ΔG_f^o $S_2O_5^{2-}$ to be -821.1 kJ mol^{-1}. This value differs from the value predicted by our model, which did not use a value for $S_2O_5^{2-}$ for calibration, by about 40 kJ mol^{-1}. If the value derived from the measurements of Connick et al. (1982) is included with the set of calibration data, an unacceptable statistical fit is obtained with R^2=0.94 compared to 0.9999 when this datum is not used. Because it did not stand up to our critical selection criteria, Connick et al.'s (1982) data for $S_2O_5^{2-}$ could be used to calibrate the model. The estimation by Latimer (1952) for this species appears quite reasonable as it agrees within 10kJ mol^{-1} of the value predicted by our model, but could not be included in our critically selected dataset because it was estimated, albeit rather well.

Figure 14 plots the average literature value of ΔG_f^o of sulfoxy anions (Latimer, 1952; Wagman et al., 1982; Barner and Scheuerman, 1978; Cobble et al., 1972) against model-generated free energy of the same. In addition, we plot the average of Latimer's (1952) and Barner and Scheuerman's (1978) estimate for pyrosulfite ($S_2O_5^{2-}$) with our model calculations using two distinct structures. Calculating ΔG_f^o using an S-S bond to link one O_2S^{III} group with one O_3S^{VI} group (the crystal structure) results in a value of -1139 kJ mol^{-1}, which is plotted in Figure 14. A model using one O_2S^{III} group and one O_3S^{IV} group yields -48.8 kJ mol^{-1}, which is clearly unacceptable, and is not plotted on the figure. Lastly, and most

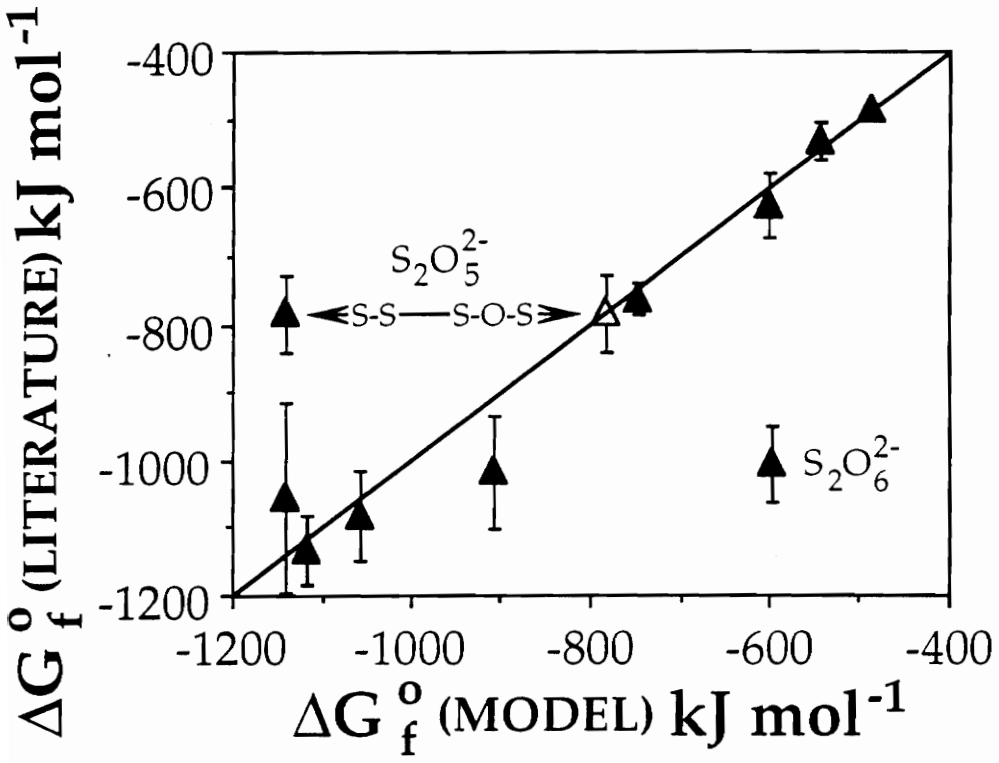

Figure 14. The agreement between average free energy values reported in the literature and model-derived data is good for a large number of species. However, the inconsistancy for $S_2O_5^{2-}$ may be reconciled by considering aqueous species to have a structure that incorporates a S-O-S linkage rather than the S-S bond observed in the crystalline material to calculate free energy. In this figure, the calculated for $S_2O_5^{2-}$ using an S-S bond is shown as a solid triangle, and the value calculated using an S-O-S linkage is shown as an open triangle. Error bars are the standard deviation in the reported values for free energy.

interesting, calculating ΔG_f^o using one bridging oxygen to link two O_2S^{III} groups produces a value of -780.8 kJ mol^{-1}. This value is consistent with the trend shown in Figure 14 and, thus, it would appear that a structure for $S_2O_5^{2-}$ that incorporates a peroxy linkage may be more suitable for the aquated disulfite ion than that determined by crystal structure refinement.

Unlike the case of $S_2O_5^{2-}$, the rather large difference between our model-predicted free energy and the value given by the literature for $S_2O_6^{2-}$ cannot be conclusively accounted for by any structural configuration. Current understanding of the structure of this anion indicates that it is two SO_3 groups, in this study considered $O^{IV}S$ and $O^{VI}S$. Unfortunately, the only ΔG_f^o value that is available in the literature for this species is based upon an estimation by Latimer (1952) in which he used the contemporary enthalpy value from NBS tables combined with his own estimation of S°. The original enthalpy measurement for $S_2O_6^{2-}$ is not cited in any reference source and remains something of an enigma. Thus, we are unable to comment on the quality of literature free energies for this species. It is possible, given the remarkable agreement among most other aqueous sulfur species, that the currently held ΔG_f^o datum for $S_2O_6^{2-}$ requires revision. The examples provided by $S_2O_5^{2-}$ and $S_2O_6^{2-}$ serve to highlight the ability of the present model to identify questionable thermodynamic data in the literature for the S-O-H system.

CONCLUSIONS

The additivity method described in this paper is a useful tool for geochemists who can use it to identify inconsistencies in available

established datasets and to estimate ΔG_f^o and ΔH_f^o values for substances that have not yet been determined. With respect to the S-O-H system, a complete, internally consistent data set has not been produced, even though intermediate, metastable oxidation states are increasingly recognized as important in a number of geologically important environments. In this paper, we show that a first-order additivity model can provide a useful, self-consistent set of thermodynamic data for complex aqueous ions. The generally large values of g_i and h_i , the coefficients resulting from multiple linear regressions, for both divalent and monovalent data sets are indicative that each of the chosen parameters makes a significant contribution to thermodynamic values of species used to calibrate the model.

Using model-derived thermodynamic data, we have illustrated the thermodynamic stability of intermediate species, relative to the end product of sulfide mineral oxidation, sulfate. In doing so, we have illustrated a series of free energy stairsteps down which the overall oxidation reaction might be expected to descend. We have shown that since $S_2O_3^{2-}$, $S_3O_6^{2-}$, $S_4O_6^{2-}$ and SO_3^{2-}, the prominent species in solution during a pyrite oxidation experiment, skirt energetic high points, any mechanistic hypothesis couched in terms of these reservoirs is thermodynamically feasible.

Although the primary purpose of this report is move toward a more unified, systematic set of thermodynamic data for the S-O-H system, the correlation between these properties and structure has been shown to have other applications. Specifically, given accurate thermodynamic data, it is

possible to offer a probable structure for a species if reasonably accurate thermodynamic data for that species exists.

REFERENCES

Barner H. E. and Scheuerman R. V. (1978) *Handbook of Thermochemical Data for Compounds and Aqueous Species*. John Wiley and Sons, New York.

Barton, P. (1978). The acid mine drainage. In *Sulfur in the Environment* (J.O. Nriagu, ed.) pp. 314-358, John Wiley & Sons, NY.

Basolo F. and Pearson R. G. (1967) *Mechanisms of Inorganic Reactions: A Study of Metal Complexes in Solution*. John Wiley and Sons, New York.

Bethke C.M. (1978) Program SOLUPLOT, Pennsylvania State University Computing Center, University Park, Pennsylvania.

Boulegue J. and Michard G. (1978) Constantes de formation des ions polysulfurés S_6^{2-}, S_5^{2-} et S_4^{2-} en phase aqueuse. *Jour. Fr. Hydrologie* **9**, 27-34.

Brewer L. (1982) Thermodynamic values for desulfurization processes. In *Flue Gas Desulfurization* (J.L. Hudson & G.T. Rochelle, eds.) ACS Symp. Series 188, pp. 1-39, Washington, D.C.,

Chermak J. and Rimstidt J. D. (1989) Estimating the thermodynamic properties (ΔG and ΔH) of silicate minerals at 298K form the sum of polyhedral contribution. *Amer. Miner.* **74**, 1023-1031.

Christidis P. C., Rentzeperis P. J., Kirfel A. and Will G. (1985) Experimental charge density in polythionate anions. I. X-ray study of electron density distribution in potassium trithionate, $K_2S_3O_6$. *Z. Kristall.* **173**, 59-74.

Cobble J. W., Stephens H. P., McKinnon I. R. and Westrum E. F., Jr. (1972) Thermodynamics of oxygenated sulfur complex ions. Heat capacity from 5 to 300 K for $K_2S_4O_6$ and from 273 to 373 K for $S_4O_6^{2-}$. Revised thermodynamic functions for HSO_3^-, SO_3^{2-}, $S_2O_3^{2-}$ and

$S_4O_6^{2-}$ at 298 K. Revised potential of the thiosulfate-tetrathionate electrode. *Inorg. Chem.* **11**, 1669-1674.

Connick R. E., Tam T. M. and vonDenster E. (1982) Equilibrium constant for the dimerization of bisulfite ion to form pyrosulfite. *Inorg. Chem.* **21**, 103-107.

Cotten F. A. and Wilkinson, G. W. (1972) *Advanced Inorganic Chemistry.* Interscience Publishers, New York.

Cox J.D., Wagman D.D. and Medvedev V.A. (1989) *CODATA Key Values for Thermodynamics*, Hemisphere Publishing Corp., New York.

Goldhaber M. B. (1983) Experimental study of metastable sulfur oxyanion formation during pyrite oxidation at pH 6-9 and 30°C. *Amer. J. Sci.* **283**, 193-217.

Graedel T. E. and Goldberg K. I. (1983) Kinetic studies of raindrop chemistry 1. Inorganic and organic processes. *J. Geophys. Res.* **88**, 10865-10882.

Herlinger A. W. and Long T. U. II (1969) An investigation of the structure of the disulfite ion in aqueous solution using Raman and infared spectroscopies. *Inorg. Chem.* **8**, 2661.

Huheey J. E. (1983) *Inorganic Chemistry.* Harper & Row, New York.

Huss A., Jr. and Eckert C. A. (1977) Equilibria and ion activities in aqueous sulfur dioxide solutions. *J. Phys. Chem.* **81**, 2268-2270.

Janz G. J. (1958) *Estimation of Thermodynamic Properties of Organic Compounds.* Academic Press, Inc., New York.

Jellenik K. (1911) Uber das elecktrolytische potential von hydrosulfitreaktionen. *Z. Elektrochem.* **17**, 157-176.

Jorgensen B. B. (1990) A thiosulfate shunt in the sulfur cycle of marine sediments. *Science* **249**, 152-154.

Langmuir D. (1979) Techniques of estimating thermodynamic properties for some aqueous complexes of geochemical interest. In *Chemical Modeling in Aqueous Systems* (E.A. Jenne, ed.), ACS Symposium Series v. 93, pp. 353-387, American Chemical Society,

Latimer W. M. (1952) *The Oxidation States of the Elements and Their Potentials in Aqueous Solutions*. Prentice-Hall, Englewood Cliffs, N.J.

Latimer W. M., Pitzer, K. S. and Slansky, C.M. (1939). The free energy of hydration of gaseous ions, and the absolute potential of the normal calomel electrode. *J. Chem. Phys.* **7**: 108 - 111.

Leffler J. E. and Grunwald E. (1963) *Rates and Equilibria of Organic Reactions, As Treated by Statistical, Thermodynamic and Extrathermodynamic Methods*. Wiley and Sons, New York.

Lindquist I. and Mörtsell M. (1957) The structure of potassium pyrosulfate and the nature of the pyrosulfate ion. *Acta Cryst.* **10**, 406-409.

Maronny G. (1959) Constantes de dissociation de l'hydrogen sulfure. *Electrochim. Acta* **1**, 58-69.

McMillan W. G., Jr., Roberts J. D. and Coryell C. D. (1942) The thermodynamic constants of dithionite (hydrosulfite) ion. *J. Am. Chem. Soc.* **64**, 398-399.

Mel H. C., Hugus Z. Z. and Latimer W. M. (1956) Thermodynamics of thiosulfate ion. *J. Amer. Chem. Soc.* **78**, 1822-1826.

Meyer B., Peter L. and Spitzer K. (1977) Trends in the charge distribution of sulfanes, sulfanesulfonic acids, sulfanedisulfonic acids and sulfurous acid. *Inorg. Chem.* **16**, 27-33.

Millero F. J. (1983) The estimation of the pK^*_{HA} of acids in seawater using the Pitzer equations. *Geochim. Cosmochim. Acta* **47**, 2121-2129.

Moses C. O., Nordstrom D.K., Herman J.S. and Mills A.L. (1987) Aqueous pyrite oxidation by dissolved oxygen and by ferric iron. *Geochim. Cosmochim. Acta* **51**, 1561-1571.

Murowchick J. B. (1984) The formation and growth of pyrite, marcasite, and cubic FeS. Ph.D. Dissertation, The Pennsylvania State University.

Nordstrom D. K. (1982) Aqueous pyrite oxidation and the consequent formation of secondary iron minerals. In *Acid Sulfate Weathering*. (L. R. Hossaer, J. A. Kittrick and D. F. Faming, eds.) pp. 37-56, Soil Science Society of America, Madison Wis.

Nordstrom D. K. and Munoz J. L. (1985) *Geochemical Thermodynamics*. The Benjamin/Cummings Publishing Co., Menlo Park, CA.

Olafsson I. V., Spitzer J. J. and Hepler L. G. (1978) Apparent molar heat capacities and volumes of aqueous electrolytes at 25 C: Na_2SO_4, K_2SO_4, $Na_2S_2O_3$, $Na_2S_2O_8$, $K_2S_2O_8$, K_2CrO_4, Na_2MoO_4, and Na_2WO_4. *Can. Jour. Chem.* **56**, 1871-1873.

Page F. M. (1953) The dissociation constant of thiosulfuric acid. *J. Chem. Soc.* 1719-1724.

Parks G. S. and Huffman H. M. (1932) *The Free Energies of Some Organic Compounds*. Chemical Catalogue Co., New York.

Pickering T. L. and Tobolsky A. V. (1972) Inorganic and organic polysulfides. In *Sulfur in Organic and Inorganic Chemistry* (A. Senning, ed.), v. 3, 19-38, Marcel-Dekker.

Pitzer K. S. (1940) The vibrational frequencies and thermodynamic functions of long chain hydrocarbons. *J. Chem. Phys.* **8**, 711-722.

Schoonen M. A. A. and Barnes H. L. (1988) An approximation of the second dissociation constant for H_2S. *Geochim. Cosmochim. Acta* **52**, 649-654.

Schwartzenbach G. and Fischer A. (1960) Die Aciditat der Sulfane and die Zusammensetzung wasseriger Polysulfidlosungen. *Helvetica Chim. Acta* **43**, 1365-1390.

Sergeant E.P. and Dempsey B. (1979) *Ionisation Constants of Organic Acids in Aqueous Solutions*. Pergamon Press, Oxford.

Simon A. and Kriegsmann H. (1953) Zu den ionengliechgewichten in den wessrigen losungen der sauren sulfite. *Chem. Ber.* **89**, 2442-2446.

Smith R. M. and Martell A. E. (1976) *Critical Stability Constants*. Plenum Press, New York.

Spirakis C.S. (1991) The possible role of tiosulfate in the precipitation of ^{34}S-rich barite in some Mississippi Valley-type deposits. *Mineral. Depos.* **26**, 60-65.

Sterns K. H. (1969) The effect of cations on the thermal decomposition of salts with oxyanions. *J. Chem. Ed.* **46**, 645-649.

Steudel R., Holdt G., Gobel T. and Hazeu W. (1987) Chromatographic separation fo higher polythionates SnO6 2- (n =3...22) and their detection in cultures of Thiobacillus ferrooxidans; molecular composition of bacterial sulfur secretions. *Angew. Chem. Int. Ed. Engl.* **26**, 151-153.

Stoffreggen R. (1986) Observations on the behavior of gold during supergene oxidation at Summitville, Colorado, USA, and implications for electrum stability in the weathering environment. *Appl. Geochem.* **1**, 549-558.

Takano B. (1987) Correlation of volcanic activity with sulfur oxyanion speciation in a crater lake. *Science* **235**, 1545-1712.

Takano B. and Watanuki K. (1990) Monitoring of volcanic eruptions at Yugama crater lake by aqueous sulfur oxyanions. *J. Volcanol. Geotherm. Res.* **40**, 71-87.

Taylor J. R. (1982) *An Inroduction to Error Analysis*. University Science Books, Mill Valley, California.

Taylor J. R., Wagman D. D., Williams M. G., Pitzer K. S. and Rossini F. D. (1946) Heats, equilibrium constants, and free energies of formation of the alkylbenzenes. *J. Res. NBS* **37**, 95-108.

Wagman D.D., Evans W.H., Parker V.B., Schumm R.H., Halow I., Bailey S.M., Churney K.L. and Nuttall R.L. (1982) *The NBS Tables of Chemical Thermodynamic Properties* J. Phys. Chem. Reference Data, volume 11.

Woods T. L. and Garrels R. M. (1987). *Thermodynamic Values at Low Temperature for Natural Inorganic Materials: An Uncritical Summary*, Oxford Univ. Press, New York.

Zachariasen W. H. (1932) The crystal lattice of potassium pyrosulfite, $K_2S_2O_5$, and the structure of the pyrosulfite group. *Phys. Rev.* **40**, 113.

Chapter 3: The Rate of Decomposition of the Ferric-thiosulfate Complex in Acidic Aqueous Solutions

ABSTRACT

The rate of decomposition of the ferric thiosulfate complex was determined by following the change in optical absorbance due to the complex as a function of time. The rate of decomposition of the complex varies as the square of the concentration of the complex. Regression of log rate vs. log $m_{FeS_2O_3^+}$ at 20°C produced the rate law

$$\frac{dm_{FeS_2O_3^+}}{dt} = -10^{2.0(\pm0.3)} m_{FeS_2O_3^+}^{2.0(\pm0.1)}$$

The decomposition of this complex in acid solutions is strongly dependent on temperature, E_a = 120(±15) kJ mol^{-1}. The rate of reaction increases with increasing ionic strength, which is consistent with the interaction of two positively charged ions to form the activated complex. This study resolves many of the inconsistencies found in earlier studies and shows that reaction with H^+ is a more important sink for $S_2O_3^{2-}$ than reaction with Fe^{3+} when pH > ~1.7.

INTRODUCTION

Thiosulfate occurs in a variety of geochemically interesting environments including the porewaters of marine and lacustrine sediments (Jorgensen, 1990; Anderson-Thode and Jorgenson, 1989; Nriagu et al., 1979), surficial geothermal waters (Veldeman et al., 1991; Webster,

1987), hot brines (Boulègue, 1978) and solutions produced during weathering of an auriferous sulfide deposit (Benedetti and Boulègue, 1991; Webster and Mann, 1984; Webster, 1986). It may be an important species in the supergene enrichment of gold (Benedetti and Boulègue, 1991; Webster and Mann, 1984; Stoffreggen, 1986) and the formation of uranium roll-front (Granger and Warren, 1969; Granger and Warren, 1974) and Mississippi Valley-type Pb-Zn sulfide deposits (Spirakis, 1991). This species is present during laboratory studies of the aqueous oxidation of pyrite (Goldhaber, 1983; Moses et al., 1987) and is present in effluents from sulfide mill tailings (Makua and Hitchon, 1978; Wolkoff and Larose, 1975).

Despite its importance as a geochemical species, an understanding of the reactivity of thiosulfate under naturally occurring conditions is far from complete. Thiosulfate forms stable aqueous complexes with many important economic metals (e.g. Ag and Au). Recently, silver thiosulfate complex activities have been shown to be similar to silver chloride complex activities in surficial geothermal waters in New Zealand (Webster, 1987). In acidic solutions, thiosulfate decomposes, forming predominantly sulfite and a colloidal sulfur compound known as a Raffo sol (Burns et al., 1981, Steudel et al., 1988). Ferric iron reacts with thiosulfate to form a highly colored solution of a labile ferric thiosulfate complex that fades as ferrous iron and tetrathionate ($S_4O_6^{2-}$) are produced (Tykodi, 1990).

$$2Fe^{3+} + 2S_2O_3^{2-} = 2FeS_2O_3^{+} \rightarrow 2Fe^{2+} + S_4O_6^{2-} \qquad (1)$$

Interest in the ferric-thiosulfate complex first arose in the chemical community owing to its utility as an analytical tool and it has received attention since the mid-nineteenth century (see references in Page, 1960). The stoichiometry of the complex has been conclusively established as $FeS_2O_3^+$ by three independent studies, using Job's method of continuous variation (Das and Patnaik, 1956, Das et al, 1956, Halder and Banerjee, 1948). The molar absorptivity, ε, of this complex has been determined at 589 nm (Page, 1953), 500 and 600 nm (Mahapatra et al., 1957). Values for the instability constant of the complex are reported in the literature for a variety of temperatures (Mahapatra et al., 1957, Page, 1954, Schmidt, 1930).

Several workers studied the kinetics of the decomposition of the ferric thiosulfate complex, beginning in the first quarter of this century, but these studies produced inconsistent results. Several different reaction orders have been proposed with correspondingly different reaction mechanisms. Only Page (1960) reports a complete rate law, although this work was performed in solutions of unspecified pH at 6°C. Patnaik et al. (1956) and Page (1960) postulate reaction mechanisms which involve intermediates that were not shown conclusively to exist.

This paper reports the rate of decomposition of the highly colored ferric-thiosulfate complex in acidic solutions. We studied the rate of reaction as a function of ferric iron, thiosulfate and ferric thiosulfate complex concentrations, temperature and ionic strength to produce a more complete description of the reaction than previously available. The present study resolves many of the apparently contradictory results from previous studies. These results are useful in evaluating the relative

importance of the ferric thiosulfate reaction as a sink for thiosulfate in acidic solutions compared to the acid-catalyzed decomposition, thus enabling more complete understanding of thiosulfate reactivity in geological environments.

METHODS

Because of the transient nature of the ferric thiosulfate complex, we constructed a stopped-flow spectrophotometer to study the kinetics of its decomposition. Figure 1 shows our experimental design. Thermostatted ferric chloride and sodium thiosulfate solutions were accurately blended by using peristaltic pumps and a Y-tube equipped with an in-line mixer. The mixed solutions immediately passed into a flow-thru cell housed in a spectrometer. Output voltages from the photodetector of the spectrometer, which was zeroed using distilled-deionized water, were recorded on a strip chart recorder. Measurement of pH was made using an in-line pH electrode that was located at the exit of the spectrophotometer flow-thru cell. The temperature of effluent fluids was monitored just after the in-line pH electrode.

Reaction solutions were prepared from analytical grade $Na_2S_2O_3 \cdot H_2O$ and $FeCl_3 \cdot 6H_2O$ and varied in concentration between 4×10^{-4} and 1.2×10^{-1} molal. For one set of solutions, constant ionic strength was maintained with addition of KCl. Variable amounts of KCl were added to another set of solutions that was used to study the rate of reaction as a function of ionic strength. Reagent grade hydrochloric acid was added to the ferric iron solutions during preparation to limit the hydrolysis of ferric

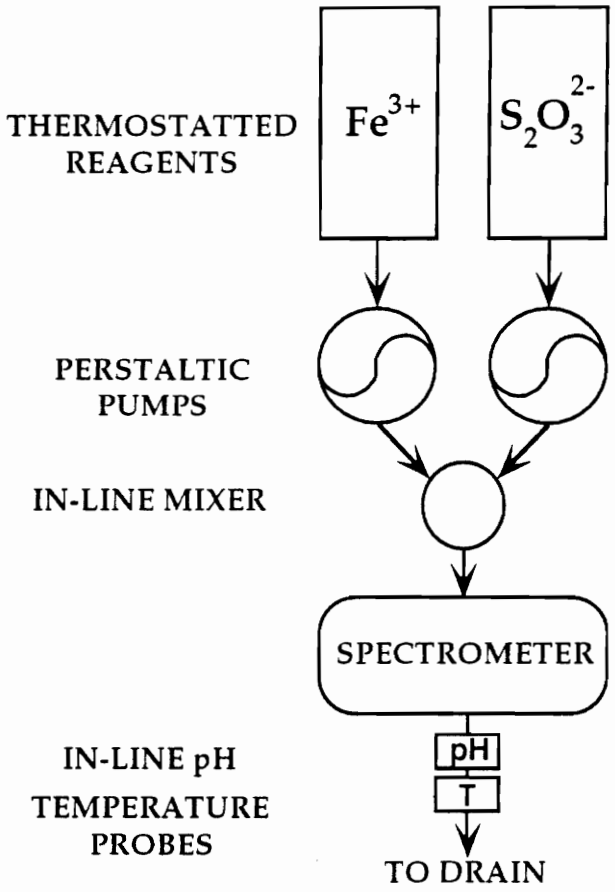

Figure 1. Schematic diagram of the stopped-flow apparatus used in the present study.

iron and to produce the low pH conditions (2.65 to 3.09) desired for this study. For one pair of ferric iron and thiosulfate concentrations, we systematically varied the temperature of reactant solutions to find the activation energy of the reaction.

An absorbance spectrum of the aqueous complex was determined by continuously pumping mixed solutions through the spectrometer flow-thru cell while measurements of the absorbance of the complex as a function of wavelength were recorded. Solutions of ferric or ferrous iron, thiosulfate or bithiosulfate did not absorb in this range of wavelengths. Hence the absorbance maximum for the ferric thiosulfate complex we observed at 490 nm was chosen as the analytical wavelength allowing us to work with the lowest complex concentrations possible.

We have refined the value of the instability constant and extinction coefficient reported by Mahapatra et al. (1957) using statistical regression techniques to improve upon their graphical approximations. Regression of the data in Mahapatra et al. (1957) yields values of 523 and 7.94×10^{-3} for ε_{500} and K_D, respectively. The value of K_A is therefore $K_A = K_D^{-1} = 126$.

With the refined value for ε_{500} and the absorbance spectrum of the complex, we calculated the value of ε_{490}. According to Beer's law

$$A = \varepsilon \beta c \tag{2}$$

$$c = \frac{A}{\varepsilon \beta} \tag{3}$$

where A is absorbance, β is the optical path length and c is the concentration of the absorbing species, in this case the ferric thiosulfate complex. For any two wavelengths (e.g. 490 and 500 nm), using the same solution concentration and optical path length

$$\frac{A_{500}}{\varepsilon_{500}} = \frac{A_{490}}{\varepsilon_{490}} \tag{4}$$

Rearranging and using our measurements for A_{500} (0.061) and A_{490} (0.1375) and the refined value of ε_{490}

$$\begin{aligned} \varepsilon_{490} &= \varepsilon_{500}\left(\frac{A_{490}}{A_{500}}\right) \\ &= 1178.9 \text{ L mol}^{-1}\text{cm}^{-1} \end{aligned} \tag{5}$$

The rate of the decomposition of the complex was determined by determining the change in absorbance as a function of time. Mixed solutions were pumped through the spectrometer until steady-state absorbance was achieved. Then the flow was stopped and the system was operated as a batch reactor. The change in absorbance with time was monitored by the trace of the chart recorder and was used to determine the rate of decomposition of the complex. Because our experimental design allowed us to accurately determine the rate of decomposition of the complex immediately after peristaltic pumps were shut off, we used the method of initial rates for kinetic analysis.

Multiple linear regression was used to determine the effect of solution composition on reaction rate. The concentration of the $FeS_2O_3^+$ complex at time, t = 0, was determined using the refined value of ε_{490}.

Fe^{3+} and $S_2O_3^{2-}$ concentrations were determined using measured pH values to speciate mixed reaction solutions to account for all ferric iron hydrolysis and protonated and fully dissociated forms of thiosulfate using equilibrium constants from Baes and Mesmer (1976) and Williamson and Rimstidt (1992). We have used the concentration of $FeS_2O_3^+$ determined by absorbance because data for the ionic strength and temperature dependance of K_A are not available, but ε_{490} is independent of these variables.

RESULTS

Table 1 lists the results of the constant ionic strength experiments. Values reported for the concentration of the complex were calculated from absorbance measurements, and ferric iron and thiosulfate are based on solution speciation calculations. Figure 2 shows the good agreement between concentrations determined for the complex from absorbance measurements and equilibrium speciation calculations. Table 2 shows the rate dependance on temperature and ionic strength.

DISCUSSION

Early studies (Holluta and Martini, 1924a, Holluta and Martini, 1924b, Holluta and Martini, 1925) produced somewhat erratic results owing to the transient nature of the colored complex and the relatively slow wet chemical methods of analysis used to follow the reaction progress. Later studies followed the reaction spectrophotometrically. Patnaik et al. (1956) and Das et al. (1956) observed an S-shaped absorbance

Table 1. Summary of experimental results at 20°C. Rate is expressed as $mol \cdot s^{-1}$. Reported complex concentrations were determined by absorbtion of the complex at 490 nm.

pH	log $m_{FeS_2O_3^+}$	log Rate
2.89	-3.57	-4.96
3.03	-3.47	-4.75
3.08	-3.39	-4.63
3.09	-3.29	-4.51
2.84	-3.68	-4.95
2.92	-3.48	-4.70
2.96	-3.29	-4.52
3.02	-3.19	-4.42
2.65	-4.22	-6.36
2.69	-3.95	-5.77
2.74	-3.73	-5.26
2.78	-3.54	-4.89
2.85	-3.42	-4.75
2.90	-3.29	-4.58
2.81	-3.52	-4.79
2.82	-3.30	-4.51
2.83	-4.14	-6.18
2.74	-3.95	-5.84
2.69	-4.22	-6.43
2.65	-3.19	-4.41

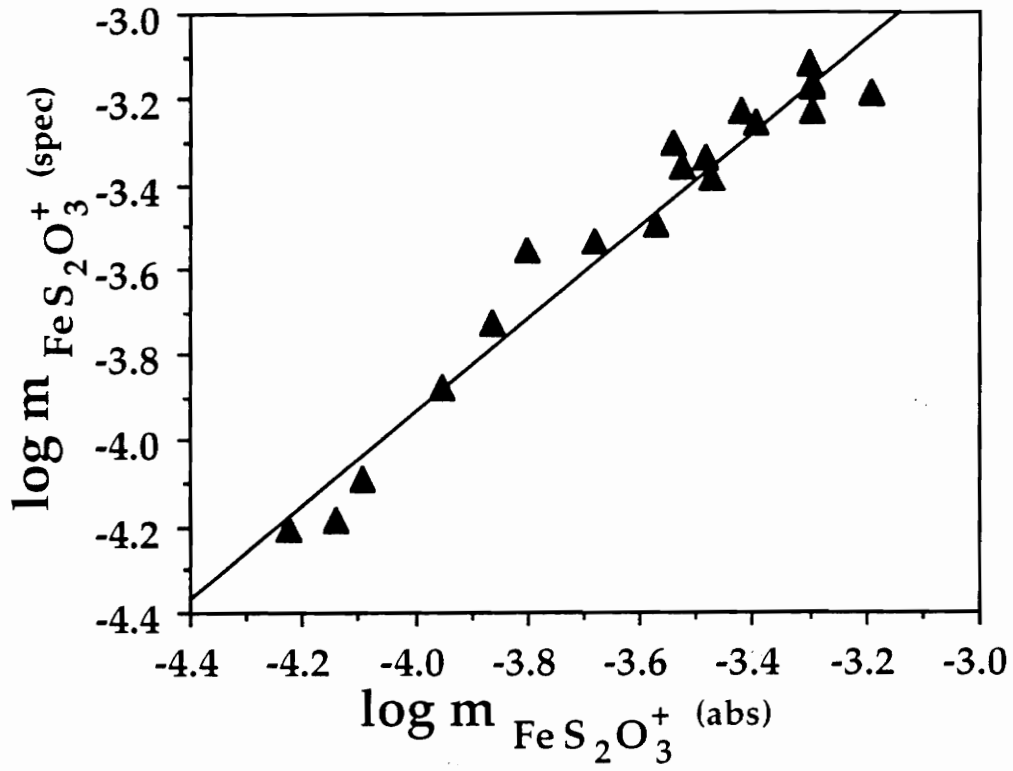

Figure 2. A graph of the concentration of the ferric thiosulfate complex at time t = 0 as determined by absorbance at 490 nm, log $m_{FeS_2O_3^+}$(abs), and speciation calcualtions, log $m_{FeS_2O_3^+}$(spec). Although concentrations determined by absorbance are more reliable, the consistency shown in this figure suggests that speciated Fe^{3+} and $S_2O_3^{2-}$ concentrations could have also been reasonable uses in formulating rate laws.

Table 2. Summary of experimental study of complex decomposition as a function of temperature and ionic strength.

Temperature °C	ln k (I=0.350)	$I^{0.5}$	ln k (27°C)
11.9	2.67	0.314	5.66
16.9	4.19	0.346	5.72
22.0	4.65	0.362	5.77
24.6	5.83	0.390	5.79
28.2	5.93	0.403	5.86
31.0	6.26		
33.7	6.35		

decay curve for the colored complex while Haldar and Banarjee (1948) and Page (1953) did not. The S-shaped curve suggested to some workers (Patnaik and Mahapatra, 1956) that the reaction was autocatalytic and led them to formulate very complex mechanisms that invoked the participation of intermediates for which no evidence could be produced. Page (1960) reports the only complete rate law found in the literature, although his work was conducted at 6°C in solutions of unspecified pH and ionic strength. Like Patnaik and Mahapatra. (1956), Page (1960) postulates a reaction mechanism which involves intermediates which have not been shown to exist.

The Rate and Mechanism of Reaction

The results of this investigation indicate that the rate of decomposition of the ferric thiosulfate complex in acidic solutions (pH~3) varies as the square of the concentration of the complex. Regression of log rate vs. log $m_{FeS_2O_3^+}$ for our experimental data (Table 1; Fig. 3) produced the rate law

$$\frac{dm_{FeS_2O_3^+}}{dt} = -10^{2.0(\pm 0.3)} m_{Fe\text{-}S_2O_3^+}^{2.0(\pm 0.1)} \qquad (6)$$

where the units on the rate constant are kg· $mol^{-1} \cdot s^{-1}$. The rate dependance on the square of the concentration of the complex suggests that the stoichiometry of the activated complex involves two ferric thiosulfate complex ions. This stoichiometry is consistent with a simple bimolecular reaction between two molecules of the colored complex,

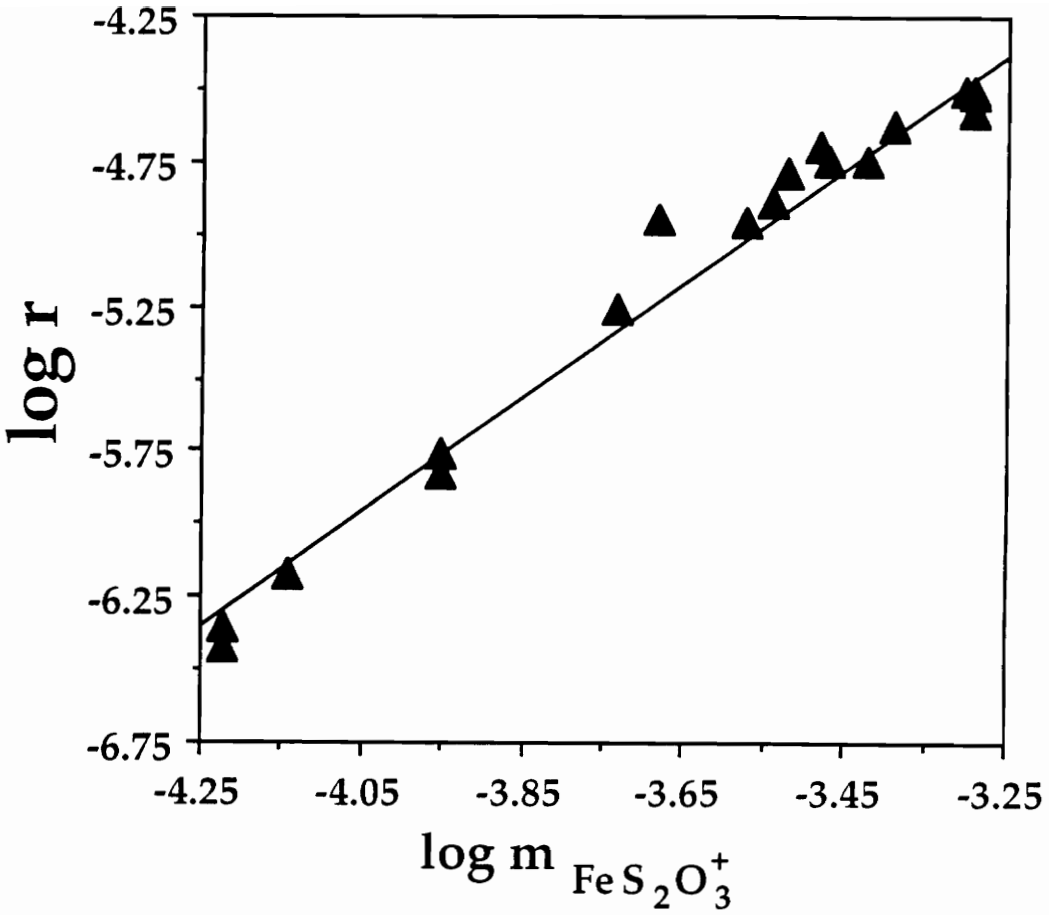

Figure 3. A graph of the log of the rate of decomposition of the $FeS_2O_3^+$ complex *versus* log of the concentration of the complex. $R^2 = 0.98$ for 20 points. The slope of the best fit line is ~2 (1.96 ±0.1, 1σ) indicating that the reaction is second order with respect to the complex concentration.

which leads directly to the formation of reaction products. Schmidt (1930) has shown that the complex forms virtually instantaneously and remains in equilibrium with ferric iron and thiosulfate throughout the course of the reaction until all reactants are consumed. Thus, the overall reaction may be represented as

$$Fe^{3+} + S_2O_3^{2-} \overset{fast}{=} [FeS_2O_3]^+ \tag{7}$$

$$\therefore \quad [FeS_2O_3]^+ + [FeS_2O_3]^+ \overset{slow}{=} [\,[FeS_2O_3]\cdots[FeS_2O_3]\,]^{2+} \tag{8}$$

$$[\,[FeS_2O_3]\cdots[FeS_2O_3]\,]^{2+} \rightarrow 2Fe^{2+} + S_4O_6^{2-} \tag{9}$$

In these equations, the terms fast and slow are relative only.

The decomposition of the ferric thiosulfate complex in acid solutions is strongly dependent on temperature. Figure 4 is an Arrhenius plot for this reaction. A regression of our data (Fig. 4) gives the relationship

$$\ln k = -\left(\frac{14500(\pm 1800)}{T}\right) + 53.9(\pm 6.2) \tag{10}$$

The activation energy calculated from the slope of this line is 120(±15) kJ·mol^{-1}. This activation energy is large compared to ~20 kJ mol^{-1} that would be expected for a diffusion-controlled reaction. In terms of a bimolecular reaction between two positively charged complex ions, shown in the rate law and eqn. (8), we expect the collision of two-like charged ions to be energetically expensive, thus the reaction has a higher E_a than would be expected for a purely diffusional process.

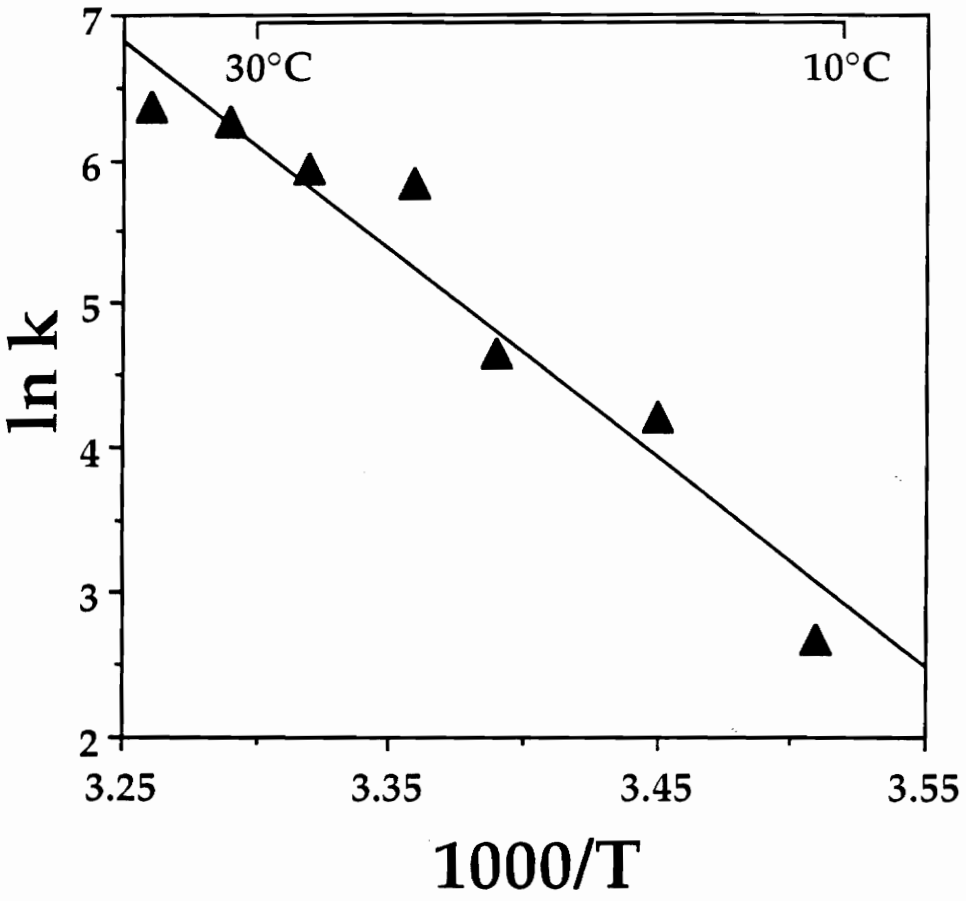

Figure 4. An Arrhenius plot for the decomposition of the $FeS_2O_3^+$ complex. The slope of the best fit line was used to calculate E_a = 120 kJ mol^{-1}, which is significantly higher than activation energies associated with diffusion-controlled reaction (~20 kJ mol^{-1}). No error bars are shown on this graph as they are approximately the size of the points plotted.

Our studies show that the rate of this reaction increases with increasing ionic strength, which is consistent with the interaction of two similarly charged ions to form the activated complex. For the simplest case,

$$\log k = 2Z_A Z_B \alpha \sqrt{I} + \log k_o \qquad (11)$$

where Z_A and Z_B are the charges on the reacting ions, I is ionic strength and α is a constant (= 0.5 at 25°C, Moore and Pearson, 1981). Appendix I provides a derivation of this relationship, which is of the form y = mx + b, and shows that a plot of log k *versus* $I^{0.5}$ should be linear with a positive slope when ions of like charge react and negative for interaction of oppositely charged ions. Further, the magnitude of the slope, under conditions of ideal behavior, equals to $2\alpha Z_A Z_B$. The slope of the best fit line shown in Fig. 5 is positive, indicating that two similarly charged species react to form the activated complex. This observation is consistent with the rate law of eqn. (6): a bimolecular reaction occurs between two 1+ charged ferric thiosulfate complex ions. The slope of the line in Fig. 5 is +0.9(±0.1), in agreement with the value predicted by theory of 1.0. The ionic strength used for this study was chosen to represent geologically meaningful conditions and exceeds 0.01m, hence the quantitative application of the relationship between the rate constant and ionic strength may be limited (Pethybridge and Prue, 1972). Many geologically relevant solutions have ionic strengths exceeding limits of Debye-Hückel (D-H) theory, and the slope of a plot of ln k *versus* $I^{0.5}$ deviates from the

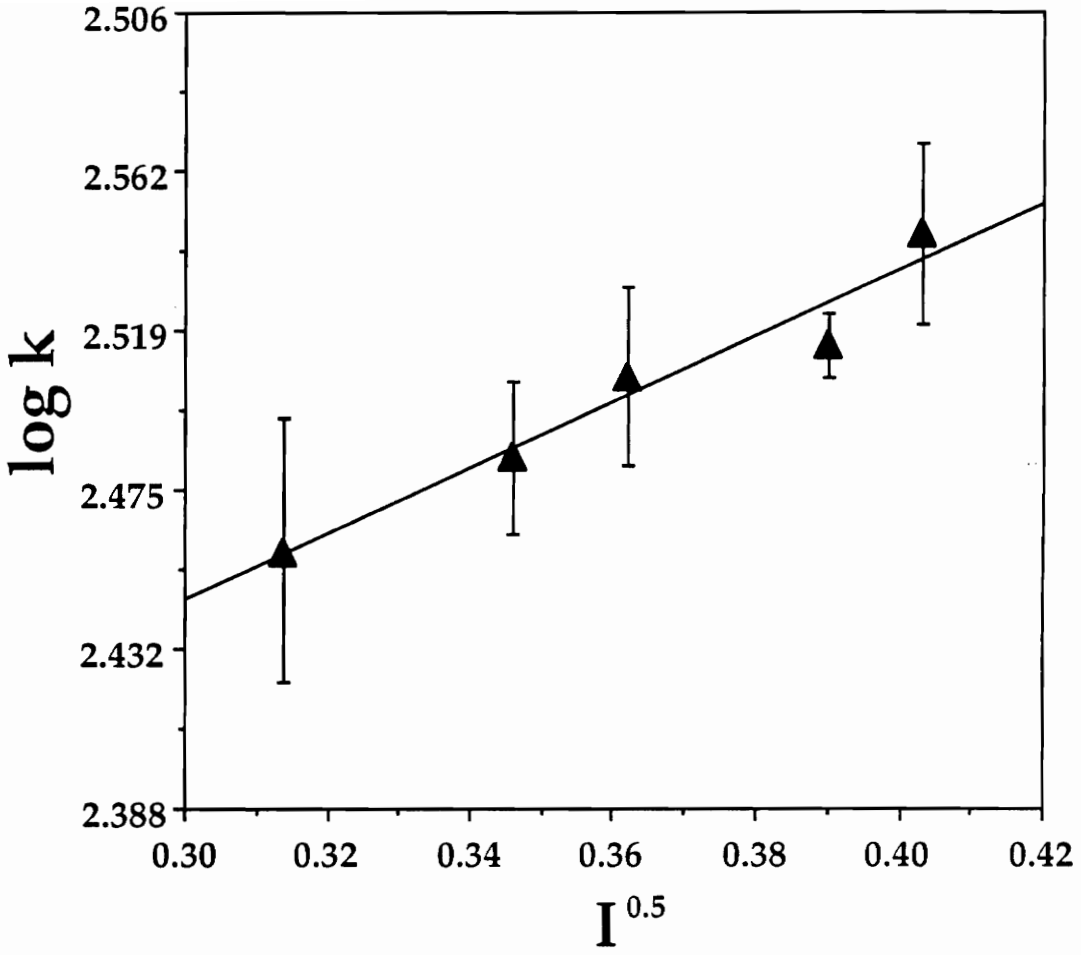

Figure 5. The decomposition of the $FeS_2O_3^+$ complex shows a positive salt effect, indicating that two species of similar charge are reacting to form the activated complex.

theoretical slope and will generally be of only qualitative value (Moore and Pearson, 1981). Even so, such a plot yields important information. Here, distinctly positive slope observed in this study indicates that two species of similar charge combine to form the activated complex.

Based on the results of our experiments, we propose that the ferric thiosulfate decomposition proceeds as illustrated in Fig. 6. The ferric thiosulfate complex remains in equilibrium with any unreacted ferric iron and thiosulfate. Two ferric thiosulfate complexes participate in a bimolecular, rate-limiting reaction that forms the activated complex with a 2+ charge. Sulfur in the activated complex condenses, eliminating two ferrous iron ions, to form tetrathionate. Unlike mechanisms proposed by earlier workers which generally involve a series of bimolecular reactions that invoke the participation of species for which no evidence exists, the present reaction mechanism is consistent with the principle of least nuclear motion (Hine, 1977). This principle dictates that elementary reactions which involve the least change in atomic position and electronic configuration will be favored over reaction pathways that tend to be more elaborate.

Although this mechanistic interpretation represents a significant departure from earlier work, our experimental data are consistent with the measured rates of reaction observed by other workers. The results of this study can be used to produce rate laws that compare favorably with earlier studies. Yet, we do not propose reaction intermediates such as $\bullet S_2O_3^-$ (Page, 1960) or $Fe(S_2O_3)_2^-$ (Holluta and Martini, 1924; Patnaik and Mahapatra, 1956) for which there is no direct experimental evidence. The slow oxidation of

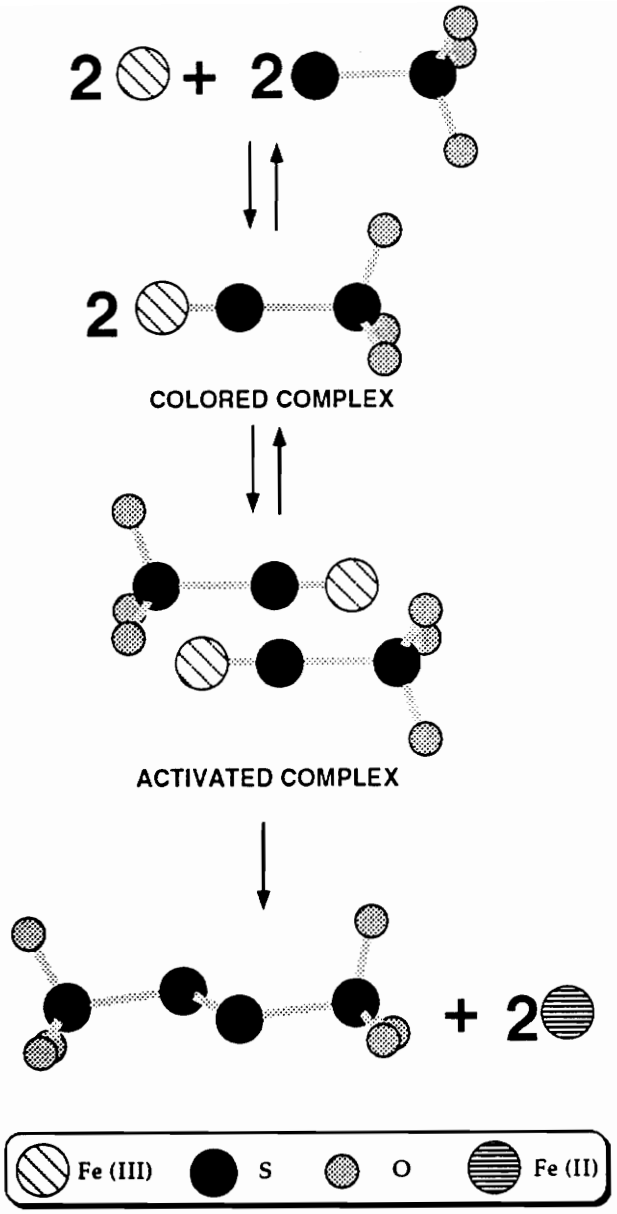

Figure 6. A schematic representation of the mechanism of reaction for the decomposition of the complex (eqns. 6-9). The colored $FeS_2O_3^+$ complex remains in equilibrium with Fe^{3+} and $S_2O_3^{2-}$ until all reactants are consumed. Two $FeS_2O_3^+$ complexes react to form the activated complex, which decomposes to form tetrathionate and ferrous iron, the observed reaction products.

$\bullet S_2O_3^-$ required in the mechanism of Page (1960) is difficult to justify since radical anions are normally strong reducing agents (Bamford and Tipper, 1972) and would be expected to react away quickly. Patnaik and Mahapatra (1956) considered autocatalysis of the decomposition of the colored complex to be important because they observed an S-shaped absorbance decay curve and, hence, they formulated a mechanism that is more complex that what the present study suggests.

The solutions used in this study produced no S-shaped absorbance decay curve. Hence, we were not compelled to consider autocatalysis by any reaction products as an important part of the reaction mechanism. However, we can produce an overall reaction model that will produce S-shaped curves as observed by Patnaik and Mahapatra (1956) considering that for any combination of $S_2O_3^{2-}$ and Fe^{3+} the rapid equilibrium established with the $FeS_2O_3^+$ complex will always leave some free $S_2O_3^{2-}$ and Fe^{3+}. These uncomplexed species react to produce more complex at the same rate at which the complex decomposes. Hence, the absorbance due to the presence of the $FeS_2O_3^+$ complex will not change for a short time at the beginning of an experiment until most of the $S_2O_3^{2-}$ and Fe^{3+} is consumed. For the low initial concentrations of reactants used in this study, the S-shape decay behavior occurs, but for such a short time that we did not observe it.

H+ *versus* Fe3+ As Sinks for $S_2O_3^{2-}$

In the geochemical environment, dissolved oxygen, H^+ and Fe^{3+} can act as inorganic sinks for thiosulfate. Rolia and Chakrabarti (1982)

have shown that thiosulfate is stable in the presence of dissolved oxygen at atmospheric pO_2, at least when transition metals are absent. Hence, a comparison of the relative importance of H^+ and Fe^{3+} is necessary and useful.

We have used the rate law from the present study (eqn. 6) for the decomposition of FeS_2O_3+ and the rate law of Johnston and McAmish (1973)

$$\frac{dm_S}{dt} = -0.336(\pm 0.018) m_{S_2O_3^{2-}}{}^{2.0} m_{H^+}{}^{1.0} \qquad (12)$$

for the rate of the acid-catalyzed decomposition of thiosulfate

$$S_2O_3^{2-} + H^+ = S + HSO_3^{2-} \qquad (13)$$

to calculate initial rates for each reaction. Values for $m_{FeS_2O_3^+}$ and $m_{S_2O_3^{2-}}$ used in these rate laws were calculated by speciating solutions over the pH range 0.5 - 7 (T = 25°C). For these calculations, $m_{S_2O_3^{2-}}(total) = 10^{-4}$ and we assume equilibrium control of Fe^{3+} by $Fe(OH)_3$, which is dominant in most geochemical environments

$$Fe(OH)_3 + 3H^+ = Fe^{3+} + 3H_2O \qquad (14)$$

$$a_{Fe^{3+}} = \frac{K}{H^+} = \frac{10^{3.4}}{H^+}$$

The result of this exercise is shown in Fig. 7 where we plot the reaction rate *versus* pH. This figure shows a rapid drop in the reaction rate for the

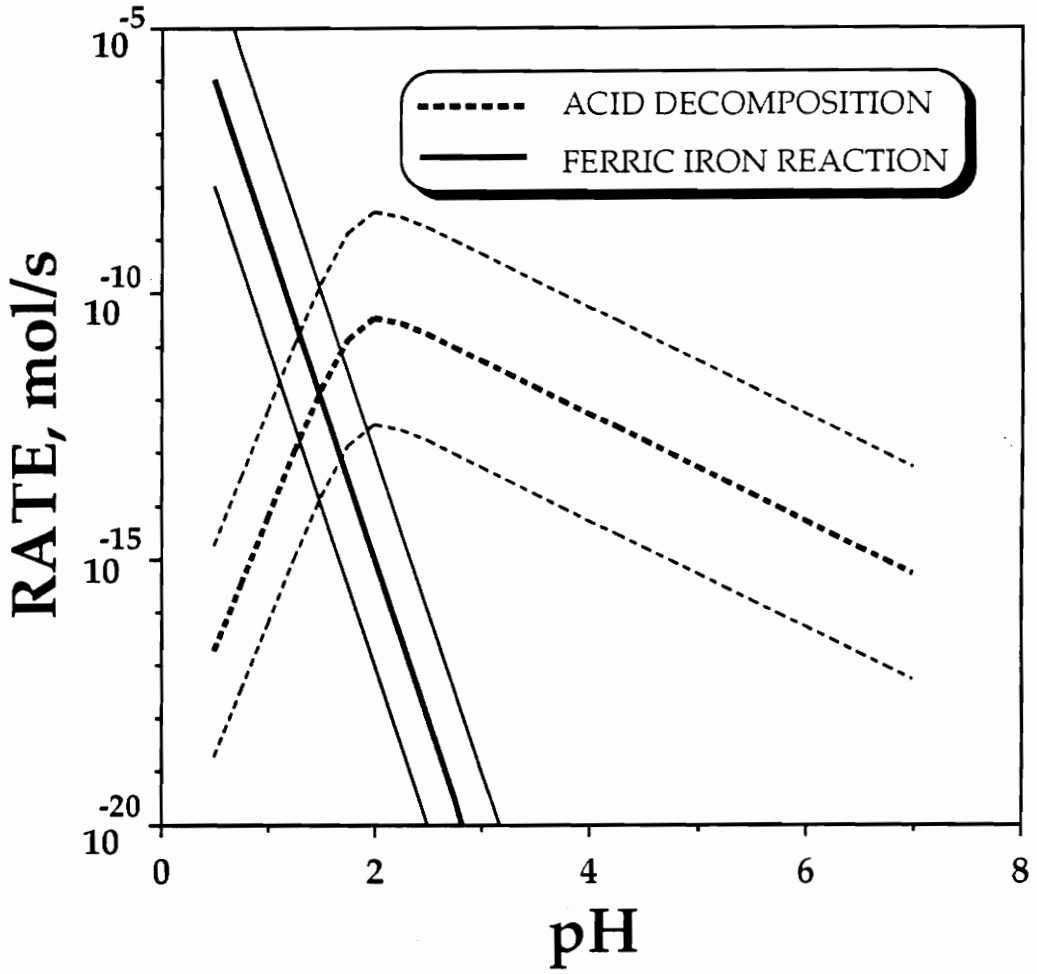

Figure 7. At 25°C, the rate of thiosulfate consumption *via* the $FeS_2O_3^+$ complex is dominated by the acid-catalyzed rate of $S_2O_3^{2-}$ decomposition at pH's above ~ 1.7. The rate of the ferric complex decomposition is limited in natural systems by the availability of Fe^{3+}, which diminishes rapidly with an increase in pH. The bold line for each reaction rate represent the rate of reaction for $m_{S_2O_3^{2-}}(\text{total}) = 10^{-4}$, while the finer lines indicate an increment or decrement of $m_{S_2O_3^{2-}}$ by one order of magnitude.

ferric thiosulfate complex with increasing pH compared to the acid-catalyzed reaction. At 25°C, the rate of the ferric thiosulfate complex decomposition is limited in natural systems by the availability of Fe^{3+}, which diminishes rapidly with increasing in pH, so the rate of the acid-catalyzed decomposition is faster at pH's above ~ 1.7.

The high activation energy for the decomposition of the ferric thiosulfate complex (120 kJ mol^{-1}) compared to the acid-catalyzed reaction (15 kJ mol^{-1}; Johnston and McAmish, 1973) suggests the decomposition of the ferric thiosulfate complex may dominate the acid decomposition at higher temperatures. However, no information is available for the temperature dependance of equilibria involving the formation of the ferric thiosulfate complex or the protonation of $S_2O_3^{2-}$, so we have confined our solution speciation calculations, and thus, rate comparisons to 25°C. An additional caveat of this comparison is that all rate laws describing the acid-catalyzed rate of thiosulfate decomposition (including Johnston and McAmish, 1973; eqn 14) have been formulated by following the rate of production of elemental sulfur which may not correlate well with the true rate of thiosulfate decomposition. Such an approach ignores any kinetic limitation on the nucleation and growth of sulfur so the rate of thiosulfate consumption may be even faster.

CONCLUSIONS

This study shows that the decomposition of the ferric thiosulfate complex is second order with respect the concentration of the $FeS_2O_3^+$ complex and that the rate law for the reaction is

$$\frac{dm_{Fe\text{-}S_2O_3^+}}{dt} = -10^{2.0(\pm0.3)} m_{Fe\text{-}S_2O_3^+}^{2.0(\pm0.1)}$$

Our results show that the rate of reaction increases with an increase in ionic strength, which is consistent with the bimolecular reaction between the two $FeS_2O_3^+$ complexes indicated in the rate law. The reaction is strongly dependent on temperature and has an activation energy of 120 kJ mol^{-1}. This high E_a is consistent with a bimolecular reaction between two positively charged ferric thiosulfate complex ions which must overcome repulsive coulombic interactions. The mechanism proposed in this study is consistent with the principles of structural economy and is, therefore, more acceptable than the series of bimolecular reactions proposed in earlier studies.

A comparison of the rate of $S_2O_3^{2-}$ decomposition by H^+ and Fe^{3+} shows that above pH = ~1.7, reaction with H^+ is a more important sink for $S_2O_3^{2-}$ at 25°C. However, because the E_a for the decomposition of thiosulfate by H^+ is an order of magnitude less than that for the ferric thiosulfate complex, it is reasonable to expect that modest increases in temperature will elevate the importance of the reaction between Fe^{3+} and $S_2O_3^{2-}$.

REFERENCES

Anderson-Thode S. and Jorgenson B. B. (1989) Sulfate reduction and the formation of 35S-labeled FeS, FeS2 and S0 in coastal marine sediments. *Limnol. Oceanogr.* **34**, 793-806.

Baes C. F. Jr. and Mesmer R. E. (1976)*The Hydrolysis of Cations* , Wiley-Interscience,

Bamford C.H. and Tipper C.F.H. (1972) *Comprehensive Chemical Kinetics. V. 7: Reactions of Metallic Salts and Complexes and Organometallic Compounds.* Elsevier, Amsterdam.

Benedetti M. and Boulègue J. (1991) Mechanism of gold transfer and deposition in a supergene environment. *Geochi. Cosmochim Acta* **55**, 1539-1547.

Boulègue J. (1978) Metastable sulfur species and trace metals (Mn, Fe, Cu, Zn, Cd, Pb) in hot brines from the French Dogger. *Am. J. Sci.* **278**, 1394-1411.

Burns D. T., Townshend A. and Carter A. H. (1981)*Reactions of the Elements and their Compounds Part B: Osmium to Zirconium* , 2, Wiley and Sons, New York.

Das J. and Patnaik D. (1956) Spectrophotometric study of the ferric-thiosulfate complex Part I. *J. Indian Chem. Soc.* **33**, 243-248.

Das J., Nanda C. and Patnaik D. (1956) Spectrophotometric study of the ferric thiosulfate complex. Part II. *J. Ind. Chem. Soc.* **33**, 459-464.

Goldhaber M. B. (1983) Experimental study of metastable sulfur oxyanion formation during pyrite oxidation at pH 6-9 and 30°C. *Am. Jour. Sci.* **283**, 193-217.

Granger H. C. and Warren C. G. (1969) Unstable sulfur compounds and the origin of roll-type uranium deposits. *Econ. Geol.* **64**, 160-171.

Granger H. C. and Warren C. G. (1974) Zoning in the altered tongue asociated with roll-type uranium deposits. Symposium on the formation of uranium ore deposits, Athens, Greece. pp. 185-199

Halder B. C. and Banerjee S. (1948) Studies on ferric-thiosulfate complex by colorimetric method. *Proc. Nat. Inst. India* **14**, 1-12.

Hine J. (1977) The principle of least motion. *Adv. Phys. Org. Chem.* **15**, 1-61.

Holluta J. and Martini A. (1924a) Kinetik und reaktionsmechanismus fur ferrisalzreduktion durch thiosulfat in schwach saurer losung. *Z. Anorg. Alleg. Chem.* **141** (in German)

Holluta J. and Martini A. (1924b) Die autokatayse bei der reaktion eisenchlorid-natriumsulfat. *Z. Anorg. Alleg. Chem.* **141**, 23-37. (in German)

Holluta J. and Martini A. (1925) Der einfluss der wasserstoffionen auf den mechanismus fer ferrisalzreduktion durch natriumthiosulfat. *Z. Anorg. Alleg. Chem.* **144**, 321-336.

Johnston F. and McAmish L. (1973) A study of the rates of sulfur production in acid thiosulfate solutions using S-35. *J. Coll. Inter. Sci.* **42**, 112-119.

Jorgensen B. B. (1990) A thiosulfate shunt in the sulfur cycle of marine sediments. *Science* **249**, 152-154.

Mahapatra G., Nanda C. and Patnaik D. (1957) Spectrophotometric study of the ferric thiosulfate complex. Part III. *J. Ind. Chem. Soc.* **34**, 458-460.

Makhua R. and Hitchen A. (1978) Determination of polythionates and thiosulphate in mining effluents and mill circuit solutions. *Talanta* **25**, 79-84.

Moelwyn-Hughes E. A. (1971) *The Chemical Statics and Kinetics of Solutions* ,

Moore J. W. and Pearson R. G. (1981) *Kinetics and Mechanism* , John Wiley and Sons, Nw York.

Moses C. O., Nordstrom D.K., Herman J.S.and Mills, A.L. (1987) Aqueous pyrite oxidation by dissolved oxygen and by ferric iron. *Geochimica et Cosmochimica Acta* **51**, 1561-1571.

Nriagu J. O., Coker R. D. and Kemp A. L. W. (1979) Thiosulfate, polythionates, and rhodanese activity in Lakes Erie and Ontario sediments. *Limnol. Ocean.* **24**, 383-389.

Page F. M. (1953) The reaction between ferric and thiosulfate ions Part 1. the determination ofthe absorption spectrum of the transient ferric-thiosulfate complex. *Trans. Faraday Soc.* **49**, 635-643.

Page F. M. (1954) The ferric thiosulfate reaction Part 2. The thiosulfate complexes of iron. *Trans. Faraday Soc.* **50**, 120-126.

Page F. M. (1960) The ferric thiosulfate reaction Part 3. The mechanism of the reaction. *Trans. Faraday Soc.* **56**, 398-406.

Patnaik D. and Mahapatra G. N. (1956) Spectrophotometric study of the kinetics of ferric thiosulfate reaction. *Curr. Sci.* **24**, 195-196.

Pethybridge A. D. and Prue J. E. (1972) Kinetic salt effects and the specific influence of ions on rate constants. In *Inorganic Reaction Mechanisms, Part II* (J. O. Edwards, ed.), Interscience Publishers, New York.

Rolia E. and Chakrabarti C. L. (1982) Kinetics of decompositon of tetrathionate, trithionite and thiosulfate in alkaline media. *Environ. Sci. Tech.* **16**, 852-857.

Schmidt H. (1930) Physikalische messungen an kurzlebigen zwischenprodukten. *Z. fur Phys. Chem.* **148**, 321-348. (in German)

Spirakis C. S. (1991) The possible role of thiosulfate in the precipitation of 34S-rich barite in some Mississippi Valley-type ore deposits. *Mineral. Deposita* **24**, 60-65.

Steudel R., Gobel T. and Holdt G. (1988) The molecular composition of hydrophilic sulfur sols prepared by acid decomposition of thiosulfate. *Z. Naturforsch* **436**, 203-218.

Stoffreggen R. (1986) Observations on the behavior og gold during supergene oxidation at Summitville, Colorado, USA, and implications for electrum stability in the weathering environment. *App. Geochem.* **1**, 549-558.

Tykodi R. J. (1990) In praise of thiosulfate. *J. Chem. Ed.* **67**, 146-149.

Veldeman E., Dack L. V., Gubels R. and Pentcheva E. N. (1991) Sulfur species and associated trace elements in south-west Bulgarian thermal waters. *App. Geochem.* **6**, 49-62.

Webster J. G. (1986) The solubility of gold and silver in the system Au-Ag-S-O_2-H_2O at 25°C and 1 atm. *Geochim. Cosmochim. Acta* **50**, 1837-1845.

Webster J. G. (1987) Thiosulfate in surfical geothermal waters, North Island, New Zealand. *App. Geochem.* **2**, 579-584.

Webster J. G. and Mann A. W. (1984) The influence of climate, geomorphology and primary geology on the supergene migration of gold and silver. *J. Geochem. Explor.* **22**, 21-42.

Williamson M. A. and Rimstidt J. D. (1992) Correlation between structure and thermodynamic properties of aqueous sulfur species. *Geochim. Cosmochim. Acta* in press.

Wolkoff A. W. and Larose R. H. (1975) Separation and detection of low concentrations of polythionates by high speed anion exchange liquid chromatography. *Anal. Chem.* **47**, 1003-1008.

APPENDIX

From absolute rate theory, for a generalized reaction

$$A + B = AB^{\neq} \rightarrow \text{Products} \tag{1A}$$

$$k = \frac{\kappa T}{h} K_c^{\neq} \tag{2A}$$

where k is the rate constant, κ is Boltzmann's constant, h is Planck's constant and K_c^* is an equilibrium constant for the formation of the activated complex in terms of concentration. In terms of activity,

$$K_a^{\neq} = K_c^{\neq} \frac{\gamma_{AB^*}}{\gamma_A \gamma_B} \tag{3A}$$

where a and c refer to activity and concentration, respectively, and γ is the activity coefficient. Equation (2A) can be rewitten

$$k = \frac{k'T}{h} K_a^{\neq} \frac{\gamma_A \gamma_B}{\gamma_{AB^*}} \tag{4A}$$

which is equivilent to the Brønsted-Bjerrum relation (Moore and Pearson, 1981)

$$k = k_o \frac{\gamma_A \gamma_B}{\gamma_{AB^*}} \tag{5A}$$

From Debye-Hükel (D-H) solution theory

$$-\log \gamma_i = \alpha Z_i^2 F(I) \qquad (6A)$$

where Z_i is the charge for an ion, i, F(I) is a function that expresses ionic strength and α is a constant (α=0.52 at 25°C). Thus for the general reaction (eqn 1A)

$$\log k = \log k_o + \left(Z_A^2 + Z_B^2 - (Z_A + Z_B)^2\right)\alpha F(I) \qquad (7A)$$

$Z_A + Z_B$ is the charge on the activated complex. Eqn (7A) may be simplified to

$$\log k = 2Z_A Z_B \alpha \sqrt{I} + \log k_o \qquad (8A)$$

Chapter 4: The kinetics of aqueous pyrite oxidation by ferric iron and dissolved oxygen

ABSTRACT

We have compiled rate data available in the literature for the reaction of pyrite with dissolved oxygen (DO) to produce a rate law that is applicable over three and one half orders of magnitude in DO concentration over the pH range 2-10. The valid rate law is

$$r = 10^{-8.19(\pm 0.10)} \frac{m_{DO}^{0.5(\pm 0.04)}}{m_{H^+}^{0.11(\pm 0.01)}}$$

where r is the rate of pyrite destruction in units of mol m^{-2} s^{-1}. In addition, we performed a series of batch, and mixed flow reactor experiments to determine the effect of SO_4^{2-}, Cl^-, ionic strength and dissolved oxygen on the rate of reaction of pyrite with ferric iron. Of these, only dissolved oxygen was found to have any appreciable effect. We combined our results with kinetic data reported in the literature to formulate rate laws that are applicable over a six order of magnitude range in Fe^{3+} and Fe^{2+} concentration for the pH range ~0.5-3.0. In N_2-purged solution, the rate law is

$$r = 10^{-8.58(\pm 0.15)} \frac{m_{Fe^{3+}}^{0.30(\pm 0.02)}}{m_{Fe^{2+}}^{0.47(\pm 0.03)} m_{H^+}^{0.32(\pm 0.04)}}$$

and when dissolved oxygen is present

$$r = 10^{-6.07(\pm 0.57)} \frac{m_{Fe^{3+}}^{0.93(\pm 0.07)}}{m_{Fe^{2+}}^{0.40(\pm 0.06)}}$$

where r is the rate of pyrite destruction in mol m^{-2} s^{-1}.

We also performed experiments in which we re-reacted the same pyrite sample with ferric iron solutions of the same composition and identical A/M. For each subsequent experiment, the rate of reaction slowed and the original behavior of the pyrite could not be re-established by washing the pyrite with concentrated HCl or EDTA. We have interpreted this behavior as representative of a change in the electrochemical properties of the solid pyrite. Pretreating pyrite samples with aqueous solutions of ferrous iron and EDTA did not change the reaction rate with ferric iron, however pretreatment with hydroxylamine hydrochloride lowered the rate significantly.

The data presented are best modelled by a non-site specific Freundlich multilayer isotherm. Good correlation was found between Eh and rate for the aqueous oxidation of pyrite with DO and ferric iron. Because the fractional orders of reaction are difficult to explain with a purely molecular-based mechanism, we favor a cathodic-anodic electrochemical mechanism to explain the transfer of the electron from pyrite to the aqueous oxidant.

Mechanistically, the results of our studies suggest a non-site specific interaction between dissolved oxidants and the pyrite surface. Rate correlates strongly with Eh (Fe^{3+}/Fe^{2+} ratio or DO concentration) and is consistent with an electrochemical mechanism where anodic and cathodic recations occur at different places on the pyrite surface.

INTRODUCTION

The mechanism of a chemical or geochemical reaction, that is the detailed manner in which it proceeds, particularly the number and nature of steps involved, is a product of our imagination. A correct mechanism cannot ever be proven, but a substantial amount of information may be gathered to test any hypothesized molecular processes (Wilkins, 1974). The chemical data which are typically gathered en route to establishing acceptable mechanisms include (1) determination of species which influence the rate of reaction with subsequent formulation of a rate law; (2) the nature of the reaction products and (3) intermediates; (4) activation parameters (i.e. activation energy, E_a); (5) bond cleavage and (6) linear free energy relationships (the dependance of rate on free energy of reaction).

Because of its importance in the formation of acid mine drainage, in hydrometallurgy, and in the geochemical cycling of sulfur and iron, the kinetics and mechanism of the aqueous oxidation of pyrite by molecular oxygen and ferric iron have received a great deal of attention. These two reactions are

$$FeS_2 + 14Fe^{3+} + 8H_2O \rightarrow 15Fe^{2+} + 2SO_4^{2-} + 16H^+ \quad (1)$$

$$FeS_2 + \frac{7}{2}O_2 + H_2O \rightarrow Fe^{2+} + 2SO_4^{2-} + 2H^+ \quad (2)$$

Studies of the aqueous oxidation of pyrite by dissolved oxygen and ferric iron prior to 1982 are summarized by Hiskey and Schlitt (1982) and Lowson (1982). Since the publication of these two review papers, Goldhaber (1983),

Wiersma and Rimstidt (1984), McKibben and Barnes (1986), Moses et al. (1987), Nicholson et al. (1988) and Moses and Herman (1991) have contributed to our understanding of these important reactions. There is general agreement that the E_a for eqns. (1) and (2) are high enough (on the order of 50-80 kJ mol^{-1}) to support a chemical rather than physical (i.e. diffusional) control of the rate limiting step. Reedy et al. (1991) provided important insight into bond cleavage by demonstrating that over the pH range 1-7, virtually all oxygen in the product sulfate is derived from water. Goldhaber (1983) and Moses et al. (1987) showed that aqueous sulfoxy intermediates could be produced during oxidation of pyrite with dissolved oxygen (DO), with the latter study demonstrating that the rate of formation of these intermediates is negligible relative to the rate of sulfate production for pH<7. This conclusion was also noted to be true for oxidation by ferric iron. However, despite the apparent active research, many factors remain to be reconciled among the various efforts regarding the solution species which influence the rate of reaction, the nature of sulfur intermediates and the mechanism by which these intermediates produce the eventual reaction products.

To formulate a rate law that accurately describes the rate of reaction and provides useful mechanistic information, the effect of species commonly found in the reaction system on the rate of reaction must be quantified. For example, there are several reports that the rates of oxidation of sulfide minerals by ferric iron are greater in chloride-rich solutions than in sulfate-rich solutions (*eg.* chalcopyrite: Dutrizac, 1982; Gerlach *et al.*, 1973. galena: Warren et al., 1987; Furerstenau *et al.*, 1986. cubanite: Dutrizac et al., 1970)

Sulfate ions could inhibit the rate limiting step of the oxidation reaction or chloride ions could catalyze it. Additionally, while some studies of the reaction of ferric iron with pyrite were conducted in oxygen-free environments (Smith et al., 1970; McKibben, 1984; Moses et al. 1987; Moses and Herman, 1991) to isolate the effect of ferric iron, the weathering environment often contains oxygen. King and Lewis (1980) reported that the oxidation reaction with ferric iron proceeds faster in the presence of DO.

The goal of this paper is to present results of our studies on the effect of sulfate (SO_4^{2-}), chloride (Cl^-), ionic strength (I) and DO on the rate of pyrite oxidation by ferric iron, and to compile available data for the kinetics of the aqueous oxidation of pyrite. We have compiled rate data available in the literature, transformed the data to consistent units and formulated empirical rate laws for the ferric iron and DO oxidation at 25°C. Our experiments with mixed ferric iron/DO solutions show that the mechanism of eqn. (1) changes when DO is present compared to N_2-purged systems studied previously. The rate laws we have formulated are applicable over a wider range of solution composition than has previously been available.

METHODS

Experimental

Measurements were performed in either a mixed flow reactor (MFR; Rimstidt and Dove, 1986) or a simple, stirred, batch reactor (BR; Fig. 1). The pyrite used in all experiments is from Peru and was obtained from Geoscience Resources The material was hand sorted, immersed in 1N hydrochloric acid overnight to remove carbonate and oxide phase impurities

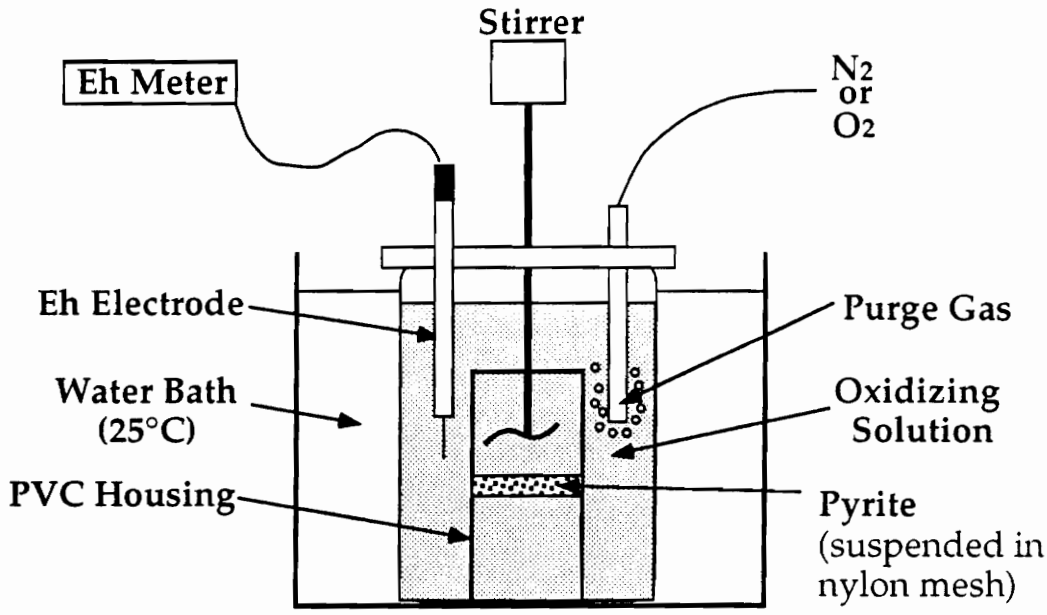

Figure 1. A schematic diagram of the reaction kettle used for batch and mixed flow experiments in this study.

and air dried in an oven at 40°C. Next the pyrite was crushed and the particles ranging in size from 150 to 250 μm were recovered by sieving. This size fraction was rinsed in acetone several times to remove any fine particles adhering to the surface of the larger grains. The specific surface area of the unreacted mineral grains was determined by N_2 adsorption to be 0.047 ± 0.002 m^2g^{-1}.

Ferric chloride run solutions were prepared by mixing aliquots of an acidified 0.5 molal ferric chloride solution into distilled water and adjusting to a final pH (<3) using reagent grade HCl. Similarly, ferric sulfate run solutions were prepared by using aliquots of an acidified 0.25 molal ferric sulfate stock solution and were acidified using reagent grade H_2SO_4. Appropriate amounts of sodium chloride and sodium sulfate were added directly to 0.0001 molal ferric chloride solutions to attain the desired Cl^- and SO_4^{2-} concentrations for investigating the effect of the anions on the rate of reaction. The pH was checked prior to each experiment with the MFR and was monitored continuously in the BR studies.

Approximately two grams of pyrite were used for each experiment. All MFR experiments were performed using ambient air-saturated solutions. BR experiments were performed using either pure N_2 or O_2 purged solutions, with the appropriate gas bubbled through them during the course of an experiment. The Eh of reactor solutions was continuously monitored using a Fisher Scientific combination Pt 4 molal KCl/Ag-AgCl Eh electrode and an Orion Research 811 meter. For MFR experiments, the reaction was stopped when steady state conditions were reached and the difference between the concentration of ferric iron in the feed and effluent solutions at this time was

used to calculate the reaction rate. For BR experiments, the Eh of the reacting solutions was monitored continuously and the ferrous and ferric iron concentrations in the solutions was calculated from Eh readings at selected intervals. The rate of reaction for BR experiments was determined by using the b-term from a second order polynomial fit to ferric iron concentration-time data (McKibben and Barnes, 1986; Rimstidt and Newcomb, 1992).

The pyrite sample from MFR experiments was removed from the reactor, rinsed in distilled deionized water, dried in an oven at 40°C, and stored in air tight containers. Finally, the specific surface area of the reacted pyrite grains was determined from a three point N_2 BET isotherm using a Quantasorb Surface Area Analyzer. Approximately 0.2 g of four different run samples was outgassed at 50°C for five days before performing the surface area measurement. The specific surface area of the reacted pyrite samples was 0.051 ± 0.009 m^2 g^{-1}; the specific surface area of the reacted grains was essentially the same as the unreacted grains within the precision of the measurement. No surface area measurement was taken for pyrite used in BR experiments after reaction.

The concentration of ferric and ferrous iron in the reaction solutions was calculated from the measured Eh and by simultaneously solving the Nernst equation, a mass balance equation, and equations relating the activity to concentration. The details of this approach are described in Wiersma, (1982) and Weirsma and Rimstidt (1984). The electrode was calibrated using a ZoBell's solution (Nordstrom, 1977). A FORTRAN program which takes into account sulfate, chloride, and hydroxide ion pairing (Wiersma, 1982) was used to calculate the activity coefficients of ferric and ferrous iron in the

effluent solution. Hence, the ferric and ferrous iron concentration in reaction solutions could be calculated from its Eh.

For MFR experiments, the difference in ferric iron concentration between the feed and effluent solutions was combined with the flow rate to compute the apparent rate of the oxidation of pyrite:

$$r' = (dn/dt)_{rxn} = [(n/M)_{in} - (n/M)_{out}]\,[dM/dt] = (dn/dM)(dM/dt), \quad (6)$$

where $r' = (dn/dt)$ is the rate of reduction of ferric iron in this experiment, $(n/M)_{in}$ is the concentration of ferric iron of the feed solution, $(n/M)_{out}$ is the ferric iron concentration of the effluent solution, and (dM/dt) is the flow rate of solution through the reactor. The specific surface area and total mass of the sample were used to adjust the reaction rate to that of a standard system with 1 m^2 surface area of pyrite.

A simple plug flow reactor (PFR) was used to evaluate the effect of addition of Ag^+, SO_3^{2-} and formaldehyde on the rate of aqueous sulfoxy anion production during oxidation by ferric iron at pH = 2. Details concerning the use of a PFR to study pyrite oxidation by ferric iron is summarized by Rimstidt and Newcomb (1992). Nitrogen-purged ferric iron solutions containing either Ag^+, SO_3^{2-} or formaldehyde were pumped through the PFR at different rates. The addition of Ag^+ was designed to complex and thus trap any thiosulfate ($S_2O_3^{2-}$) that might be released to solution during reaction and extend its lifetime in solution so as to enable its detection. Luttrell and Yoon (1984) suggested polysulfides could be produced on the surface of an oxidizing sulfide. Accordingly, sulfite was

added to cleave, via nucleophilic attack, any polysulfides (S_n^{2-}) which might form on the surface of the mineral and release $S_2O_3^{2-}$ to solution. Addition of formaldehyde will complex any SO_3^{2-} produced and stabilize it in solution (Moses et al., 1984). These additives were used in separate experiments and not together. Solutions which flowed out of the PFR were immediately analyzed for SO_4^{2-}, SO_3^{2-} and $S_2O_3^{2-}$ with an ion chromatograph according to a procedure outlined by (Schoonen, 1988).

Compilation of Literature Rates

In addition to the experimental studies outlined above, we have collected rate data from a variety of sources (Smith et al., 1970; McKibben, 1984; Nicholson et al., 1988 and Moses and Herman, 1991). All sources provided sufficient information to allow us to determine the reaction rate for a standard system of 1 m^2 surface area. Data were recast to consistent SI units so the rate of pyrite destruction expressed as mol m^{-2} s^{-1}.

These literature data were combined with the results of this investigation to produce a database representing a wide range of rates and aqueous solution compositions. This set of data was analyzed to produce rate laws for pyrite oxidation by ferric iron and dissolved oxygen over a very wide range of solution composition.

Multiple Linear Regression and Leverage Plots

Multiple linear regression analyses were performed using the statistical program JMP 2.0 for the Apple Macintosh computer, which is produced by the SAS Institute, Cary, NC, USA. In addition to reporting the

coefficients for all independent variables in a regression, this program produces leverage plots, which are discussed in detail by (Sall, 1990).

In effect, a leverage plot graphically depicts the influence of an independent variable on the overall model dependant variable. The slope of the leverage plot is numerically represented by a regression coefficient and its associated standard error. For a simple regression, one dependent and one independent variable, points on a leverage plot for simple regression are actual data coordinates. On a leverage plot for a model that incorporates multiple effects (more than one independent variable), the points are no longer actual data values (see Sall, 1990). However, the intuitive interpretation of the plot is the same for multiple linear regression as for simple linear regression. A horizontal graph on a leverage plot indicates that the regressor does not significantly influence the dependant variable. Hence, the slope of a leverage plot is numerically equal to the coefficient normally associated with multiple linear regression. Leverage plots are useful for graphically displaying the effect of regressor on the dependent variable and portray in a glance which regressors are significant and which are not.

RESULTS

Experimental and compiled data for aqueous pyrite oxidation are found in Tables 1-3. Multiple linear regressions of these data are illustrated in Figures 2-4. We describe the results in greater detail below.

Compiled data for the oxidation of pyrite by DO are found in Table 1. Multiple linear regression of these data produced the rate law

Table 1. Data for the oxidation of pyrite by DO. The rate of pyrite destruction has units of mol $m^{-2}s^{-1}$ and concentration, mol kg^{-1}.

log r	log m_{O2}	log H^+	Ref	log r	log DO	log H^+	Ref
-9.13	-2.24	-2.00	1	-9.88	-3.49	-2.00	1
-9.00	-2.05	-2.00	1	-9.92	-3.64	-2.00	1
-9.64	-2.90	-2.00	1	-9.94	-3.61	-2.00	1
-9.13	-2.24	-2.00	1	-10.05	-3.79	-2.00	1
-8.80	-1.71	-2.00	1	-9.28	-2.90	-1.50	1
-9.14	-2.24	-2.00	1	-9.26	-2.90	-2.00	1
-9.15	-2.24	-2.00	1	-9.10	-2.90	-4.00	1
-9.13	-2.24	-2.00	1	-8.99	-2.90	-6.00	1
-9.05	-2.05	-2.00	1	-8.98	-2.90	-6.00	1
-8.88	-1.84	-2.00	1	-8.87	-2.90	-7.00	1
-9.13	-2.24	-2.00	1	-8.71	-2.90	-8.00	1
-8.90	-1.93	-2.00	1	-8.55	-2.90	-9.00	1
-8.75	-1.71	-2.00	1	-8.48	-2.90	-10.00	1
-9.39	-2.43	-2.00	1	-9.23	-2.94	-1.89	2
-9.28	-2.35	-2.00	1	-9.19	-2.94	-2.33	2
-9.13	-2.24	-2.00	1	-9.29	-2.94	-2.94	2
-9.45	-2.97	-2.00	1	-9.31	-2.94	-3.85	2
-9.23	-2.53	-2.00	1	-9.57	-3.63	-1.89	2
-9.24	-2.56	-2.00	1	-9.42	-3.63	-1.89	2
-9.25	-2.56	-2.00	1	-9.19	-2.86	-1.89	2
-9.29	-2.64	-2.00	1	-9.25	-2.99	-1.89	2
-9.41	-2.83	-2.00	1	-9.03	-2.94	-7.00	3
-9.61	-3.11	-2.00	1	-9.02	-2.94	-7.00	3
-9.65	-3.22	-2.00	1	-9.03	-2.94	-7.00	3
-9.73	-3.34	-2.00	1	-9.00	-2.94	-6.00	3
-9.85	-3.46	-2.00	1				

Reported data are from [1]Smith et al. (1970), [2]McKibben (1984) and [3]Moses and Herman (1991).

Table 2. Experimental rate data from this study for the oxidation of pyrite with ferric iron in the presence of DO. Rate of destruction of pyrite is expressed as mol $m^{-2}s^{-1}$ and concentration as mol kg^{-1}.

log r	log mFe^{3+}	log mFe^{2+}	Eh	log mH^{+}	log mSO_4^{2-}	log mCl^{-}	I	Note
-7.58	-4.58	-5.30	0.813	-2.05	-10.00	-4.10	0.00908	1
-7.59	-4.07	-4.84	0.815	-1.84	-10.00	-3.59	0.01499	1
-6.90	-3.57	-4.30	0.812	-2.06	-10.00	-3.09	0.01043	1
-7.11	-3.54	-4.54	0.829	-2.06	-10.00	-3.06	0.01050	1
-6.60	-3.01	-4.69	0.869	-2.13	-10.00	-2.53	0.01332	1
-6.20	-2.51	-3.87	0.849	-2.03	-10.00	-2.03	0.02814	1
-6.36	-2.51	-4.08	0.862	-2.06	-10.00	-2.03	0.02742	1
-6.51	-3.08	-5.55	0.917	-2.53	-10.00	-2.60	0.00794	1
-6.31	-2.78	-4.14	0.851	-2.39	-10.00	-2.31	0.01411	1
-6.55	-2.61	-4.01	0.854	-2.35	-10.00	-2.13	0.01939	1
-7.14	-4.24	-5.95	0.871	-1.57	-10.00	-3.77	0.02726	1
-7.14	-3.98	-4.55	0.805	-1.57	-10.00	-3.50	0.02761	1
-7.68	-3.73	-4.33	0.807	-1.57	-10.00	-3.25	0.02813	1
-7.68	-3.57	-2.76	-	-2.00	-2.54	-10.00	0.02500	2
-7.82	-3.44	-2.79	-	-2.00	-2.54	-10.00	0.02500	2
-8.63	-4.72	-3.74	-	-1.79	-3.52	-10.00	0.01772	2
-8.67	-4.77	-3.74	-	-1.79	-3.52	-10.00	0.01772	2
-8.19	-4.04	-3.26	-	-1.97	-3.02	-10.00	0.01552	2
-9.11	-5.48	-4.22	-	-1.75	-3.02	-10.00	0.01826	2
-8.67	-4.59	-3.76	-	-1.75	-2.52	-1.00	0.12000	2
-8.65	-4.72	-3.74	-	-1.50	-2.52	0.00	1.00000	2
-8.64	-4.77	-3.74	-	-1.90	-2.52	-2.00	0.01200	2
-8.67	-4.63	-3.75	-	-1.82	-2.52	-1.00	0.12000	2
-8.63	-4.72	-3.74	-	-1.95	-2.52	0.00	1.00000	2
-8.57	-5.27	-3.71	-	-2.10	0.01	-10.00	3.00000	2
-7.78	-3.73	-3.09	-	-1.92	-10.00	-1.82	0.01802	2
-8.72	-4.89	-4.06	-	-1.94	-10.00	-1.92	0.01208	2
-8.22	-4.15	-3.60	-	-1.95	-10.00	-1.92	0.01314	2
-7.41	-2.94	-2.69	-	-1.98	-10.00	-1.82	0.02967	2
-8.55	-5.24	-3.71	-	-1.90	-0.96	-10.00	0.30200	2
-8.60	-4.92	-3.73	-	-2.10	-1.98	-10.00	0.03200	2

[1] Batch reactor [2] Mixed flow reactor.

Table 3. Rate data for oxidation of pyrite with ferric iron in the absence of dissolved oxygen. Rate of pyrite destruction is mol $m^{-2}s^{-1}$ and concentrations are mol kg^{-1}.

log r	log Fe^{3+}	log Fe^{2+}	Eh	log H^+	Ref
-6.67	-3.83	-4.94	0.838	-1.97	1
-6.77	-3.52	-4.64	0.837	-1.95	1
-6.59	-3.15	-4.38	0.843	-1.92	1
-6.54	-3.08	-4.64	0.863	-1.91	1
-6.50	-2.78	-4.39	0.866	-1.87	1
-6.64	-2.63	-4.24	0.866	-1.90	1
-6.43	-2.52	-4.13	0.866	-1.84	1
-6.81	-4.21	-5.36	0.839	-1.37	1
-6.69	-4.49	-5.07	0.806	-2.22	1
-6.86	-4.45	-4.32	0.763	-2.21	1
-7.39	-2.72	-4.70	-	-1.15	2
-7.10	-2.70	-4.70	-	-1.55	2
-6.88	-2.71	-4.24	-	-1.89	2
-6.95	-2.70	-4.62	-	-2.10	2
-7.05	-2.71	-4.06	-	-1.70	2
-7.16	-2.72	-4.15	-	-1.29	2
-6.79	-2.41	-4.19	-	-1.89	2
-8.88	-7.57	-2.01	0.441	-2.50	3
-9.11	-4.30	-2.61	0.670	-0.50	3
-8.91	-3.75	-2.23	0.680	-0.50	3
-8.68	-2.99	-1.72	0.695	-0.50	3
-8.43	-6.43	-3.28	0.583	-2.00	3
-8.51	-5.72	-2.95	0.606	-2.00	3
-9.01	-3.99	-2.41	0.676	-0.50	3
-8.83	-3.50	-2.06	0.685	-0.50	3
-8.76	-3.25	-1.91	0.690	-0.50	3
-8.60	-2.77	-1.57	0.699	-0.50	3
-8.51	-2.48	-1.38	0.705	-0.50	3
-8.45	-5.98	-3.05	0.596	-2.00	3
-8.41	-6.69	-3.40	0.575	-2.00	3
-8.33	-5.91	-2.96	0.595	-2.00	3
-9.56	-7.45	-2.04	0.450	-0.50	3
-9.77	-7.59	-1.99	0.439	-0.50	3
-9.89	-7.82	-1.99	0.425	-0.50	3
-10.10	-8.23	-1.96	0.399	-0.50	3
-10.40	-8.67	-1.98	0.374	-0.50	3
-9.44	-7.25	-2.00	0.459	-0.50	3
-9.29	-7.09	-2.01	0.469	-0.50	3
-9.55	-7.50	-2.01	0.445	-0.50	3
-9.56	-7.47	-1.98	0.445	-0.50	3
-9.52	-8.42	-2.98	0.448	-0.50	3
-9.56	-7.43	-1.99	0.448	-0.50	3
-9.53	-7.43	-1.99	0.448	-0.50	3
-9.49	-7.51	-1.97	0.442	-0.50	3
-9.68	-7.48	-1.97	0.444	-0.50	3
-9.56	-7.35	-1.96	0.451	-0.50	3
-10.19	-8.36	-1.97	0.392	-0.50	3
-9.98	-7.86	-1.98	0.422	-0.50	3
-8.76	-4.84	-1.93	0.597	-0.50	3
-9.70	-7.50	-2.00	0.445	-0.50	3
-8.84	-5.74	-2.01	0.549	-0.50	3
-8.87	-5.33	-2.00	0.668	-0.50	3
-8.68	-3.71	-2.01	0.669	-0.50	3
-8.72	-3.94	-2.02	0.656	-0.50	3
-8.72	-4.33	-2.02	0.633	-0.50	3
-9.47	-6.99	-2.01	0.475	-0.50	3
-9.15	-6.58	-2.02	0.500	-0.50	3
-8.92	-6.15	-2.01	0.525	-0.50	3
-10.65	-9.10	-1.99	0.349	-1.00	3
-9.99	-8.07	-1.98	0.410	-1.00	3
-9.76	-7.82	-1.98	0.425	-1.00	3
-9.64	-7.68	-1.98	0.433	-1.00	3
-9.53	-7.48	-2.01	0.446	-1.00	3
-9.39	-7.23	-1.97	0.459	-1.00	3
-9.34	-7.21	-1.98	0.460	-1.00	3
-9.42	-7.21	-2.02	0.463	-1.00	3
-9.29	-7.30	-2.00	0.456	-1.00	3
-10.38	-9.13	-1.98	0.347	-2.00	3
-10.24	-8.86	-1.98	0.363	-2.00	3
-9.88	-8.49	-1.99	0.385	-2.00	3
-9.77	-8.20	-1.98	0.402	-2.00	3
-9.68	-8.05	-1.99	0.411	-2.00	3
-9.53	-7.97	-1.99	0.416	-2.00	3
-9.32	-7.81	-1.98	0.425	-2.00	3
-9.34	-7.66	-1.98	0.434	-2.00	3
-9.23	-7.48	-1.98	0.445	-2.00	3
-8.93	-7.43	-2.04	0.451	-2.00	3
-9.14	-7.68	-2.01	0.434	-2.00	3
-9.77	-8.39	-1.97	0.390	-2.00	3
-9.58	-7.97	-1.97	0.415	-2.00	3
-9.24	-7.50	-1.98	0.443	-2.00	3
-8.33	-3.40	-1.66	0.667	-2.00	3
-9.24	-7.59	-2.00	0.439	-2.00	3
-9.32	-7.62	-2.00	0.437	-2.00	3

Table 3. (continued)

log r	log Fe^{3+}	log Fe^{2+}	Eh	log H^+	Note
-8.90	-7.24	-2.00	0.460	-2.00	3
-8.33	-4.25	-2.00	0.637	-2.00	3
-8.45	-4.49	-2.01	0.623	-2.00	3
-8.43	-5.01	-2.00	0.592	-2.00	3
-8.46	-5.37	-2.01	0.571	-2.00	3
-8.47	-5.76	-2.01	0.548	-2.00	3
-8.54	-6.16	-2.01	0.542	-2.00	3
-8.86	-6.98	-2.00	0.475	-2.00	3
-8.66	-6.57	-2.01	0.500	-2.00	3
-8.41	-4.49	-1.99	0.622	-2.00	3
-9.78	-8.76	-1.99	0.369	-2.50	3
-9.60	-8.55	-1.99	0.382	-2.50	3
-9.49	-8.33	-1.99	0.395	-2.50	3
-9.32	-8.04	-1.99	0.412	-2.50	3
-9.19	-7.87	-1.99	0.422	-2.50	3
-8.99	-7.47	-1.98	0.445	-2.50	3
-8.82	-7.34	-1.98	0.453	-2.50	3

[1]Present Study, [2]McKibben (1984), [3]Smith et al. (1970).

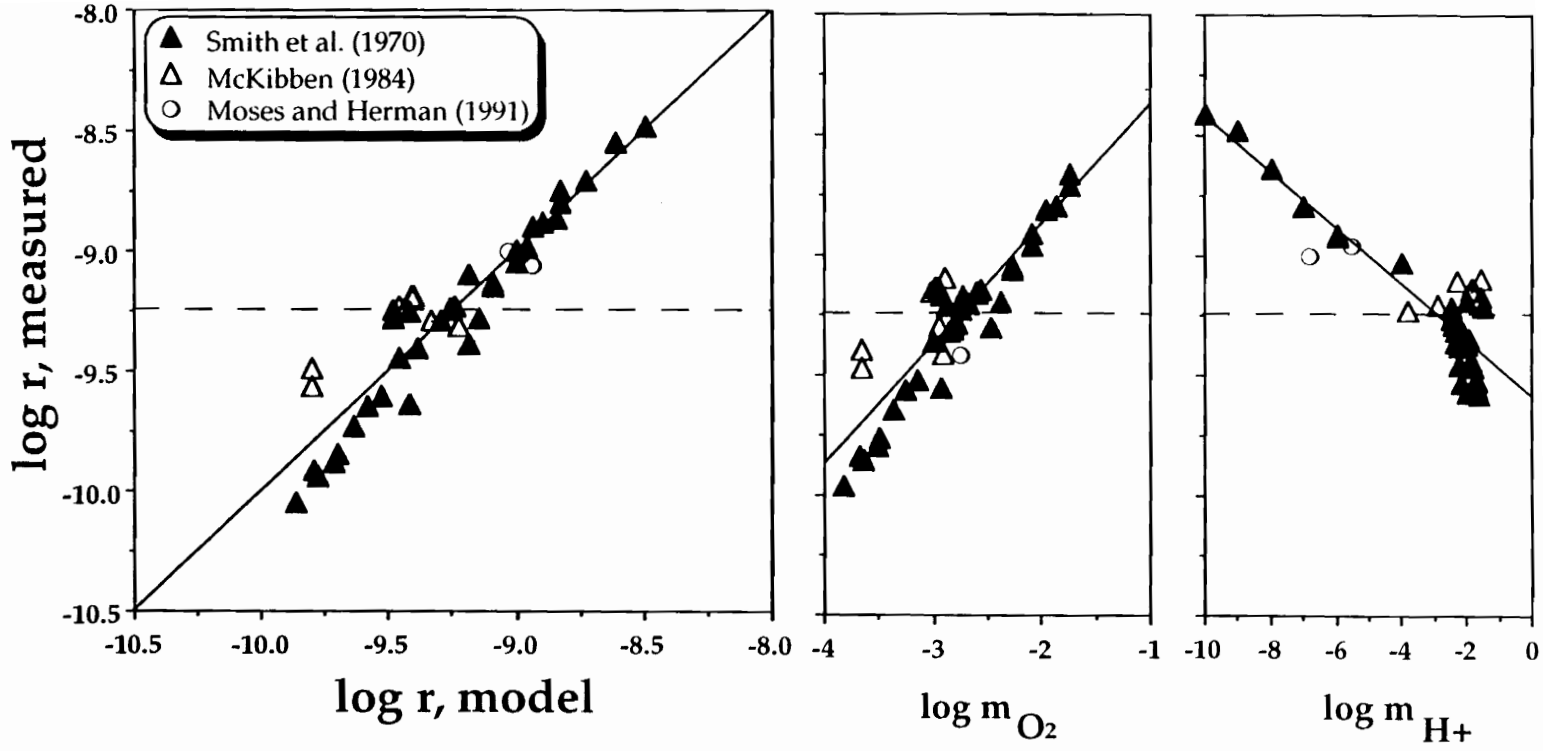

Figure 2. Whole model and leverage plots for multiple linear regresion analysis of rate data for the aqueous oxidation of pyrite by dissolved oxygen.

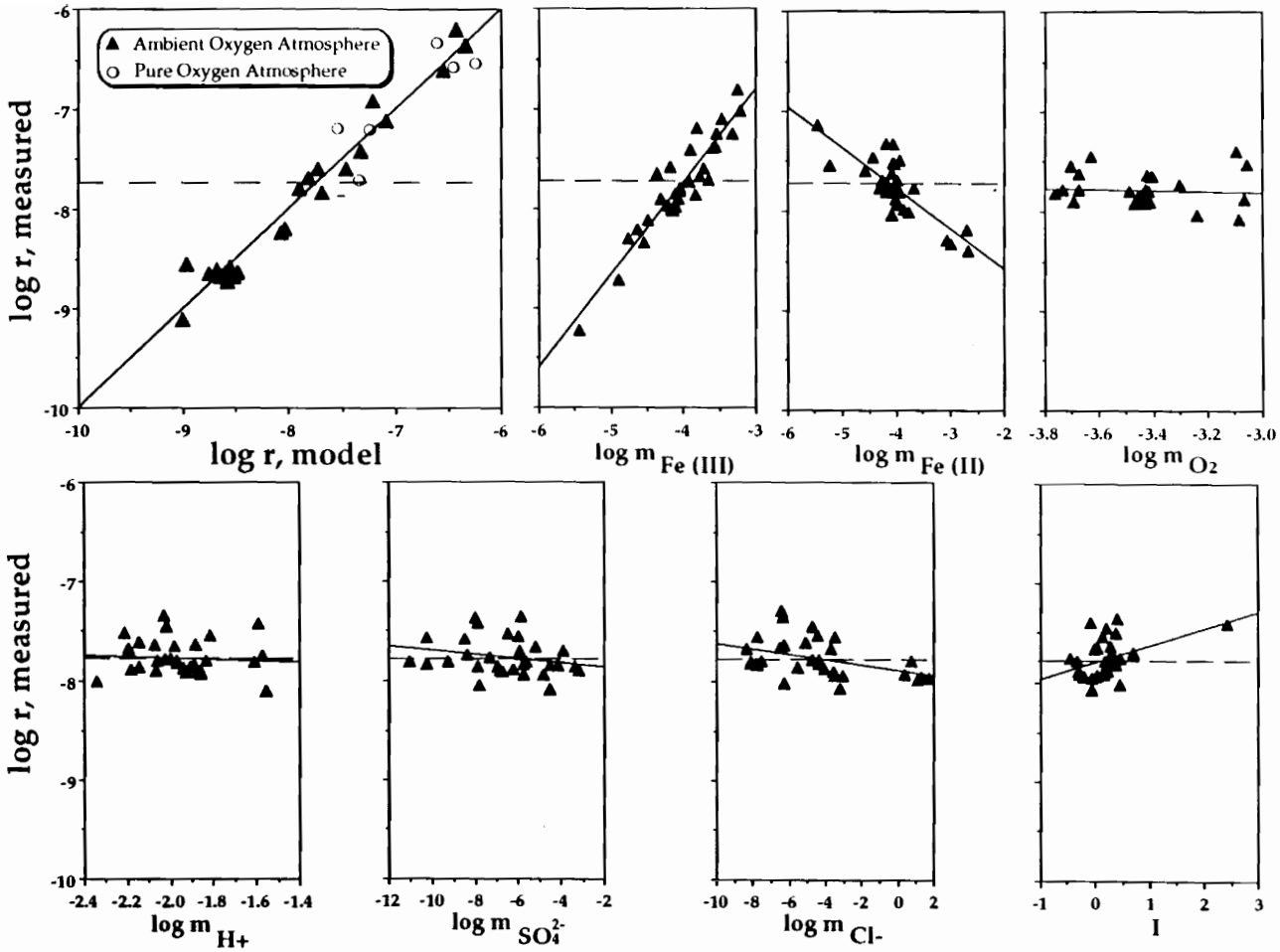

Figure 3. Whole model and leverage plots for multiple linear regresion analysis of rate data for the aqueous oxidation of pyrite by ferric iron in the presence of dissolved oxygen. Slopes for the leverage plots for O_2, H^+, SO_4^{2-}, Cl^- and I are nearly zero indicating that these parameters do not significantly affect the rate of reaction.

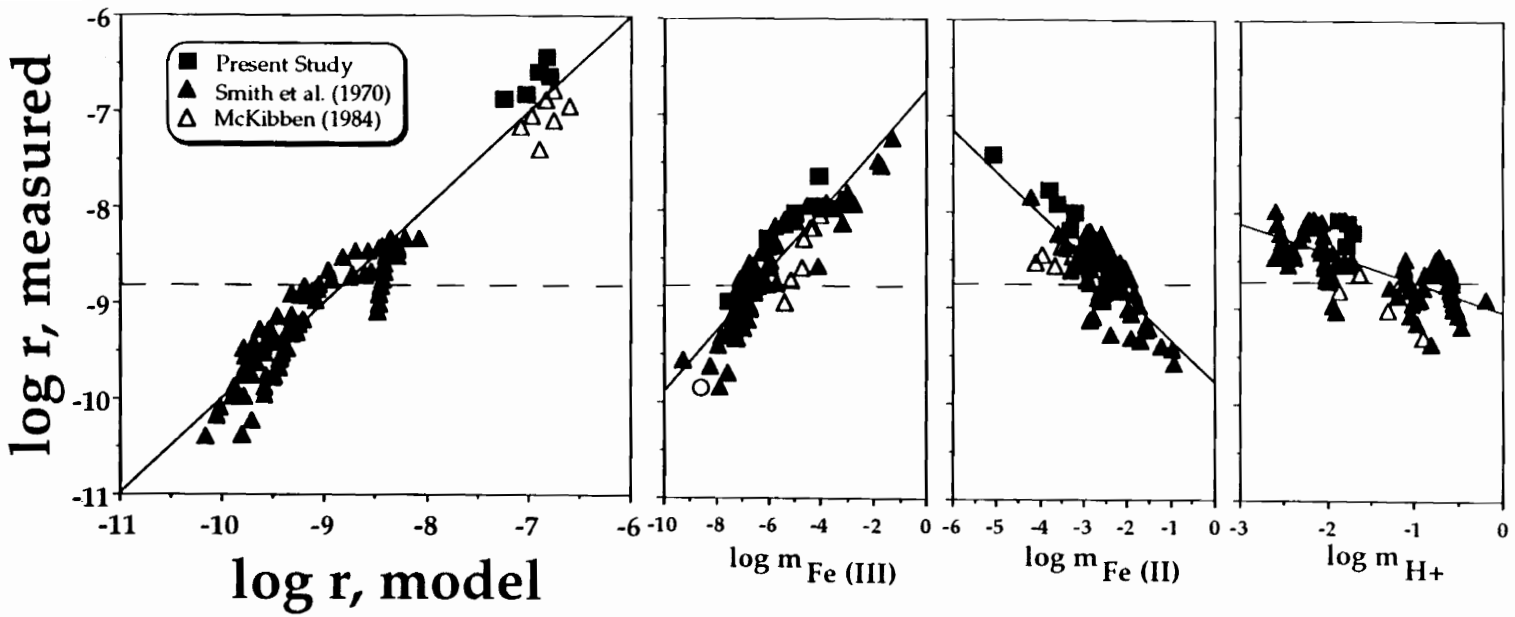

Figure 4. Whole model and leverage plots for multiple linear regresion analysis of rate data for aqueous pyrite by ferric iron under an N_2 atmosphere.

$$r = 10^{-8.19(\pm 0.10)} \frac{m_{DO}^{0.5(\pm 0.04)}}{m_{H^+}^{0.11(\pm 0.01)}} \quad (4)$$

where r is the rate of pyrite destruction in mol m^{-2} s^{-1}. The result of this regression is illustrated in Fig. 2 (numerically in Table 4) which shows a slight discrepancy between the data of Smith et al. (1970) and McKibben (1984). This difference is about a half an order of magnitude or less at the lowest DO concentration studied by McKibben (1984). This analysis confirms a reaction order for dissolved oxygen of 0.5, consistent with McKibben and Barnes (1986) and many previous studies (see reviews by Hiskey and Schlitt, 1982 and Lowson, 1982). Although, McKibben and Barnes (1986) report that the rate is independent of pH, our results indicate an order of 0.11(±0.01) which cannot be interpreted as an order of zero within the error limits of the regression. Figure 5 shows that the residuals for the model show no pronounced systematic error.

Results for our MFR and BR studies of the reaction of ferric iron and pyrite in the presence of oxygen are found in Table 2. Multiple linear regression of these data revealed that the reaction between ferric iron and pyrite is independent of the concentration of sulfate, chloride and ionic strength (I). As illustrated in the leverage plots of Fig. 3 (numerically in Table 4), SO_4^{2-}, Cl^-, H^+ and I exert no statistically significant influence on the rate of pyrite oxidation by ferric iron in the presence of oxygen. Although the experiments represented in Table 2 and Fig. 3 were performed under partial pressures of O_2 of ambient air and under pure O_2, no difference could be discerned between the two data sets (see leverage plot for DO in Fig. 3).

Table 4. Summary of multiple linear regression alaysis to determine rates laws for pyrite oxidation by dissolved oxygen (Py/DO), ferric iron in the presence of dissolved oxygen ($Py/Fe^{3+}/DO$) and ferric iron in nitrogen-purged solutions ($Py/Fe^{3+}/N_2$).

	TERM	COEFFICIENT	STD ERROR	R^2
Py/DO				
	Intercept	-8.19	±0.10	
	log mO_2	0.50	±0.04	
	log mH^+	-0.11	±0.01	0.87 (n=51)
$Py/Fe^{3+}/DO$				
	Intercept	-6.07	±0.57	
	log mFe^{3+}	0.93	±0.07	
	log mFe^{2+}	-0.40	±0.06	
	log mH^+	-0.07	±0.19	
	log mSO_4^{2-}	-0.02	±0.02	
	log mCl^-	-0.03	±0.01	
	I	0.17	±0.07	0.96 (n=31)
	Intercept	-19.71	±0.86	
	Eh	12.93	±1.04	
	pH	1.00	±0.29	0.88 (n=31)
$Py/Fe^{3+}/N_2$				
	Intercept	-8.58	±0.15	
	log mFe^{3+}	0.30	±0.02	
	log mFe^{2+}	-0.47	±0.03	
	log mH^+	-0.32	±0.04	0.95 (n=101)
	Intercept	-12.7	±0.11	
	Eh	6.10	±0.19	
	pH	0.37	±0.04	0.93 (n=93)

Model Residuals

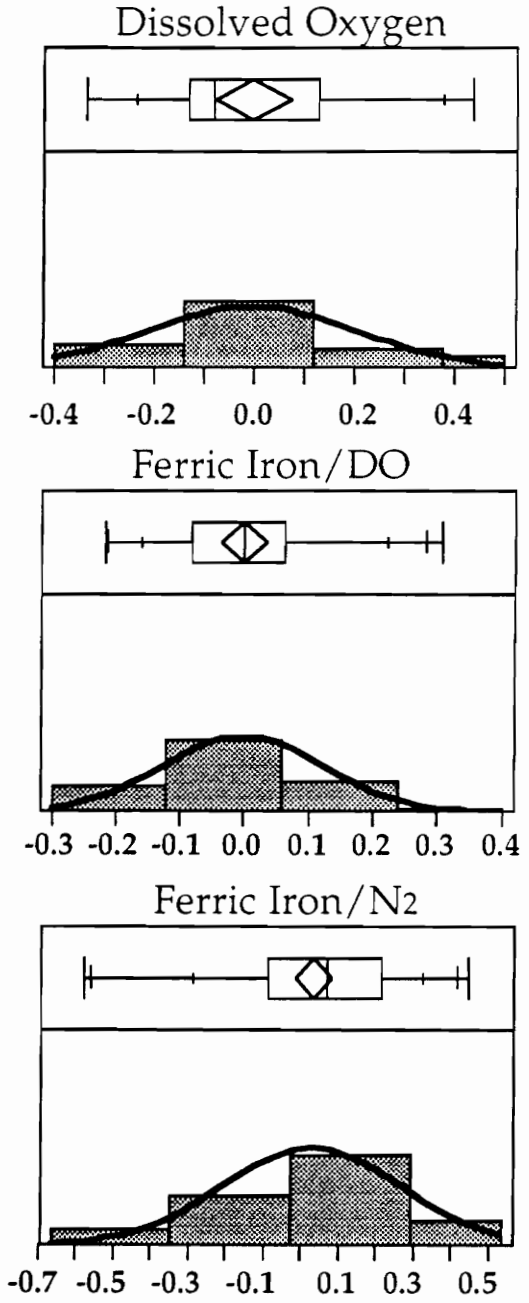

Figure 5. Plots of whole model residuals for regressions of Fig. 2-4. The absence of pronounced asymmetry in the distribution indicates that errors in the model fit are nearly random.

When DO is present, the rate of oxidation is appreciably affected by ferrous and ferric iron only and the applicable rate law is

$$r = 10^{-6.07(\pm 0.57)} \frac{m_{Fe^{3+}}^{0.93(\pm 0.07)}}{m_{Fe^{2+}}^{0.40(\pm 0.06)}} \quad (5)$$

Smith et al. (1970) noted a slight difference in the rate of reaction when using ferric chloride instead of ferric sulfate as the oxidant, but did not specifically quantify the effect. Unfortunately, it was not possible for us to incorporate Smith et al. 's (1970) data for chloride and sulfate additions into the present dataset as those authors did not provide sufficient detail in their report to satisfactorily correlate tabulated rates with solution composition. Smith et al. (1970) studied the effect of Cl^- and SO_4^{2-} over a half an order of magnitude variation in concentration, whereas the present study reports data spanning about 6 orders of magnitude. However, if the graphs of Smith et al.'s (1970) data are examined (their figure 27), it can be seen that only modest differences in the rate for Cl^- and SO_4^{2-} solutions are indicated. Additionally, they consider only two concentrations of both Cl^- and SO_4^{2-}, and this is not a significant range of variation. By performing a series of experiments using a wide range of Cl^- and SO_4^{2-} concentrations, we have been able to produce a reliable basis for evaluating the effect of these species at 25°C and atmospheric pressure. No significant systematic error was found for the model regression (Fig. 5)

Our results and data compiled from the literature for the reaction of ferric iron and pyrite in N_2-purged solutions are summarized in Table 3. Analysis of these data reveals distinctly different behavior from experiments

performed in the presence of DO (Fig. 4; Table 4). For these experiments, the applicable rate law is

$$r = 10^{-8.58(\pm 0.15)} \frac{m_{Fe^{3+}}^{0.30(\pm 0.02)}}{m_{Fe^{2+}}^{0.47(\pm 0.03)} m_{H^+}^{0.32(\pm 0.04)}} \quad (6)$$

Similar to the oxygen-present experiments, the rate is dependant on Fe^{3+} and Fe^{2+} concentrations. However, in the absence of oxygen, the pH of the solution has a significant effect on the rate, consistent with the findings of McKibben and Barnes (1986). As with the other regressions, analysis of residuals does not reveal any pronounced systematic error in the analysis, hence, all error is random (Fig. 5).

The positive correlation with Fe^{3+} and negative correlation with Fe^{2+} suggests a correlation of rate with the Eh of the experimental solutions. Table 4 reports the results of a multiple linear regression model of log r as a function of Eh and log m_{H+}, which show that the kinetics of the reaction of pyrite with ferric iron are strongly influenced by the Eh of the solution. For cases where DO was present

$$r = 10^{-19.71(\pm 0.86)} Eh^{12.93(\pm 1.04)} pH^{1.0(\pm 0.29)} \quad (7)$$

and for N_2-purged solutions

$$r = 10^{-12.7(\pm 0.11)} Eh^{6.10(\pm 0.19)} pH^{0.37(\pm 0.04)} \quad (8)$$

This result was first presented by Garrels and Thompson (1960), and is strong evidence for an electrochemical mechanism for the reaction.

Consistent with McKibben (1984), who reported the rate of sulfate production to be stoichiometrically equivalent to ferrous iron production, we found that only sulfate is produced in significant quantities during pyrite oxidation with ferric iron. PFR experiments with added sulfite and formaldehyde did not affect the rate of production of sulfate. Therefore, we do not believe that aqueous polysulfides or sulfide species are involved in the production of sulfate. When Ag^+ was added to reaction solutions, a small amount of thiosulfate, $S_2O_3^{2-}$ was detected, but was not abundant enough to be a significant intermediate for sulfate production.

DISCUSSION

Pyrite Oxidation by Dissolved Oxygen

Because Moses (1982) and Goldhaber (1983) reported the formation of aqueous sulfur intermediates at pH . 6 during the reaction of pyrite with DO, McKibben and Barnes (1986) called into question some data from Smith et al. (1970), which assumed the stoichiometry of eqn. (2) to be correct at all pH's. However, the data reported by Moses et al. (1987) clearly show that the assumption of Smith et al. (1970) is valid for the pH range ~2-8 (2.22-7.85) as the formation of sulfoxy intermediates was not observed under these conditions. At pH=9.06, Moses et al. (1987) showed that the rate of sulfate production is one-half the total sulfur production. Hence, only a factor of two error (0.3 log units in rate) can be expected for Smith et al.'s (1970) data of pH 9 and 10. As seen in Fig. 2, the measurements of Moses and Herman (1991)

are consistent with those of Smith et al. (1970) at pH = 6-7 and clearly establish the order of reaction for H^+. However, the small reaction order of the present report for H^+ indicates that pH has a negligible effect on observed rate which increases only one order of magnitude over a nine order of magnitude change in H^+ molality.

The results of Nicholson et al. (1988) cannot be accurately compared with our results, as those authors do not report analytically determined surface area for the pyrite used in their experiments and do not report the specific pH of each individual experiment. However, using their surface area estimates (10^{-2} m^2g^{-1}) and an assumed pH of 7.6, our rate law can be used to calculate rates of reaction that agree with the observations of Nicholson et al. (1988) within a factor of 1.7 (0.2 log units on average).

It could be argued that the observed increase in rate with pH may be related to the oxidation of ferrous iron released from pyrite according eqn. (2). This process would produce ferric iron which could subsequently react with pyrite according to eqn. (1). Moses and Herman (1991) present arguments for the adsorption of ferrous iron and DO, and suggest that the oxidation of adsorbed ferrous iron has a significant effect on rate at circumneutral pH. Smith et al. (1970) report the results of several experiments at pH=2 with their Warburg apparatus (an externally cycled batch reactor) in which they placed amberlite cation exchange resin in-line to remove the ferrous iron produced by the reaction of pyrite with DO. They observed no difference in rate for experiments when ferrous iron was removed *versus* when it was not. Therefore, at pH 2, oxidation of ferrous iron to produce ferric iron to oxidize pyrite is not significant. It is possible that the slight break in slope of the

leverage plot for log H^+ in Fig. 2, which occurs very nearly at the pH when ferrous iron oxidation increases rapidly (Williamson et al., 1992), is significant and supports the hypothesis that iron oxidation is important in this reaction. However, our data do not allow us to evaluate this further.

The data in this paper for the rate of oxidation of pyrite by DO are not adequately modeled using a simple, ideal Langmuir isotherm. Under Langmuir adsorbtion behavior, saturation of the mineral surface will occur with increasing P_{O2}. Nicholson et al. (1988) presented evidence that they believe indicated such behavior and that the rate of reaction became zeroth order in DO at high DO concentrations. The data tabulated in Table 1 represent DO concentrations that extend to higher values than those reported by Nicholson et al. (1988), but do not suggest surface saturation (see leverage plot for DO in Fig. 2). Deviations from ideal, Langmuir adsorption behavior is not uncommon (Laidler, 1987). Alternatively, a non-ideal, multilayer adsorption model can be constructed. According to this approach, the amount of a substance adsorbed, Θ, is related to the concentration c by

$$m_{sfc} = k_F\, m_{sol}^n \tag{9}$$

where k_F and n are empirical constants. This expression is known as the Freundlich isotherm (Adamson, 1982; Laidler, 1987) and, as above, can be substituted into the general form of the rate expression for rate expressed as a function of fraction of mineral surface covered by the oxidant

$$\begin{aligned} r &= k\, m_{sfc} \\ &= k\, k_F\, m_{sfc}^n \\ &= k'\, m_{sfc}^n \end{aligned} \tag{10}$$

or, alternatively

$$\log r = \log k' + n \log m_{sfc} \qquad (11)$$

where k' is the apparent rate constant. As shown in Fig. 2, this relationship between log r and log m_{O2} concentration is linear over two orders of magnitude variation in DO. It is important to note the Freundlich isotherm does not allow saturation of the surface and that the amount of adsorbate found on the surface of the mineral, and hence rate keeps increasing with increasing DO concentration. This effect is clearly illustrated in Fig. 2. The Freundlich isotherm was developed theoretically on the basis of distributions of surface sites of different energies (see references in Laidler, 1987). Such behavior is consistent with the non-uniform attack of the pyrite surface by aqueous oxidants at sites of high excess surface energy as suggested by SEM studies of McKibben and Barnes (1986).

Oxidation by Ferric Iron

Our results show that the rate of reaction between Fe^{3+} and pyrite is enhanced by the presence of DO at high Fe^{3+}/Fe^{2+} ratios, but that the rate is faster in the absence of DO when Fe^{3+}/Fe^{2+} is low. Figure 6 illustrates this result by comparing the influence of Fe^{3+}/Fe^{2+} on reaction rate for a constant pH = 2 and atmospheric DO concentration *versus* no DO, using the rate laws presented above. Because the two trends cross, the reaction in mixed Fe^{3+}/DO systems is not simply a linear combination of the rate laws for Fe^{3+} in N_2 and for O_2 oxidations At high Fe^{3+}/Fe^{2+}, the experimental conditions

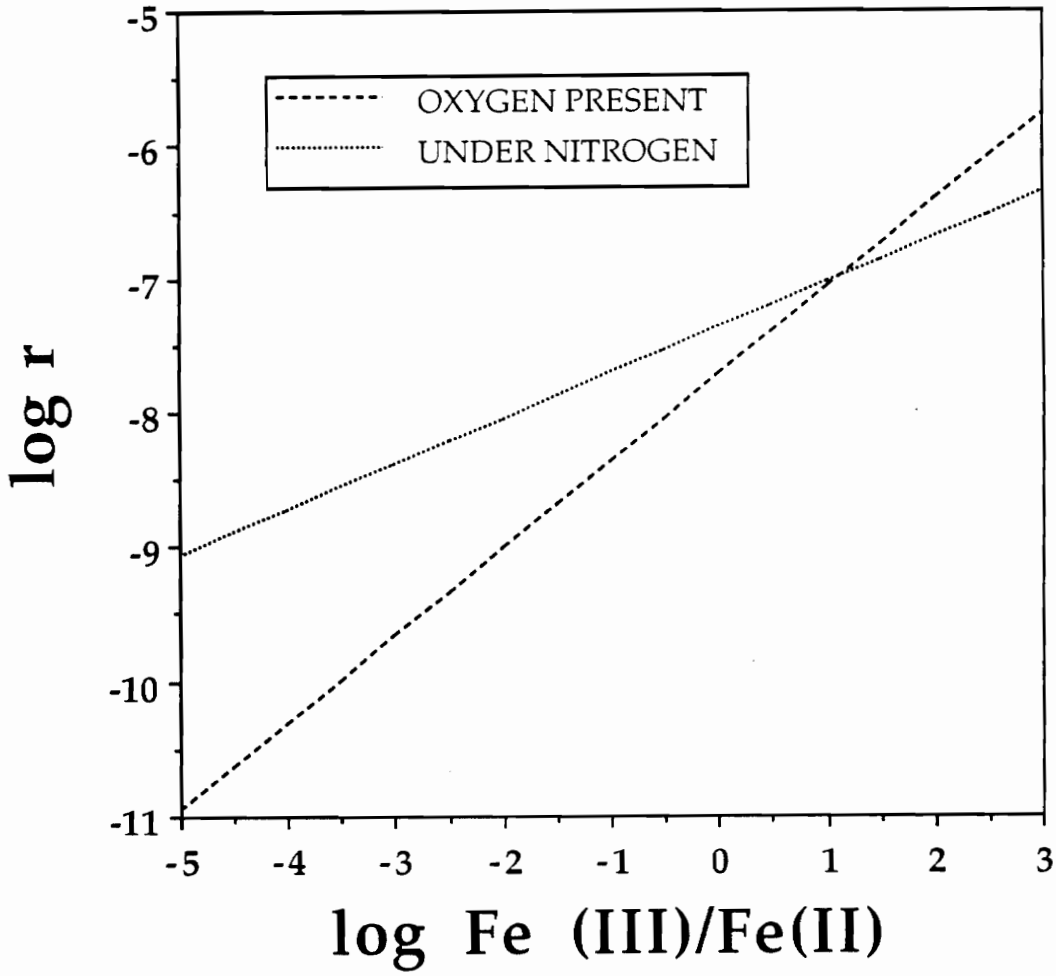

Figure 6. Plot of log r vs. log (Fe^{3+}/Fe^{2+}) at pH = 2 for the rate of pyrite oxidation by ferric iron under a nitrogen atmosphere and in the presence of DO calculated from the regression data in Table 4. In oxygenated acid mine drainage solutions, log (Fe^{3+}/Fe^{2+}) ~ 4.5.

of King and Lewis (1980), McKibben and Barnes (1986), Moses et al. (1987) and Moses and Herman (1991), the rate is very nearly equal for the O_2 absent and O_2 present experiments. Consistent with Fig. 6, King and Lewis (1980) reported that the reaction rate at ambient pO_2 was no different than the rate under N_2. This effect also accounts for the agreement between the reports by McKibben and Barnes (1986) and Rimstidt and Newcomb (1992) which were performed under N_2 and ambient air, respectively. Significantly, in weathering environments like acid mine drainage (AMD), the Fe^{3+}/Fe^{2+} is generally much lower (~$10^{-4.5}$ at pH~2; Williamson et al., 1992) than most experimental studies to date. As seen in Fig. 6, this results in rates of reaction between ferric iron and pyrite that are about two orders of magnitude slower than would be expected based on the rates laws determined in N_2-purged solutions.

Similar to the results for the DO oxidation of pyrite, the results of this study do not support a simple, site specific adsorption model to explain the kinetics of aqueous oxidation of pyrite by ferric iron. A simple Langmuir isotherm model for competitive, site-specific adsorption between Fe^{3+}, Fe^{2+} and H^+ (to account for pH variation) produced an $R^2 = 0.92$. However, despite the high correlation coefficient, a plot of the residuals for the model fit shows a significant degree of asymmetry, indicative of pronounced systematic error. (Fig. 7) Hence, it is difficult to place a great deal of confidence in an ideal adsorption process to explain the kinetics. Because we are able to correlate log r with log m_{Fe3+} and log m_{Fe2+}, with model residuals normally distributed, we believe that a non-site specific Freundlichadsorbtion process may be part of the reaction mechanism.

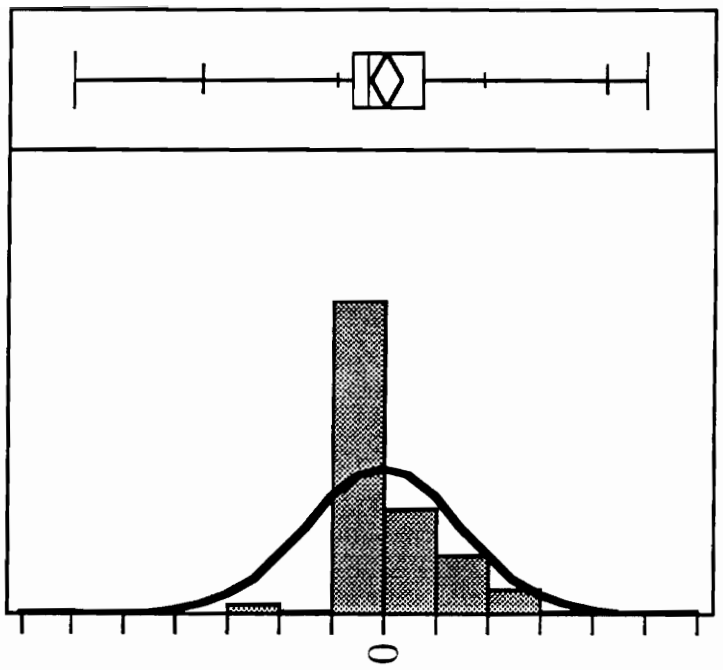

Figure 7. Residuals from an adorption model for the ferric iron oxidation of pyrite show a pronounced asymmetry, indicating that systematic error is present in the model and that an ideal, site-specific model of the adsorption of the oxidant onto the mineral does not explain the data

Mechanistic Implications

Much of the difficulty in formulating a reaction mechanism for the aqueous oxidation of pyrite by DO and ferric iron is centered on whether a molecular adsorption process (effectively chemical reactions at the pyrite surface) or an electrochemical process involving distinct anodic and cathodic sites on is operative. The evidence in the present study may be used to address this dilemma and provide a convincing arguement for the electrochemical mechanism.

Central to molecular mechanisms (McKay and Halpern, 1959; Smith et al., 1970; Mathews and Robins, 1974; Moses et al., 1987; Nicholson et al., 1988; Moses and Herman, 1991) is isite-specific adsorption of the oxidant. Several studies have derived Langmuir-like relationships that appear to fit the experimental data and thus, have been taken as ample evidence for the validity of the model. The evidence presented in this paper does not support an adsorption mechanism because saturation of the mineral surface by the oxidant cannot be demonstrated. This is particularly true for the oxidation by ferric iron where rate increases with increase in ferric iron over a six order of magnitude range in ferric iron. Further, our efforts to model the rate of pyrite destruction by ferric iron with an adsorption model produced residuals that show pronounced assymmetry and indicate that pronounced systematic error is present in the model. However, further analysis shows that the rate of pyrite destruction can be fit with a Freundlich isotherm, which entails a multi-layer, non-site specific process.

Fractional orders of reaction for heterogeneous reaction, such as aqueous pyrite oxidation, are oftern viewed as evidence for adsorption of

reactants or desorption of products as rate limiting (McKibben and Barnes, 1986). Our results show that the oxidation of pyrite by ferric is independant of sulfate concentration, which is the primary sulfur product (Moses et al., 1987). Similarly, our PFR experiments using chemical probes to track aqueous sulfur speciation showed that only a small amount of thiosulfate could be isolated when using Ag^+ as an additive. Further, no sulfite, aqueous polysulfides or polythionates could be detected. Hence, the desorption of primary product sulfate from the pyrite surface cannot be the rate limiting step for the overall reaction. Similarly, because the rate data do not conform to a site specific adsorption model, the adsoprtion of the oxidant is probably not rate limiting.

The rate of pyrite destruction is positively correlated with the concentration of the oxidant only, hence we can infer that electron transfer from the mineral to the aqueous oxidant is rate limiting. This is consistent with activation energies reported for the reaction (50-80 kJ mol^{-1}; see Lowson, 1982 and McKibben and Barnes, 1986) which indicate a chemical rather than physical barrier to reaction is rate-limiting. The correlation we present between rate of mineral destruction and Eh coupled with non-site specific interaction of the aqueous oxidant with the mineral is good evidence for an electrochemical mechanism involving distinct anodic and cathodic sites. Such a mechanism would conveniently account for product sulfate acquiring oxygen from the solvent water (Reedy et al., 1991) and would also account for the observed first order dependance of the reaction on water (Lowson, 1982).

In summary, the evidence we have presented supports a reaction between pyrite and the aqueous oxidant that is an electrochemical reaction

involving non-site specific, multilayer adsorption of the oxidant for which the electron transfer is rate-limiting. Figure 8 illustrates the cathodic, rate-limiting portion of this mechanism that we feel is supported by the evidnece. This mechanism does not require the oxidant to directly contact the mineral surface, but does imply that electrons from the mineral are transferred to the oxidant within a a discreet zone of solvent near the mineral surface. We envision this process as somewhat analagous to an electron tunnelling process for electrodes (Bockris and Reddy, 1970). The probability of finding an electron adjacent to the mineral surface decreases with distance away from the surface (e.g. its potential energy becomes greater). Similarly, the probability of electron being located some position away from the aqueous oxidant decreases with an increase in distance. The potential energy maximum (really a surface in three dimensions) illustrated in Fig. 8, is the energy barrier through which an ejected electron must pass to be received by the aqueous oxidant and thereby oxidize the mineral. The passage of an electron through this energy barrier is the rate determining step for the aqueous oxidation of pyrite, as supported by the kinetic evidence we presented earlier. This cathodic process is coupled with an as yet poorly understood anodic reaction wherein electron-deficient sulfur will react with solvent water, eventually releasing the most stable aqueous sulfur species to solution (SO_4^{2-} in the case of oxidation by ferric iron at high Eh). This interpretation is consistent with the demonstrated non-site specific interaction of the pyrite and the oxidant, activation energies, oxygen isotopes and the principle of molecular economy.

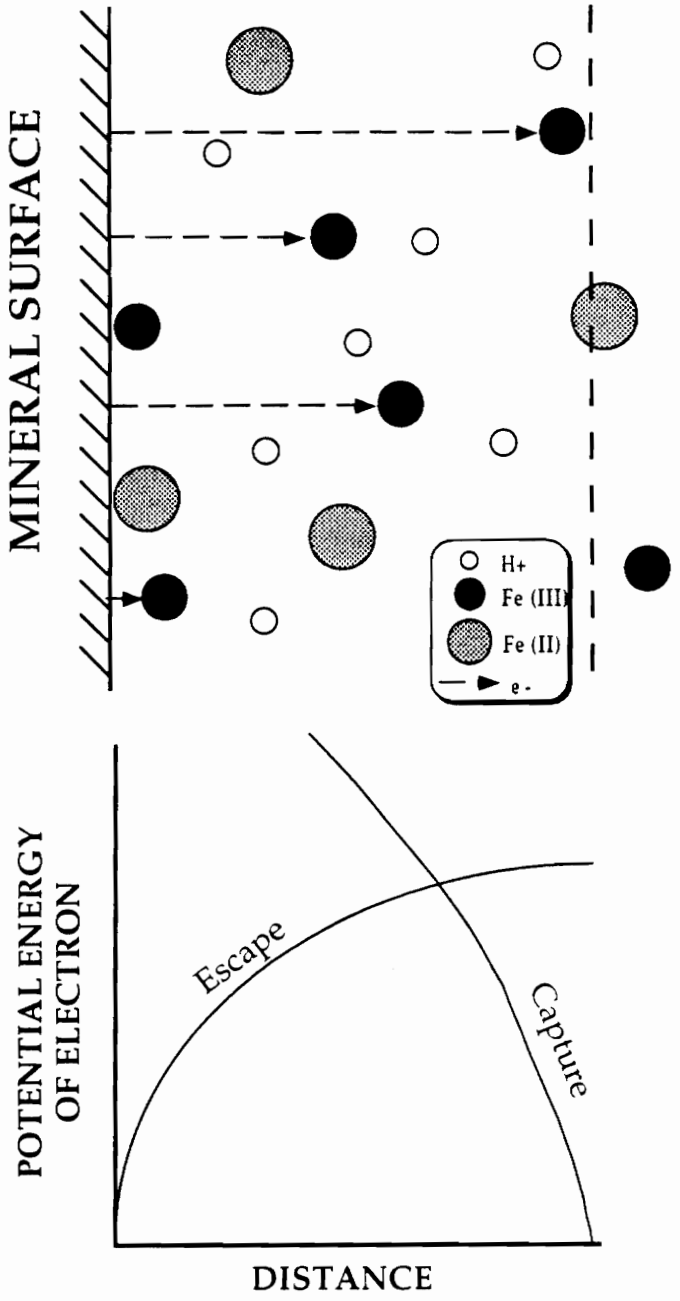

Figure 8. This figure schematically illustrates how an electron transfer occurs at the cathodic site for pyrite oxidation. Such an explanation is consistent with our rate law based upon a non-site specific Freundlich isotherm interaction between the mineral and the aqueous oxidant.

Evolution of the Pyrite Surface

Moses and Herman (1991) reported that the ferric iron oxidation of pyrite at pH 6-7 could not be sustained in N_2-purged solutions and that the rate of sulfate production became irreproducible after a few hundred seconds until oxygen was introduced. In this study, we observed reproducible, consistent and smooth consumption of ferric iron in BR experiments with ferric iron and DO mixtures. However, a detailed examination of the data revealed that a slowing of the rate occurred that cannot be attributed to consumption of oxidant in those experiments. Figure 9 is a graph of log r and log k *versus* time for a BR experiment with Fe^{3+} and DO at pH = 2. Although it is reasonable to expect the rate of reaction will slow as Fe^{3+} is consumed in the closed system (which would not be regenerated to any appreciable extent by ferrous oxidation at the low pH), the rapid drop in log k over the 2225 seconds of the experiment illustrated is counterintuitive. If the same mechanism is operative over the duration of the experiment, the value of log k should remain constant. The apparent change in log k must be due to either a corresponding change in solution composition or a change in the pyrite. This phenomenon was observed by Rimstidt and Newcomb (1992) who found that the reaction order with respect to time (n_T) was larger than the reaction order with respect to concentration (n_C). These workers concluded that an inhibitor was produced during the reaction.

For a series of experiments in which we re-reacted the same pyrite solids with identical solution compositions and volumes in the same BR, we are able to conclude that the ability of the pyrite to tranfer charge to the aqueous oxidant changes over time. We measured the rate of ferric iron

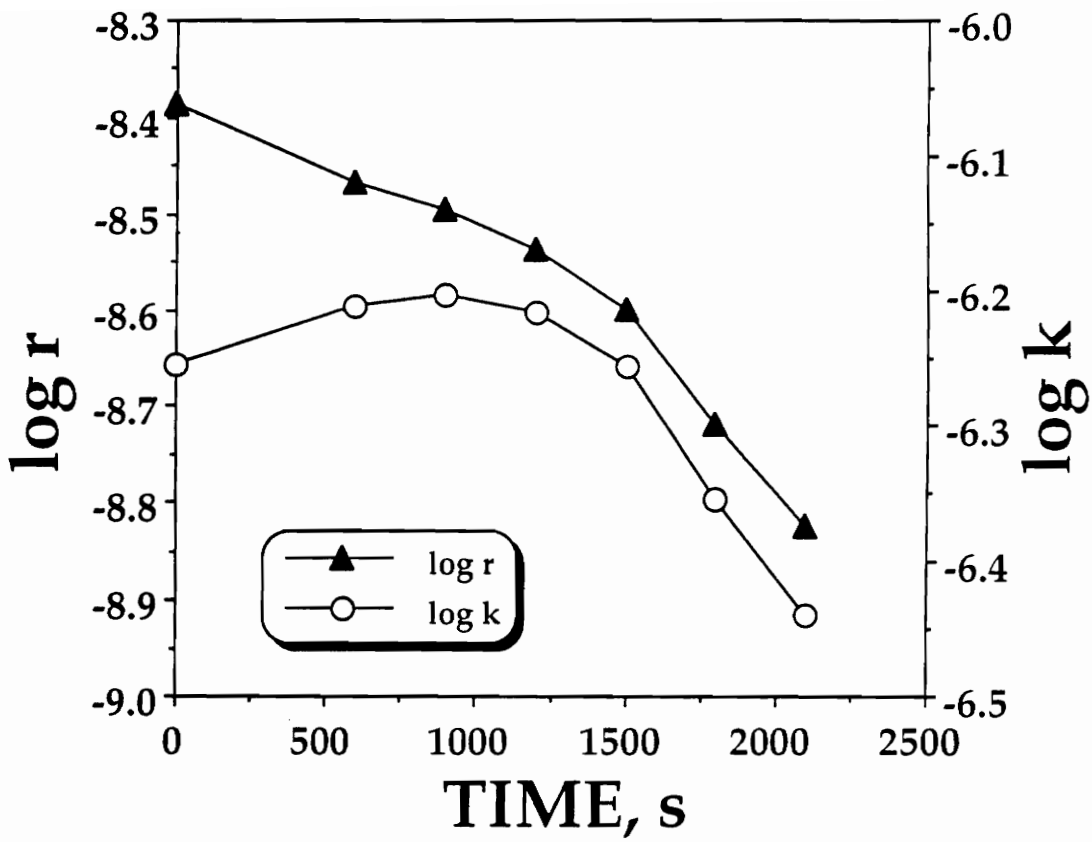

Figure 9. A graph of log r and log k as a function of time for a single batch reactor experiment of pyrite oxidation by ferric iron in the presence of DO. The drop in the rate constant indicates a change in either the reaction mechanism or a change in the pyrite solid.

consumption for a series of six experiments. For the second, third, and fourth experiments, the pyrite was simply rinsed off between with a few milliliters of distilled-deionized water. As illustrated in Fig. 10, the rate constant dropped from one experiment to the next. Between the fourth and fifth experiment, we washed the residual pyrite in concentrated HNO_3, and as shown in Fig. 10, were unable to recover the original kinetic behavior of the mineral. Similarly, treatment of reacted pyrite with EDTA failed to regenerate the original behavior. The infinitesimal change in surface area during this series of reactions could not account for an 85% reduction in the rate constant.

As an extension of the experiments described above, we pretreated three pyrite samples prior to reaction with ferric iron (plus DO) with 0.4 m Fe^{2+} (pH=1), 1 m EDTA and 1 m $NH_2OH{\cdot}HCl$ (hydroxylamine hydrochloride) for one hour, then rinsed the solids with a few milliliters of water. Pretreatment with ferrous iron and EDTA had little effect on the reaction rate (Fig. 10). However, $NH_2OH{\cdot}HCl$ pretreatment depressed the rate constant by 50%.

Because washing the reacted mineral grains with water, concentrated HNO_3 or EDTA failed to reproduce original rates, we are able to discount the hypothesis that the lowering of k over time is due to solution effects (i.e. adsorbtion of an inhibitor from solution). We hypothesize that a change in the electrochemical behavior of the solid has occurred. The semiconductor properties of pyrite have been reported to influence the rate of reaction in systems similar to the weathering environment (Lowson, 1992). However, the present data do not allow further interpretation.

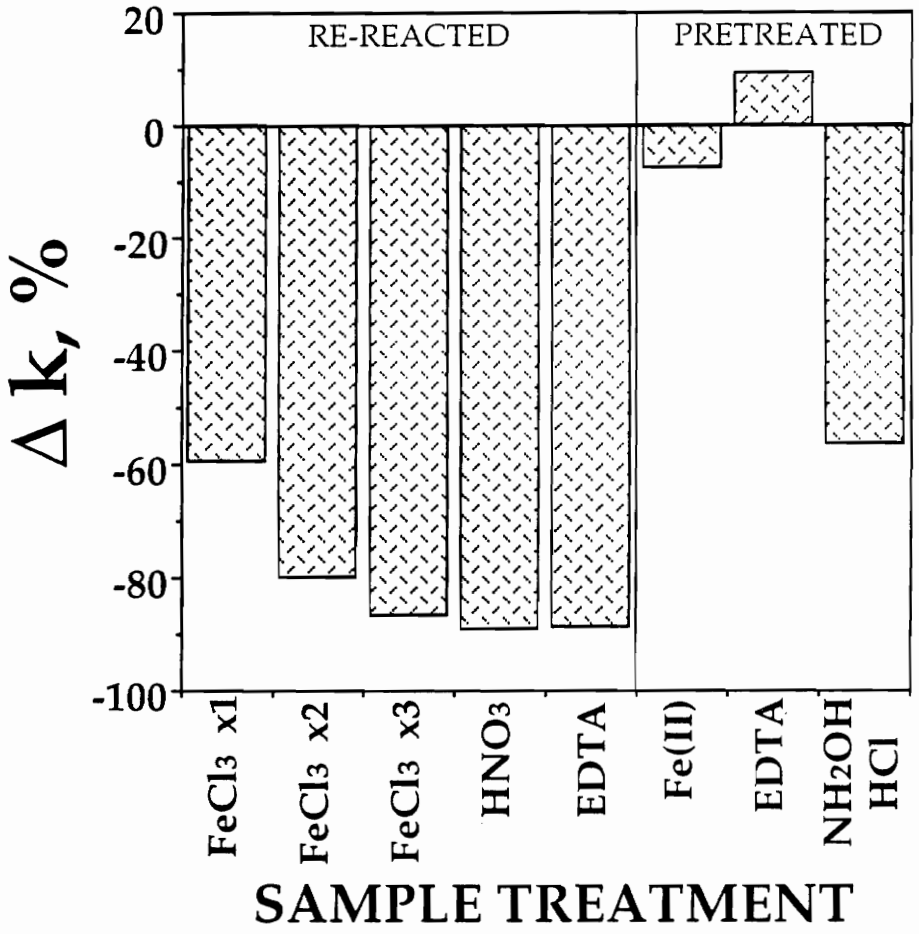

Figure 10. This figure illustrates the drop in k that occurs when the same pyrite sample is re-reacted with the same volume of identical composition ferric iron solution. The zero line indicates the original sample. Note that washing with concentrated HCl and EDTA is unable to restore the original behavior and indicates that a change in the pyrite sample has occurred. Pretreating pyrite with aqueous solutions of ferrous iron and EDTA does not affect the rate of reaction with ferric iron, while hyroxyamine hydrochloride ($NH_2OH{\cdot}HCl$) diminishes the rate.

CONCLUSIONS

We have developed rate laws for the oxidation of pyrite by molecular oxygen and ferric iron that are applicable over a wide range of solution composition. Multiple linear regression of rate data available in the literature for the reaction of pyrite with DO produced the rate law shown in eqn. (4) The rate dependance on DO was not observed to level off over a three and one half order of magnitude variation in DO concentration.

The rate of reaction of pyrite with ferric iron is not influenced by SO_4^{2-}, Cl^- or I but is significantly affected by the presence of DO (but not its concentration). For N_2-purged solutions, the applicable rate law (eqn. 5) contrasts markedly with the rate law determined for oxygenated solutions (eqn. 6). For these two rate laws, the order with respect to ferric iron is dramatically different, suggesting a difference in the reaction mechanism.

The rate of pyrite oxidation by ferric iron is strongly correlated with solution Eh, which underscores the importance of considering an electrochemical mechanism for the reaction. The fractional orders of reaction shown in the rate laws for the oxidation with ferric iron are difficult to interpret based strictly on a molecular mechanism. An electrochemical mechanism, involving distinct anodic and cathodic sites, which need not be proximal to each other, is consistent with the isotopic studies of Reedy et al. (1991) showing virtually all sulfate oxygen derived from water, and high E_a values which are typically well beyond that which can be expected from diffusion-controlled processes.

An important result of the work presented in this paper is the remarkable agreement between datasets from different workers. The studies

from which the present report has drawn upon span 20 years and represents as many as three different investigators using at least three different experimental procedures to follow the rate of this geochemically significant reaction. This results in our ability to produce rate laws for the aqueous oxidation of pyrite by DO and ferric iron that have a significant degree of confidence.

REFERENCES

Adamson A. W. (1982) Physical Chemistry of Surfaces , Wiley & Sons, New York.

Bockris, J.O. and Reddy, A.K.N. (1970) Modern Electrochemistry. vol 2, Plenum Press, New York.

Dutrizac J. E. (1982) Ferric ion leaching of chalcopyrites from different localities. *Metallurgical Transactions* **13B**, 303.

Dutrizac J. E., MacDonald R. J. C. and Ingraham T. R. (1970) The kinetics of dissolution of cubanite in aqueous acidic ferric sulfate solutions. *Metallurgical Transactions* 1, 3083-3088.

Fuerstenau M. C., Chen C. C., Hank. N. and Palmer B. R. (1986) Kinetics of galena dissolution in ferric chloride solutions. *Metal. Trans.* **17B**, 415-423.

Garrels, R.M. and Thompson, M.E. (1960) Oxidation of pyrite by iron sulfate solutions. *Am. J. Sci.* **258-A**, 57-67.

Gerlach J. K., Gock E. D. and Ghosh S. K. (1973) Activation and leaching of chalcopyrite concentrates with dilute sulfuric acid. Chapter 16 in *International Symposium on Hydrometallurgy*, D.J. I. Evans and R. S. Schoemaker eds. A.I.M.E., New York. pp. 403-416.

Goldhaber M. B. (1983) Experimental study of metastable sulfur oxyanion formation during pyrite oxidation at pH 6-9 and 30°C. *Am. Jour. Sci.* **283**, 193-217.

Hiskey J. B. and Schlitt W. J. (1982) Aqueous oxidation of pyrite. Interfacing Technologies in Solution Mining. Proceedings 2nd SME-SPE Internatl. Sol. Mining Symp., Denver CO. pp. 55-74

King W. E. and Lewis J. A. (1980) Simultaneous effects of oxygen and ferric iron on pyrite oxidation in an aqueous slurry. *Ind. Eng. Chem. Process Des. Dev.* **19**, 719-722.

Laidler K. J. (1987) Chemical Kinetics , 3rd ed., Harper and Row, New York.

Lowson R. T. (1982) Aqueous pyrite oxidation by molecular oxygen. *Chem. Rev.* **82**, 461-497.

Luttrell G. H. and Yoon R.-H. (1984) Surface studies of the collectorless flotation of chalcopyrite. *Colloids and Surfaces* **12**, 239-254.

Mathews, C.T. and Robins, R.G. (1974) Aqueous oxidation of iron disulfide ny molecular oxygen. *Aust. Chem. Eng.* **15**, 19-24.

McKay D. R. and Halpern J. (1959) A kinetic study of the oxidation of pyrite in aqueous suspension. *AIME Trans.* **212**, 301-309.

McKibben M. A. (1984) Kinetics of aqueous oxidation of pyrite by ferric iron, oxygen and hydrogen peroxide from pH 1-4 and 20-40°C, Ph.D. Thesis, Pennsylvania State University.

McKibben M. A. and Barnes H. L. (1986) Oxidation of pyrite in low temperature acidic solutions: rate laws and surface textures. *Geochim. Cosmochim. Acta* **50**, 1509-1520.

Moses C. O. and Herman J. S. (1991) Pyrite oxidation at circumneutral pH. *Geochim. Cosmochim. Acta* **55**, 471-482.

Moses C. O. Nordstrom, D.K., Herman, J.S., Mills, A.L. (1987) Aqueous pyrite oxidation by dissolved oxygen and by ferric iron. *Geochim. Cosmochim. Acta* **51**, 1561-1571.

Nicholson R. V., Gillham R. W. and Reardon E. J. (1988) Pyrite oxidation in carbonate-buffered solution: I. Experimental kinetics. *Geochim. Cosmochim. Acta* 52, 1077-1085.

Nordstrom D. K. (1977) Thermochemical redox equilibria of ZoBell's solution. *Geochim. Cosmochim. Acta* , **41**, 1836-1841.

Reedy B. J., Beattie J. K. and Lowson R. T. (1991) A vibrational spectroscopic ^{18}O tracer study of pyrite oxidation. *Geochim. Cosmochim. Acta* **55**, 1609-1614.

Rimstidt J. D. and Dove P. M. (1986) Mineral/solution reaction rates in a mixed flow reactor: wollastonite hydrolysis. *Geochim. et Cosmochim. Acta* **50**, 2509-2516.

Rimstidt J. D. and Newcomb W. D. (1992) Mesurement and analysis of rate data: The rate of reaction of ferric iron with pyrite. *Geochim. Cosmochim. Acta, in press*

Sall J. (1990) Leverage plots for general linear hypotheses. *Am. Stat.* **44**, 308-315.

Schoonen M. A. A. (1988) Mechanisms of pyrite and marcasite formation from solutions between 25 and 300° celsius, Ph.D. Thesis, Pennsylvania State University.

Smith E. E., Svanks K. et al. K., (1970) Sulfide to sulfate reaction mechanism, *Fed. Water Qual. Admin. Water Poll. Contrl. Res. Study* # 14010-FPS-02-70

Warren G. W., Kim S.-H. and Henein H. (1987) The effect of chloride ion on the ferric chloride leaching of Galena concentrate. *Metallurgical Transactions* B **18**, 59-65.

Wiersma C. L. (1982) Relative rates of reaction of pyrite and marcasite with ferric iron at low pH, Thesis, Virginia Polytechnic Institute and State University.

Wiersma C. L. and Rimstidt J. D. (1984) Rates of reaction of pyrite and marcasite with ferric iron at pH 2. *Geochim Cosmochim Acta* **48**, 85-92.

Wilkins R. G. (1974) The Study of kinetics and Mechanisms of Reactions of Transition Metal Complexes , Allyn and Bacon, Boston.

Williamson M. A., Kirby C. S., Rimstidt J. D. and Nordstrom D. K. (1992) Kinetics of acid mine drainage. *Geochim. Cosmochim. Acta, in press.*

Chapter 5: Conclusions

Taken together, the studies reported in this dissertation are a significant step toward developing a fundamental, quantitative understanding of the geochemistry of sulfur. Owing to an ability to exist in a wide variety of oxidation states, there is a tremendous richness to the inorganic geochemistry of sulfur which compounds the difficulties associated with understanding its behavior in the geochemical environment. Despite the apparently complex behavior this versatile element, this study has found simple quantitative approaches to understanding its stability and reactivity.

The correlation between structure and thermodynamic properties of aqueous sulfur anions is the first self-consistent thermodynamic dataset produced for the aqueous S-O-H system. Thus, it meets the need for data describing the stability of these species as they are increasingly recognized as important participants in the global cycling of sulfur. The technique employed in this study illustrates a simple approach to modeling a complex system and can be utilized to identify questionable data currently in use. The data produced by this study can provide insight into the relative stability's of the many aqueous forms of sulfur and can be used to predict the eventual equilibrium composition of sulfur-containing solution, but of course this method does not evaluate the rate at which such an equilibrium will be attained.

Quantification of the rate of thiosulfate destruction by ferric iron was demonstrated in Chapter 3 and a mechanism consistent with the derived rate law was established. This study illustrated the utility of a stopped-flow spectrophotometric kinetic apparatus to study the kinetics of a relatively rapid

geochemical reaction. It also illustrates the use of rate measurements over a range of ionic strength as a chemical probe of the mechanism of reaction. The rate derived in this study can be used to determine the lifetime of thiosulfate in aqueous ferric iron-containing solutions and forms a solid groundwork from which to evaluate the catalytic effects of common geochemical species like Cu^{2+} on the rate of this reaction, which may be important during the weathering sulfide mineral-containing rock outcrops and tailings piles.

Through timely experimental study and collection of data reported in the literature, rate laws for the aqueous oxidation of pyrite by dissolved oxygen and ferric iron were produced and reported in Chapter 4. These rate laws are applicable over a wide range of solution composition. By identifying the factors which most directly affect the rate of reaction, this study identified and confirmed the electron transfer from the mineral to the aqueous oxidant as the rate determining step for the reaction. The study has shown further that the rate of reaction can be expressed as a function of Eh and pH and has, therefore, provided substantial support for developing a quantitative electrochemical model of pyrite oxidation.

Vita

I was born in Bainbridge, Maryland, and for the first 14 years of my life I moved frequently as my father, Harry R. Williamson, was enlisted in the U.S. Navy as a member of the Seabeas. During this time I lived in Lambertville, New Jersey, Doylestown, Pennsylvania, Oxnard, California, China (Taipei, Taiwan), Key West, Florida and Virginia Beach, Virginia. I graduated from Bayside High School (Virginia Beach), Old Dominion University (Norfolk, Virginia; B.S. Chemistry), Northern Arizona University (Flagstaff, Arizona; M.S. Chemistry) and Virginia Polytechnic Institute and State University (Blacksburg, Virginia; Ph.D. Geology). With the completion of this dissertation, I will return to the western United States where I intend to work to preserve what little wild still remains in that inspiring territory and to continue my search for the back of beyond.

Mark A. Williamson